PAUL SCHERRER INSTITUT

u^b

b
**UNIVERSITÄT
BERN**

LABOR FÜR RADIO- UND UMWELTCHEMIE
DER UNIVERSITÄT BERN UND
DES PAUL SCHERRER INSTITUTS

Annual Report 2011

January 2012

u^b

b
UNIVERSITÄT
BERN

LABOR FÜR RADIO- UND UMWELTCHEMIE
DER UNIVERSITÄT BERN UND
DES PAUL SCHERRER INSTITUTS

Annual Report 2011

January 2012

Editors: A. Türler
M. Schwikowski
A. Blattmann

TABLE OF CONTENTS

Analytical Chemistry

Radwaste Analytics

Radionuclide Development

Environmental Radionuclides Universität Bern

EDITORIAL

Another year has passed very quickly and I am very pleased to present the next issue of our already traditional annual report.

Our report allows us to present a snapshot of ongoing research in our unit and to give an up-to-date answer to the question: What is the Laboratory for Radiochemistry and Environmental Chemistry and what are we doing? Nonetheless, the LCH annual report is not intended to replace publications in peer-reviewed papers.

In 2011, the LCH was still in a phase of consolidation. Our three, large scale projects are proceeding as planned.

As the photograph on this years title page shows, the new research and development laboratory for radiopharmaceuticals in the SWAN house on the premises of the Insel University Hospital in Bern, which is operated by the LCH, became an engineering marvel and has already attracted several new research collaborations, especially also with the nuclear medicine department. Due to the close collaboration with SWAN Isotopen AG, which is operating the new building and producing radiopharmaceuticals on a commercial level, we were able to negotiate favourable conditions with suppliers of equipment and circumvent the pitfalls that one meets when establishing a laboratory intended to produce pharmaceuticals suitable for human use. Also, the new patient floor for nuclear medicine is one of the most modern in Europe and consequently our research focus will also include therapeutic radiopharmaceuticals. Our collaboration with the Centre of Radiopharmaceutical Sciences at PSI has already resulted in very promising new results.

Again through the generous support of Bern University and the sympathetic assistance of my colleagues, rooms in the basement of the Department of Chemistry and Biochemistry (DCB) adjacent to our radioactive laboratories were remodelled and made ready for the installation of the MICADAS accelerator mass spectrometer at Bern University for ultralow level ^{14}C measurements. The instrument is currently assembled in the Laboratory of Ion Beam Physics (LIP) at ETHZ. Only after thorough testing, the instrument will then be transferred to the DCB.

After the PSI Forschungskomission had approved the project of establishing a near ambient pressure photoelectron spectrometer at SLS, also the application to R'Equip at the Swiss National Science Foundation was successful and the instrument recently passed the factory acceptance tests. With this new instrument we will be able to investigate gas phase – surface interactions at conditions relevant for processes occurring on aerosols in the atmosphere. This project is conducted in collaboration with the heterogeneous catalysis group of Prof. Jeroen van Bokhoven.

A further activity concerned the organisation of the second, very well attended ERAWAST workshop at PSI, where specialists discussed the manifold scientific applications of exotic radionuclides found in accelerator beam dumps.

But, our activities are not only confined to PSI! An expedition to Kilimanjaro was able to retrieve ice cores, which safely arrived still in frozen condition at PSI and will allow us to answer the long standing question of the age of the Kilimanjaro glaciers.

This years social event took us to the picturesque town of Haigerloch in Baden-Wuerttemberg, Germany, where in the former beer storage cellar renowned German scientists, among them Werner Heisenberg and Carl Friedrich von Weizsäcker, performed research on a heavy-water-moderated nuclear reactor during the last days of the second world war, although without reaching criticality. After spending lunch sitting outside, a heavy thunderstorm cut the visit to the town short and reunited us for coffee and cake in a dry place.

We concluded the year with a bowling party (Swiss style!) which generated lots of laughter and left us hungry for the subsequent spaghetti dinner.

In 2012, we are eagerly anticipating first results from our large scale installations and instruments and, hopefully, harvest the fruits of our labour and investments!

Andreas Türler

ON THE THERMAL RELEASE OF SUPERHEAVY ELEMENTS

D. Wittwer, R. Eichler, H.W. Gäggeler (Univ. Bern & PSI)

Experimental data and literature data was used to estimate thermal release characteristics of superheavy elements.

INTRODUCTION

For future investigation of superheavy elements (SHE) a possible change from gas phase chromatographic systems [1] towards a vacuum chromatographic system is envisaged. The expected rapidity of a vacuum system shall be advantageous for the investigation of very short-lived SHE. Due to the absence of gas as a stopping medium for the SHE a new approach is required to transfer SHE from the production site into the vacuum chromatographic setup. Our idea to this task is to provide thin metal foils to implant the SHE for thermalization. However, for the very short-lived SHE the release after the implantation in these foils must be very fast. Previously, release experiments with the lighter elements in group 12 and 14 were conducted to investigate their release characteristics [2]. Using the results of these experiments and additional literature data [3] allows for an extrapolative prediction of the diffusion coefficients and therefore also the thermal release properties of SHE. Here, we show the principle of this prediction.

THEORY

R. Tendler et al. [4] refined the principle suggested by H. Bakker [5] which was based on the Miedema model [6] and correlated $\ln(D_{Imp}/D)$ versus V_{Imp}/V where D is the self diffusion coefficient of the matrix material and D_{Imp} is the diffusion coefficient of the impurity. V and V_{Imp} are the molar volumes of the matrix material or the impurity respectively. All but V_{Imp} are experimental values. V_{Imp} can be calculated using values from [5] and formulas from [6] as:

$$V_{Im\,p} = V - \Delta V_{Im\,p} \text{ and}$$

$$\Delta V_{Im\,p} = \frac{P_0 V_A^{2/3}(\phi_A^* - \phi_B^*)}{(n_{WS}^A)^{-1/3} + (n_{WS}^B)^{-1/3}} \times \left[(n_{WS}^A)^{-1} - (n_{WS}^B)^{-1}\right]$$

V_A and V_B are the molar volumes of the element A dissolved in B at infinite dilution. Φ_A and Φ_B are the chemical potentials of A and B and n_{WS} are the electron densities at the Wigner–Seitz cell boundary. P_0 is an empirical constant. Fig. 1 shows such a plot for a tungsten matrix with data from [3] and experimental data from our experiments [2]. The two different lines represent either interstitial diffusion (green) or vacancy diffusion (black). From such a plot the diffusion coefficient of a SHE can be derived and by using data for SHE e.g. from [7] the release properties can be assessed according to [8] using the following equation:

$$F = 1 - \frac{8}{\pi^2} \cdot \exp\left(-\frac{D \cdot t}{d^2}\right)$$

D is the diffusion coefficient, t is the time, and d is the thickness of the matrix material. The position of the relevant SHE (112 - 116) are marked in Fig. 1, implying a fast release from a zirconium matrix.
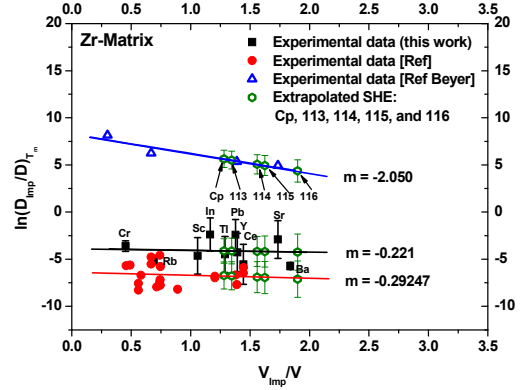
Fig. 1: Plot of $\ln(D_{Imp}/D)$ versus V_{Imp}/V at the melting point of the metal matrix zirconium. The red line is the extrapolation for vacancy diffusing elements [3]. The black squares illustrate the experimental data [2] and the calculated SHE 112 to 116 are shown as green circles. Blue triangles are literature data from [9].

REFERENCES

[1] R. Eichler et al., Radiochim. Acta, **98**, 133 (2010).

[2] D. Wittwer et al., Ann. Rep. Lab. of Radio- & Environ. Chemistry, Uni. Bern & PSI (2010), p. 3.

[3] G. Neumann et al., in „Self-diffusion and Impurity Diffusion in Pure Metals", Pergamon Materials Series (2008).

[4] R. Tendler et al., J. of Nucl. Mat. **150**, 251 (1987).

[5] H. Bakker, J. Less-Common Met., **105**, 129 (1985).

[6] A.R. Miedema, J. Less-Common Met., **45** 237 (1976).

[7] B. Eichler, "Metallchemie der Transaktinoide" PSI-Report 00-09 (2000) ISSN 1019-0643.

[8] J. Crank in "Mathematics of Diffusion". Oxford Univ. Press (1975).

[9] G.J. Beyer et al., Nucl. Instr. and Meth in Phys. Res. B, **204**, 225 (2003).

THERMAL RELEASE EXPERIMENTS AT THE OSLO CYCLOTRON LABORATORY

D. Wittwer, R. Eichler, H.W. Gäggeler (Univ. Bern & PSI), D. Piguet (PSI), E.A. Olsen, J.P. Omtvedt, A. Semchenkov, F. Schulz (Oslo University)

Volatile fission products from proton induced fission of ^{238}U have been thermally released from various solid catcher matrices at high temperatures in vacuum modeling superheavy element behavior.

INTRODUCTION

The most interesting isotopes of elements Cn - Lv (Z = 112 - 116) have half-lives usually well below 30 s. In preparation to investigate SHE, we tried to use short-lived isotopes of their lighter homologues. To produce p-elements of the 5th period recoiling at energies comparable to SHE produced in heavy ion induced nuclear fusion reactions, proton induced fission of ^{238}U is a very efficient way. A proton beam with energy up to 35 MeV and high intensities is accessible at the Oslo Cyclotron Laboratory at Oslo University, Norway. Here, we show the experimental setup that was used to investigate isotopes with half-lives in the minute time scale in a first experiment.

EXPERIMENTAL

A 0.73 mg/cm^2 ^{238}U target on a 3 μm Pd backing was irradiated for 60 min with a 30 MeV proton beam at an intensity of 500 nA. The cross section of the proton induced fission is around 1500 mb [3]. The setup is shown in Fig. 1 and Fig. 2. It consists of a vacuum chamber, see Fig. 1. This chamber has an interchangeable side plate, where the target, the cold catcher holder (CC), and a collection box to prevent unwanted contamination (CB) are mounted (see Fig. 2). Because of the random angular distribution of the fission fragments only a small fraction of fission fragments implant into a stack of hot-catcher (HC) foils (10 mm diameter), which were mounted inside of a Ta heat susceptor about 5 cm away from the target (bent away from the beam axis). This susceptor is a cylindrical Ta crucible, which has a thin metallic entrance window where the fission products enter and an outlet hole covered by the CC. This entire Ta crucible could be independently heated using an induction source (the copper coil surrounding the crucible is visible in Fig. 1). Thus, temperatures of about 1000°C were achieved in the middle of the crucible. The principle is as follows: The products entering through the thin entrance window of the crucible are stopped in the hot HC materials and are on-line released. They escape through the outlet in the crucible and are adsorbed on a water–cooled CC, which was a gold foil. Various HC materials have been investigated: Ni, Y, Zr, Nb, Mo, Hf, and Re. Before irradiation was started the box was pumped down to pressures of ~10^{-4} mbar and the crucible was heated up to the highest possible temperatures. After the irradiations the heating was switched of and the Ta crucible was cooled down for 30 min before the box could be opened. HC and CC foils were extracted. Both of them were immediately measured by standard γ-spectroscopy. To determine the absolute release a direct catch measurement was made putting a 20 μm Al foil at the place of the HC foils resulting in a 100% measurement.

Fig. 1: Picture of the Al-box with the Ta crucible where the hot-catcher foil stack was mounted in. The crucible is surrounded by the heating coil of the induction furnace. Bottom right insertion: HC foil holder.
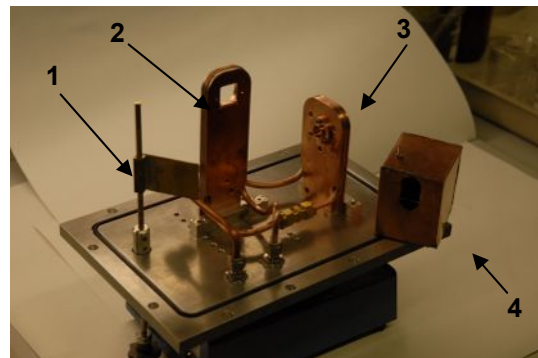
Fig. 2: Picture of the side plate holding a beam monitoring device (1), the cold catcher holder (2), the target holder (3), and not put in place the collection box to prevent contaminating the box (4).

RESULTS

First analysis indicates release of all volatile p-elements such as Sb and Te from the investigated HC. The data analysis is still in progress. Therefore, no release yields are available yet.

REFERENCES

[1] D. Wittwer et al., Ann. Rep. Lab. of Radio- & Environ. Chemistry, Uni. Bern & PSI (2010), p. 3.
[2] I. Usoltsev et al., this report, p. 5.
[3] S. Isaev et al., Nuclear Physics A **809**, 1, (2008).

INTERMETALLIC TARGETS FOR HIGH INTENSITY IRRADIATIONS

I. Usoltsev, R. Eichler, A. Türler, D. Wittwer (Univ. Bern & PSI),
R. Dressler, D. Piguet, R. Brütsch (PSI)

A new method of intermetallic target preparation is described. Based on the molecular plating technique, this method allows producing stable and homogeneous metallic targets for high intensity irradiations.

INTRODUCTION

The stability of actinide targets during the irradiation with intense heavy ion beams at near coulomb barrier energies is crucial for the performance of experiments with transactinide elements. It is believed that there are four major properties defining the overall target stability: thermal conductivity; electrical conductivity; chemical stability, and mechanical stability. The molecular plating (MP) technique is typically used for homogeneously depositing target materials on various backing materials [1]. However, poor thermal, electrical, and mechanical properties significantly limit the overall stability of such targets during irradiation. Here, we suggest a method to produce thin layers of intermetallic compounds of actinides with noble metals to overcome the disadvantages of MP targets given above.

EXPERIMENTAL

Layers of lanthanide/actinide material (0.73 mg cm^{-2} calculated for the metallic state) were deposited from nitrate solutions in isopropanol by MP on a previously polished and sonicated Pd foil (thickness 25 μm) in potentiostatic mode. In case of thin 2 μm or 3 μm foils, the foil was only rinsed with acetone prior to electrodeposition. The resulting plated material was evenly distributed on the foil if MP was performed in five consecutive steps (50 min each) at low current density (1.4 mA cm^{-2} – 2.8 mA cm^{-2}). The deposition yields were quantified by α and γ spectrometry using ^{152}Eu and ^{241}Am as tracers. Subsequently, the foil was heated up in a flow of pure hydrogen reducing the plated material in a so called "coupled reduction" process. α- and γ-spectra were taken from both sides of the foil for assessing diffusion parameters (e.g. for americium in palladium).

RESULTS AND CONCLUSIONS

It was observed that deposition performed in several consecutive steps at low current density is superior to fast single step deposition at high currents. All examined elements (Gd, Eu, Nd, U, Am, Th) were deposited on Pd surface with 90% - 100% yields. The chemical reaction equation of a "coupled reduction" [2] process of an actinide (Ac) oxide in contact with a noble metal (Me) contact can be written as:

$$xMe + Ac_xO_y + yH_2 = xAcMe + yH_2O$$
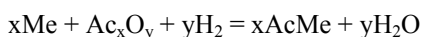
The most suitable temperature for the reduction of all examined elements on Pd foils appeared to be 1100°C. The chemical composition and lateral distribution was investigated by means of REM combined with energy dispersive X-ray spectrometry (EDX). It

appeared that the coupled reduction process is complete, since only very small traces of oxygen were present on the target surface. Due to the reduction process a pronounced diffusion of the lanthanides and the ^{241}Am tracer into the depth of the Pd foil was observed. After 3 h of reduction at 1200°C ^{241}Am and presumably also the lanthanide metal were equally distributed within the 25 μm Pd foil. The AASI 2.0 software [3] was used for alpha spectra simulation and allowed for the determination of the mean penetration depth of ^{241}Am based on the measured alpha spectra. Thus the diffusion coefficient, activation energy and the pre-exponential factor of the diffusion coefficient of Am in Pd were estimated (Fig. 1). Similar investigations will be performed using ^{238}U and ^{232}Th as target materials and also using ^{239}Pu and ^{249}Cf instead of ^{241}Am as tracers. The high melting Rh appears to be also a suitable candidate serving as coupled reduction partner. First irradiation test experiments with intermetallic targets have been carried out this year at the Oslo Cyclotron Laboratory, University of Oslo, Norway. A 3.5 μm ^{238}U/Pd target withstood perfectly irradiations with a 500 nA proton beam at vacuum conditions for several hours [4]. Finally, it is scheduled for Spring 2012 to prepare and to irradiate a stationary intermetallic ^{243}Am target using intense beams of ^{48}Ca at the U-400 cyclotron of the FLNR Dubna, Russia to really test its stability in the transactinide production environment.
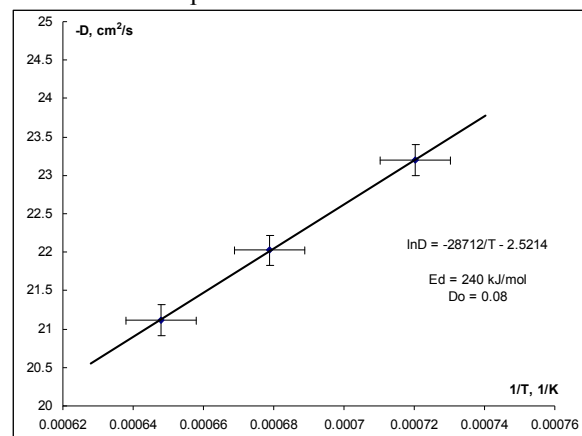
Fig. 1: Diffusion parameters for Am in Pd.

REFERENCES

[1] W. Parker et al., Nuclear Instruments and Methods 26 (1964) 61.
[2] S. Möbius, L. Hellwig, C. Keller, Journal of the Less-Common Metals, 121 (1986) 43.
[3] T. Siiskonen, et al., ESARDA BULLETIN, 40 (2008) 26.
[4] D. Wittwer et al., this report,4.

DIAMOND DETECTORS FOR TRANSACTINIDE CHEMISTRY

P. Steinegger, R. Eichler, A. Türler (Univ. Bern & PSI), R. Dressler (PSI)

First tests of diamond detectors for future SHE chemistry experiments.

INTRODUCTION

Common Si-PIN diodes feature a band gap of 1.12 eV. Thus, certain thermal energies (i.e. T > 40°C) or incident IR/VIS radiation are sufficient for partial electronic excitation, preventing any spectroscopic measurement. However, transactinide elements such as 113 and 115 are predicted to have rather high adsorption enthalpies ($-\Delta H_{ads}$) on surfaces. Hence, they can not be resolved in a thermochromatography experiment with the current COLD array. Diamond with a band gap of 5.5 eV can be seen as semiconductor and is therefore well suited for α-spectroscopy [1]. Its rather large electronic band gap allows for heating the detector up to temperatures significantly higher than 40°C and for operation in the close vicinity of an oven or even at daylight. Furthermore, based on its low dielectric constant of 5.6 (low preamplifier input capacitance) and its high resistivity (high band gap leads to a low intrinsic charge carrier density) diamond features an extremely low detector noise contribution. Hence, this new detector material shall pave the way towards various applications for future SHE chemistry experiments.

EXPERIMENTAL

The used diamond sample was provided by [2]. They consist of a 60 μm single-crystal chemical vapor deposition diamond layer (scCVDD) followed by a ~ 275 μm thick boron-doped (~ 100 ppm) high pressure / high temperature (HP/HT) diamond. Both sides of the sample were metalized with 50 nm gold, forming the detector electrodes. The sample was fixed on one side to a ceramic chip carrier with conductive high temperature glue (ground contact) while the upper electrode was wire-bonded from top down (bias contact). Subsequently, for a first measurement at high temperatures, the carrier with the detector was mounted on a copper block which was heated from the back by a resistive heating cartridge (Fig. 1). The 3-line α source (^{239}Pu, ^{241}Am, ^{244}Cm → mean penetration depth of the α-particles in diamond: 14 μm) was fixed at a distance of ~ 5 mm from to the detector surface. The spectra of this preliminary study are shown in Fig. 2 with the red line indicating the spectrum recorded at high temperature.

DISCUSSION / OUTLOOK

The achieved energy resolution of 7% (20°C) and 9% (200°C) dissatisfies. Even more if Si-like resolutions of 0.3% are reported for this kind of detector material [1]. For this reason, another type of CVD diamond from [3] (plain scCVDD) is now tested.
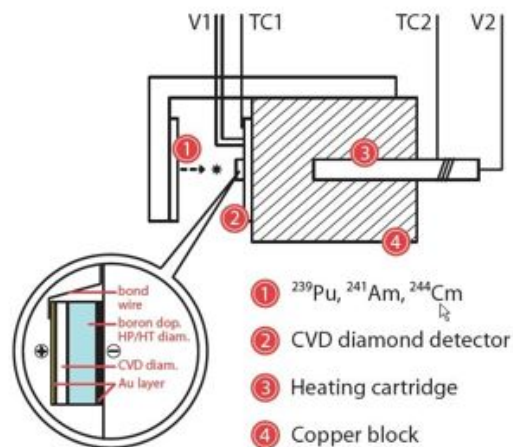
Fig. 1: Experimental setup for the high temperature alpha-spectroscopy study.
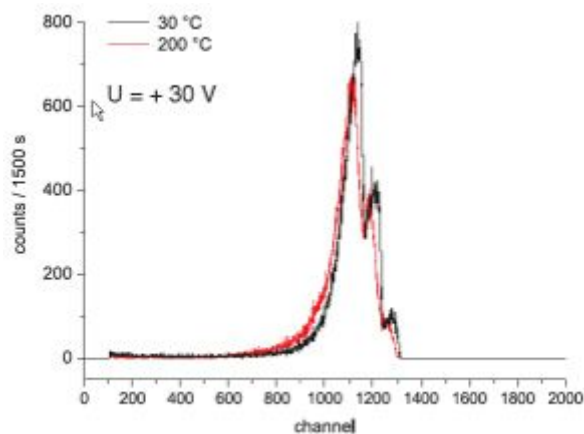
Fig. 2: Resulting spectra of the high temperature alpha-spectroscopy study.

We are convinced that the unique diamond material properties open up new experimental possibilities for the chemistry with transactinide elements, such as the mentioned increased COLD array temperature range or isothermal vacuum chromatography applications. Furthermore, the high chemical stability of diamond, should allow for fast aqueous phase chemical, e.g. electrochemical deposition experiments, directly on the detector surface.

REFERENCES

[1] M. Pomorski et al., Phys. Stat. Sol. (a), **203**, 12 (2006).
[2] DBS Microwave SA, CH – 2087 Cornaux NE.
[3] Element Six, King's Ride Park, Ascot, UK.

PREDICTING THE RETENTION OF NUCLEAR REACTION PRODUCTS IN THE PSI RECOIL CHAMBER USING COMSOL MULTIPHYSICS

R. Dressler (PSI), R. Eichler (Univ. Bern & PSI)

An optimum gas flow pattern minimizing the retention time of nuclear reaction products in the PSI recoil chamber was obtained via finite element simulations using the COMSOL Multiphysics® package.

INTRODUCTION & METHODS

The transport of the recoiling nuclear reaction products thermalized in a recoil chamber to the used chemistry setup and finally to the detection system must be performed as fast as possible. In contrast to the capillary transport, which can be described well as plug flow over long distances, the retention of volatile reaction products out of the recoil chamber needs more efforts. The COMSOL Multiphysics® software package [1] was used to perform finite element calculation to simulate the established flow pattern of the carrier gas as well as the transport of diluted species. The geometry used during the simulations based on the CAD drawing of the PSI recoil chamber used in the experiments with superheavy elements. The initial ion distribution in the recoil chamber was calculated using SRIM-2011 [2]. Due to the Z-limitations of the SRIM code, radon as reaction product and uranium as target material was used. The stopping force of ^{206}Rn was determined in argon [3]. Starting with a initial recoil energy of 53.7 MeV the ions were propagated through a U_2O_3 target (0.0 μm, 0.6 μm, and 1.2 μm thickness), through a Ti backing (2.0 μm), and stopped in a 1:1 He:Ar gas mixture at a pressure of 1.3 bar. In [3] a deviation of the experimental results to the SRIM predictions of about a factor two in terms of the stopping force was found. Therefore, the density of the stopping gas was adjusted using the ratio of experimentally determined and SRIM predicted stopping forces of radon in argon taken from [3]. The resulting ion distribution of ^{206}Rn for each target thickness was independently fitted perpendicular to the beam direction in equidistant slices using a Gaussian distribution (free fit parameter distribution width w_s) and for the projected distribution along the beam direction x using the function given in Eq. (1) (free parameters peak position x_p and distribution width w_l).

$$f(x) \propto \frac{1}{w_l} \cdot \exp\left(\frac{(x-x_p)}{w_l} - \left(1 - \exp\left(\frac{-x}{w_1}\right)\right) \cdot \exp\left(\frac{-(x-x_p)}{w_1}\right) \right) \quad (1)$$

All distributions can reasonably be described with the same width parameters (w_l = 5.2 mm and w_s = 2.2 mm). The initial ^{206}Rn density in the flow simulations was obtained by integration of Eq. (1) over the full target range assuming a constant production rate.

RESULTS & DISCUSSION

The calculations were preformed with a constant total carrier gas flow of 1.5 l/min, whereas the ratio of the flows entering inflow tube 1 (in1) and inflow tube 2 (in2) was varied. Fig. 1 shows, as an example, the initial ^{206}Rn distribution and the distributions after
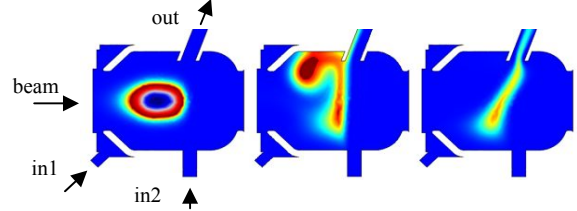
Fig. 1: ^{206}Rn density after 75 ms. The beam direction, both inflow tubes and the out-flow tube are indicated. From left to right: initial, 20% and 80% in1-flow.

75 ms for 20% and 80% in1-flow, respectively.

These results were used to estimate the flush out yield for interesting reaction products, in particular for Flerovium (Fl, Z = 114) isotopes ^{287}Fl ($t_{1/2} \sim 0.5$ s), ^{288}Fl ($t_{1/2} \sim 0.8$ s), and ^{289}Fl ($t_{1/2} \sim 2.6$ s). The results are depicted in Fig. 2. Maximal yields are predicted with 60% - 90% of the gas flow entering tube in1. In the case of ^{288}Fl about 50% of the produced atoms will be available for further transport to the detector. These calculations represent conservative yield predictions. Improved calculations will be done including the heat load induced by interactions with the beam.
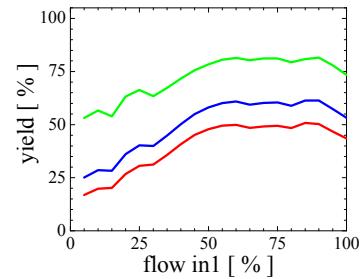
Fig. 2: Total yield of flushed out reaction products after 15 s for different half-lives $t_{1/2} = 0.5$ s (red), $t_{1/2} = 0.8$ s (blue), $t_{1/2} = 2.6$ s (green).

ACKNOWLEDGMENT

REFERENCES

[1] COMSOL Multiphysics® version-4 http://www.comsol.com (2010).

[2] J. F. Ziegler SRIM-2011, http://www.srim.org (2011).

[3] D. Wittwer et al., Nucl. Instr. Meth., **B 268**, 28 (2010).

OBSERVATION OF IN-SITU HYDRIDE FORMATION OF Bi AND Po

R. Eichler for a PSI-Univ. Bern-FLNR-ITE-LLNL collaboration

The transport of Bi and Po was observed in the IVO-COLD setup used to chemically identify element Fl (Z = 114). From the dependency of the transport yield on the dew point of the carrier gas and on the existence of a Ta-getter in the gas loop system we conclude the in-situ formation of BiH_3 and PoH_2. This observation might be important for a future chemical investigation of the elements 115 and Lv (Z = 116) and for safety assessment of LBE-spallation targets.

INTRODUCTION

Gas phase adsorption chromatography methods are typically used to separate and chemically identify transactinide elements. Therefore, the efficient in-situ formation of volatile molecules or a volatile element appeared to be important. Here, we report on the observation of a volatile compound class, presumably hydrides, for group 15 and 16 elements observed in our transactinide experiments. The in situ formation of this compound class, predicted already by Mendeleev, was experimentally observed for the first time in 1918 [1].

EXPERIMENTAL

Recently, experiments to investigate the new super-heavy transactinide elements Cn (Z = 112), 113, and Fl (Z = 114) comprise an experimental technique named IVO-COLD described elsewhere [2] and references therein. This technique is used to efficiently separate and chemically isolate volatile elements or compounds from by-products of nuclear fusion reactions as used for the production of super-heavy elements. The main constituents of this on-line setup are a recoil chamber attached to a stationary or rotating target setup followed by a hot quartz-wool filter to prevent aerosol transport and a hot Ta-getter to remove traces of water and oxygen. This part is connected via a 2 m - 3 m long PFA-Teflon capillary to the thermochromatography detector COLD shielded behind a 2 m concrete wall. The carrier gas is typically looped back to the recoil chamber after passing the COLD detector, Sicapent® drying units and again a large Ta-getter. The COLD detector is able to unambiguously identify α- and SF decaying nuclides as elements or compounds deposited on the detector surfaces in a temperature gradient between 35°C and -180°C.

RESULTS AND CONCLUSIONS

In our experiments ^{244}Pu and ^{243}Am targets have been irradiated with intense beams of ^{48}Ca. In multi-nucleon transfer reactions $^{219-222}$Rn, $^{211-214}$Pb, and $^{211-214}$Bi are formed. The production of $^{210-212}$At, $^{210-213}$Bi, and $^{210-212}$Po are attributed to multinucleon-transfer reactions with small contaminations of lead or other heavy metals in the target. The gas phase transport of radon (^{220}Rn→^{212g}Po) and astatine to the COLD detector and their deposition behavior is expected. The transport of ^{213}Bi and ^{212m2}Po during the ^{244}Pu irradiations (Fig. 1) was so far not understood. The only difference between the two irradiations was the use of the large Ta-Getter in the ^{244}Pu irradiations. We investigated the transport efficiency of Po and Bi in dependence of the getter oven temperature and of the water content in the carrier gas and measured their deposition behavior in the COLD detector (Fig. 2).
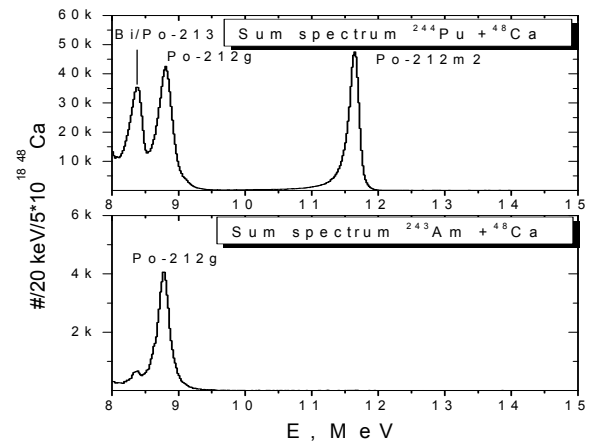
Fig. 1: α-Spectra from the ^{243}Am and ^{244}Pu irradiations.
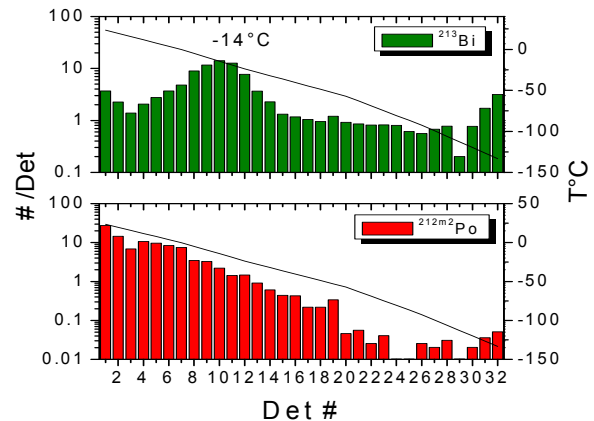
Fig. 2: COLD depositions for ^{213}BiH$_3$ and ^{212m2}PoH$_2$.

A clear correlation between the observed formation of ^{213}BiH$_3$ and ^{212m2}PoH$_2$ and the dew point in the carrier gas in the range −75°C - −100°C and to the use of the Ta-getter was found. We assume that traces of hydrogen are formed in the Ta getter by water decomposition. Hence, at beam plasma conditions atomic hydrogen becomes available for the in-situ formation of the hydrides in the recoil chamber. From a decay analysis we can attribute this observation to reaction and transport properties of Po and Bi, and not of Pb.

REFERENCES

[1] F. Paneth, Chem. Berichte 51 (1918) 1704.

[2] R. Eichler et al., Nature 447 (2007) 72.

METAL CARBONYL COMPLEXES – A NEW COMPOUND CLASS ACCESSIBLE FOR TRANSACTINIDES

J. Even (GSI & Univ. Mainz), A. Yakushev (GSI), Ch.E. Düllmann (GSI & Univ. Mainz & HIM),
J. Dvorak (HIM), R. Eichler (Univ. Bern & PSI), O. Gothe (LBNL), D. Hild (Univ. Mainz), E. Jäger (GSI),
J. Khuyagbaatar (GSI & HIM), J.V. Kratz (Univ. Mainz), J. Krier (GSI), L. Niewisch (Univ. Mainz),
H. Nitsche (LBNL), I. Pysmenetska (Univ. Mainz), M. Schädel (GSI & JAEA), B. Schausten (GSI),
A. Türler (Univ. Bern & PSI), N. Wiehl (Univ. Mainz), D. Wittwer (Univ. Bern & PSI)

First low oxidation state compound class of transition metals becomes available for transactinide research.

Gas-phase chemical studies of transactinide elements were so far restricted to simple, thermally stable, inorganic compounds. Metal-carbonyl complexes would provide a link to metal-organic chemistry. Binary, mononuclear, volatile carbonyl complexes are known for all lighter elements of group 6 and 8 of the periodic table. Seaborgium hexacarbonyl has been predicted to be stable [1]. Its experimental study would be interesting, because relativistic effects are predicted to influence the metal-CO bond. We explored the method of rapid in-situ synthesis of transition-metal carbonyl complexes with short-lived isotopes. First tests were performed at the TRIGA Mainz reactor, using the ^{249}Cf(n,f) reaction. Recoiling fission products were thermalized either in pure N_2 or in a CO/N_2- mixture. All volatile compounds were transported in a gas stream to an activated charcoal trap, which was monitored with a γ-ray detector. Fig. 1 shows a typical spectrum from the CO/N_2 measurements.
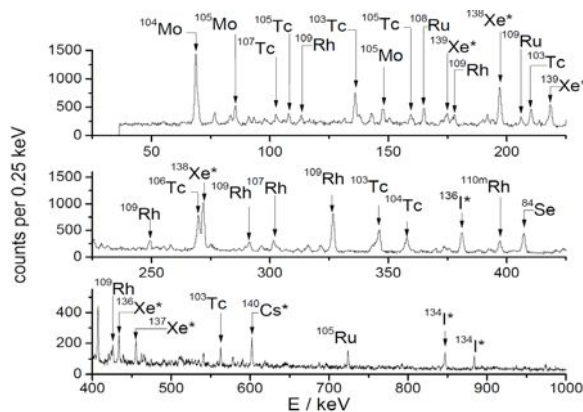
Fig. 1: γ-spectrum of fission products transported in a CO/N_2 mixture collected for 2 min and measured for 2 min. *γ-lines visible also in experiments with pure N_2.

Short-lived isotopes of Se, Mo, Tc, Ru, and Rh were only observed in the spectra when CO was added. These elements form volatile compounds with the CO. Transport with cluster (aerosol) material can be excluded. To test this method under experimental conditions relevant for transactinides, α-decaying ^{163,164}W and ^{170,171}Os were produced in ^{144}Sm(^{24}Mg, 4-5n) and ^{152}Gd(^{24}Mg, 4-5n) reactions, respectively, at the gas-filled recoil separator TASCA. Evaporation residues were separated from the primary beam and from unwanted transfer products within TASCA. They were thermalized in mixtures of He and CO in a

Recoil Transfer Chamber (RTC) [2] at the TASCA focal plane. Volatile carbonyl complexes – most likely $Os(CO)_5$ and $W(CO)_6$ – were formed in the RTC and were transported with the gas stream to the thermochromatography detector COMPACT [3]. The COMPACT detector array is a chromatography channel consisting of SiO_2 covered PIN diodes, suitable to register α particles emitted from volatile species inside the channel. A negative temperature gradient was applied along the chromatography column. Fig. 2 shows thermo-chromatograms of $Os(CO)_5$ and $W(CO)_6$. The measurements are compared to Monte Carlo Simulations. From the deposition patterns of W and Os, adsorption enthalpies of $W(CO)_6$ of (-46.5 ± 2.5) kJ/mol and $(-43^{+3.5}_{-2.5})$ kJ/mol for $Os(CO)_5$ were deduced. These values indicate physisorption of these carbonyl complexes on SiO_2.
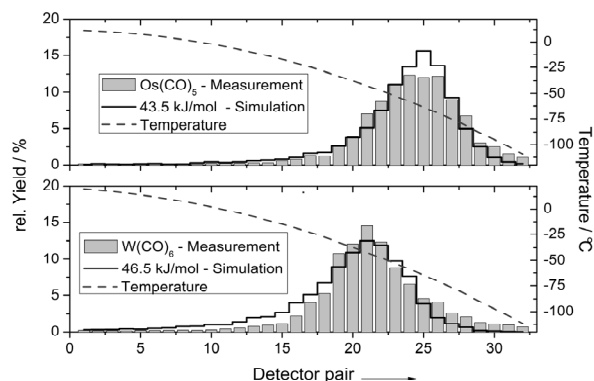
Fig. 2: COMPACT thermo-chromatograms. Upper graph: $^{170,\,171}Os(CO)_5$. Lower graph: $^{163,\,164}W(CO)_6$

Based on the results of our experiments, $Sg(CO)_6$ and $Hs(CO)_5$ are now within reach for transactinide chemistry. These compounds are suitable for chemical characterization by thermochromatography and appear highly promising for nuclear spectroscopy under low background conditions.

REFERENCES

[1] C.S. Nash, B.E. Bursten, J. Am. Chem. Soc., **121,** 10830 (1999).
[2] J. Even et al., Nucl. Instr. Meth. A. **638**, 157 (2011).
[3] J. Dvorak et al., Phys. Rev. Lett. **100**, 132503 (2008).

ADSORPTION INTERACTION OF MERCURY OXIDE ON QUARTZ AND GOLD

A. Serov, R. Eichler, A. Türler, D. Wittwer, H.W. Gäggeler (Univ. Bern & PSI),
R. Dressler, D. Piguet, A. Vögele (PSI)

The adsorption interaction of Hg was observed in thermochromatography experiments to be influenced by the presence of oxygen in the carrier gas. An at least intermediate formation of HgO is postulated.

INTRODUCTION

During the last years copernicium (Cn, Z = 112) has been characterized chemically. It was shown that its chemical behavior in the elemental state is similar to the nearest lighter homologue – mercury [1]. Mercury in the elemental state was studied as well [4]. Information about a chemical interaction of copernicium with oxygen would be desirable for a better understanding of relativistic effects in heavy transactinides. Here, we targeted HgO to establish experimental conditions and a possible design of experiments for a future study of CnO.

EXPERIMENTAL

^{197}Hg was produced as a decay product of ^{197}Tl, which was synthesized via irradiation of a ^{nat}Au target with ^{4}He at the PSI PHILIPS cyclotron applying beam intensities between 10^{11}-10^{12} particles per second. A 30 μm thick metallic gold target stack was irradiated with ^{4}He entering the target at an energy of (80±3) MeV. The gold foils were directly used as sources for thermo-chromatographic investigations.

RESULTS AND CONCLUSIONS

The results of the thermochromatography experiments with gold as stationary surface with O_2 and O_2/H_2O as carrier gases are shown in Fig. 1. A deposition temperature of one mercury species, presumably HgO, was determined as $T_{dep}^{Au}(HgO)$ = (120±25)°C, and $-\Delta H_{ads}^{Au}(HgO)$ = (95±5) kJ mol^{-1} (Fig. 1, Panels A and B). Surprisingly, this value is in good agreement with the adsorption enthalpy reported for mercury in the elemental state on gold surface $-\Delta H_{ads}^{Au}(Hg)$ = (88±2) kJ mol^{-1} [2]. The possible explanation is that the gas mixture used in the previous works was not completely oxygen free. Experiments using fused silica as stationary surface at otherwise the same experimental conditions resulted in one deposition peak at $T_{dep}(HgO)$ = (117±20)°C. A corresponding adsorption enthalpy was evaluated as $-\Delta H_{ads}^{SiO2}(HgO)$ = (92±2) kJ mol^{-1} (Fig. 2). In [3] the mercury deposition peak in a broad temperature range from 25°C to 80°C was observed. However no conclusions about the deposited species were drawn. Surprisingly, the data obtained for HgO adsorption on SiO_2 coincide with the adsorption enthalpy of HgO on the gold surface. Adsorption enthalpies obtained for HgO allow us to estimate for the first time its sublimation enthalpy using the empirical correlations from [4] as $\Delta H_{subl}(HgO)$ = (125±3) kJ mol^{-1}.
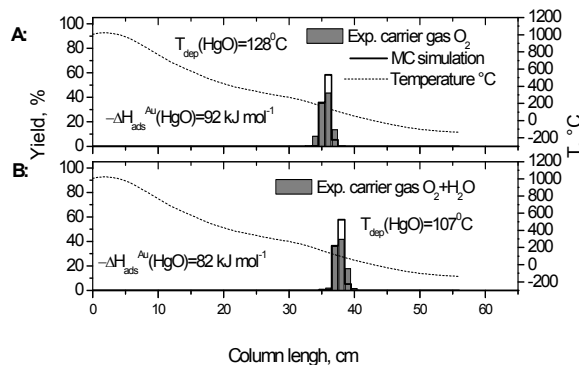
Fig. 1: Thermochromatograms of ^{197}HgO (grey bars, left hand axis) on gold surface using as carrier gas: Panel A: 25 ml min^{-1} O_2; Panel B: 25 ml min^{-1} O_2/H_2O mixture. The solid stepped lines represent the results of the Monte Carlo simulations. The temperature gradients are indicated (dashed line, right hand axis).
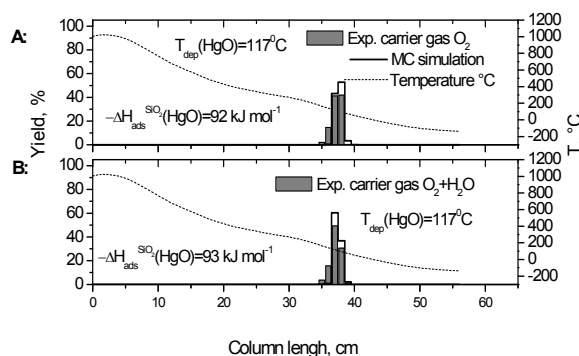
Fig. 2: Thermochromatograms of ^{197}HgO (grey bars, left hand axis) on quartz surface using as carrier gas: Panel A: 25 ml min^{-1} O_2; Panel B: 25 ml min^{-1} O_2/H_2O mixture. The solid stepped lines represent the results of the Monte Carlo simulations applying the adsorption enthalpies given on the panels. The temperature gradients are indicated (dashed line, right hand axis).

Further experiments have to show if the observed adsorption process is superimposed by a reversible chemical formation reaction of HgO from the elements.

REFERENCES

[1] R. Eichler et al., Angew. Chem. Int. Ed. **47(17),** 3262 (2008).

[2] S. Soverna et al., Radiochim. Acta **93,** 1 (2005).

[3] B. Bayar et al., Dubna report P12-7164 (1973).

[4] B. Eichler, R. Eichler, In *The Chemistry of Superheavy Elements.* (M. Schädel, ed.), Kluwer Academic Publishers 2003.)

NITROGEN ANALYSIS AT ORANGE COLOURED ZINC OXIDE SAMPLES USING PGAA

S. Soellradl (Univ. Bern & PSI & FRM II), M. Greiwe, V. J. Bukas, T. Nilges (TUM)
A. Senyshin, L. Canella, P. Kudejova (FRM II), A. Türler (Univ. Bern & PSI), R. Niewa (Univ. Stuttgart)

Based on a recent publication in 2009 [1] the synthesis took place and a study about hydrogen, nitrogen, carbon and zinc was performed and analysed with Prompt Gamma Activation Analysis (PGAA) at FRM II in Munich.

INTRODUCTION

Pure Zinc Oxide is a direct, wide band gap semiconductor with a band gap of about 3.4 eV [2]. Pure large crystals are transparent in the visible part of the spectrum. As fine powder it has normally a white colour. Based on a publication in 2009 [1] samples for detection limit measurements of Nitrogen in a ZnO matrix were prepared for prompt gamma activation analysis (PGAA) measurements at FRM II in Munich. More Information about the technique of PGAA can be found in [3-5].

EXPERIMENTAL

The synthesis was performed as described in [1]. The sample is analysed with Raman spectroscopy, powder x-ray diffraction (PXRD) and PGAA and the results were compared with the results described in literature [1]. During experiments with different ratios of Urea:$Zn(NO_3)_2 \cdot 6H_2O$ an additional phase was detected at a molar ratio of 2.3:1. The product has a pale orange colour. It shows the 4 Raman bands which were discussed in [1] to indicate the presence of nitrogen at 277 cm^{-1}, 509 cm^{-1}, 580 cm^{-1}, and 604 cm^{-1}. Two additional bands were detected at 751 cm^{-1} and 1046 cm^{-1}. The PXRD measurements showed additional reflexions (Fig. 1).
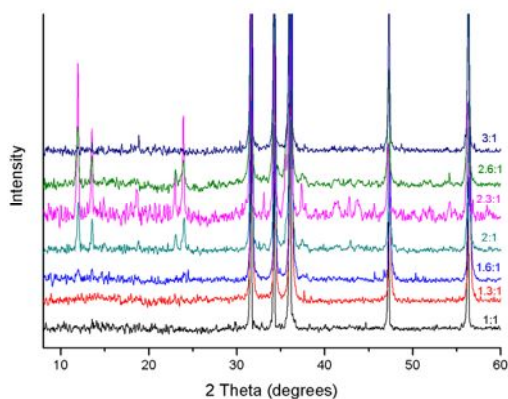
Fig. 1: Increase of an additional phase with a maximum intensity at a preparation ratio of 2.3:1. [Cu $K\alpha_1$, λ=1.5405 Å]

The phase is under further investigation. PGAA measurements were performed with the pale orange sample with a molar ratio of Urea:$Zn(NO_3)_2 \cdot 6H_2O$ 2.3:1. In addition to Zn, also H, C, N were detected. Oxygen cannot be measured with PGAA in such a matrix due to the low neutron capture cross section. During tests about the solubility, a white crystalline substance could be separated. Subsequently, the orange powder containing ZnO and the additional phase was dissolved in HCl (conc. 20%) at 70°C. Upon cooling at about 65°C white crystals formed on the surface of the acid. Qualitative EDX (energy dispersive x-ray spectroscopy) measurements showed no occurrence of Zn or Cl within the substance. Only H, C, N, O were detected in EDX. Tab. 1 compares the results of the PGAA measurement of the 2.3:1 ratio, orange coloured ZnO powder containing the additional phase with an HCN elemental analysis measurement of the white crystals. Due to the low neutron capture cross section of C, the relative error is much larger than of the other elements.

Tab. 1: Comparison of the PGAA measurements of orange coloured ZnO (molar ratio 2.3:1) with the separated white crystals separated from HCl (HCN analysis) in %$_{atom}$

Elements	HCN of crystals	PGAA of orange ZnO
H	32.5 % ± 0,6%	16% ± 5%
C	32.3 % ± 0,6%	23% ± 25%
N	35.1% ± 0,6%	16% ± 6%
Zn	not measured	44% ± 5%

CONCLUSION

PGAA and HCN elemental analysis show a similar relative abundance of the elements H, C, N. PGAA was able to measure these elements within the ZnO. It is expected that an additional organic phase forms, which resists the harsh conditions during the flame synthesis. The properties of the additional phase are not completely resolved yet.

REFERENCES

[1] M. Mapa, C.S. Gopinath, 21, 351 (2009).
[2] C. Klingshirn, ChemPhysChem (2007).
[3] G.L. Molnár, Handbook of Prompt Gamma Activation Analysis with Neutron Beams (Kluwer Academic Publishers, 2004).
[4] P. Kudejova, T. Materna, J. Jolie, G. Pascovici, X-Ray Spectrom. 34, 350 (2005).
[5] M. Crittin, J. Kern, J.L. Schenker, Nucl. Instrum. Methods Phys. Res., A 449, 221 (2000).

GAS-PHASE CHEMISTRY OF CARBONYL COMPLEXES FORMED IN HOT-ATOM REACTIONS WITH SHORT-LIVED ISOTOPES OF Mo

Y. Wang, Z. Qin, F. Fan, S. Cao, X. Wu, L. Tian, L. Zhao, J. Guo (IMP), H.W. Gäggeler (PSI)

Volatile ^{104}Mo-carbonyl complexes were synthesized using hot atom gas chemical reactions with carbon monoxide and a ^{252}Cf fission source. From the results of isothermal chromatography experiments, an adsorption enthalpy on a Teflon surface was determined as -39 kJ/mol. This experiment confirms a recent discovery that carbonyls can be formed under ambient condition in hot-atom reactions [1].

INTRODUCTION

Isotopes of superheavy elements are short-lived and available only at a level of one-atom-at-a-time. Experimental systems used in such studies are therefore preferentially tested with short-lived isotopes of homologous elements of the periodic table that may be partly produced in nuclear fission processes [2]. Radioisotopes of molybdenum, technetium, and ruthenium as homologues of Sg, Bh, and Hs can be produced from a ^{252}Cf fission source. Metal carbonyl complexes as a class of highly volatile complexes provide a chance to investigate these superheavy elements in the gas-phase.
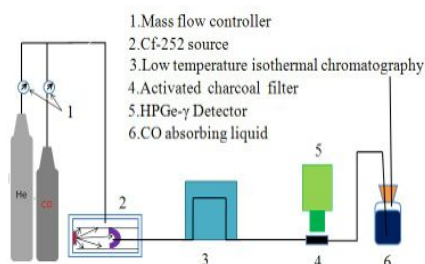
Fig. 1: Schematic of the experimental setup

EXPERIMENTAL

A ^{252}Cf source produced short-lived isotopes of Mo, Tc, and Ru. High-purity helium served as carrier gas to which CO was added as reactive gas to reach a total gas flow rate of 1 L/min. Volatile metal carbonyls were synthesized *in situ* in the chamber and transported through a 4 m long Teflon capillary (i.d. 2 mm) to a chromatography column kept at a variable isothermal temperature. The capillary was put into a low temperature cooling circulating unit (>−80°C). After passing through this chromatography column, the carbonyls were transported through a 1 m long Teflon capillary to a charcoal filter facing a HPGe γ-detector.

RESULTS

A direct implantation catch collected by a stainless steel plate on top of the ^{252}Cf source showed many fission products, mainly isotopes of Ba, Ce, Te, Mo, Rh, Xe, and Ru. When CO was introduced into the ^{252}Cf source, and the formed volatile products transported at room temperature to the γ-detector as depicted in Fig. 1, the spectrum of peaks was reduced to γ-lines of Mo, Tc, Ru, Rh, besides some lines as-

signed to the transport of Xe. From the direct catch it is possible to deduce a chemical yield of Mo carbonyl formation of about 50%. The yield as function of CO concentration in the He carrier gas for ^{104}Mo is shown in Fig. 2. It indicates that the formation of this metal carbonyl follows first-order kinetics. For further experiments an optimal CO/He ratio of 1:1, each gas with 500 mL/min was used. Fig. 3 shows the relative yield vs. isothermal temperature curve for ^{104}Mo(CO)$_6$. The solid line is the result of a Monte-Carlo simulation of the experiment assuming an enthalpy of adsorption ΔH_{ads} of −38 kJ/mol. The dashed lines indicate the 1σ-error range.
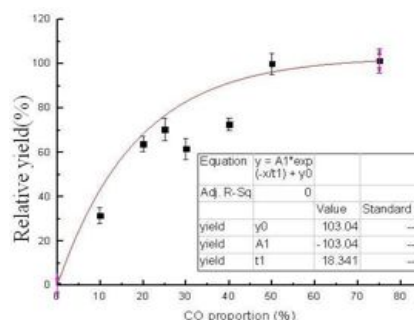
Fig. 2: Relative yields of ^{104}Mo(CO)$_6$ as function of the CO concentration in the He carrier gas.
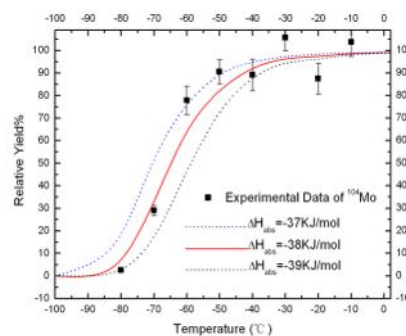
Fig. 3: Relative yield of ^{104}Mo(CO)$_6$ as a function of isothermal temperature.

REFERENCES

[1] J. Evens, Metal Carbonyl Complexes: a metal organic compound class within the Reach of Transactinide chemistry, Presentation TAN'11, Sochi, Russia 5-11 Sept. 2001.

[2] C.E. Düllmann et al., Nucl.Instr. Meth., **A 512**, 595 (2003).

CHEMICAL PROPERTIES OF VOLATILE Mo, Tc, & Ru CARBONYL COMPLEXES

Y. Wang, Z. Qin, F. Fan, S. Cao, X. Wu, L. Tian, L. Zhao, J. Guo (IMP), H.W. Gäggeler (PSI)

Volatile carbonyl complexes of Mo, Tc, and Ru were synthesized using hot-atom gas chemical reactions with carbon monoxide and a ^{252}Cf fission source. The isothermal chromatographic curves show that these metal carbonyls all have very similar adsorption enthalpies on quartz surfaces. This observation points to a physisorption process. Carbonyls might therefore be well suited to study the transactinide elements Sg, Bh, Hs, and Mt.

INTRODUCTION

Short-lived radioisotopes of molybdenum, technetium and ruthenium as homologous elements of the super-heavy elements seaborgium, bohrium, and hassium can be produced in a ^{252}Cf fission source. We have used this fission source to form very volatile metal carbonyls of Mo, Tc, Ru, Rh [1]. One should, however, be aware that in the fission process many isotopes of an isobar are formed. Tab. 1 summarizes calculated independent yields in SF of ^{252}Cf [2].

Tab. 1: Some estimated fractional independent yields of fission fragments from the SF decay of ^{252}Cf in % (from [2], not corrected for prompt neutron emission).

Isobar	Y	Zr	Nb	Mo	Tc	Ru	Rh
104	0.4	21	67	12	0.1		
106		1.2	35	58	5.3		
108			2	51	44	2	
110				8	63	28	0.8

As an example, the nuclide ^{104}Tc which is well observed in the γ-spectra is not produced as primary fission product but formed via β-decay from its precursor ^{104}Mo. Therefore, not all the isotopes observed represent the chemical properties of the corresponding element. A chemical interpretation of observed chromatographic properties requires i) an analysis of the nuclide's half-life, ii) a comparison with the fission yield (see Tab. 1), iii) knowledge on the transport time from the chamber to the activated charcoal filter, and iv) what members of the fission isobar can form volatile metal carbonyls.

RESULTS

The relative yields of $^{104-106}$Mo(CO)$_6$, ^{107}Tc(CO)$_x$, ^{109}Ru(CO)$_x$ are shown in Fig. 1. The deduced adsorption enthalpies on the quartz column surface for Mo, Tc, and Ru were -37 kJ/mol, -35 kJ/mol, and -34 kJ/mol, respectively. These values are very similar. As expected, the $T_{50\%}$ values of the different isotopes of Mo are depending on their half-life, similar to an observation made in a study of Tc oxides [3]. This observation points to a reversible mobile adsorption process assumed for the Monte-Carlo simulations. We assume that ^{104}Mo ($T_{1/2}$ = 60 s), ^{105}Mo ($T_{1/2}$ = 35.6 s) and ^{106}Mo ($T_{1/2}$ = 8.4 s) were transported in the form of Mo (CO)$_6$ to the filter, because they are formed directly or via Nb which does not form carbonyls.

We also assume that ^{107}Tc ($T_{1/2}$ = 21.2 s) is at least partly representing the chemical property of technetium. We also take ^{109}Ru as a good representative for ruthenium because the half-life of the precursor ^{109}Tc is very short ($T_{1/2}$ = 0.9 s).

In conclusion, we showed that the adsorption behavior of Mo, Tc, and Ru carbonyls on quartz surfaces is very similar. They all exhibit a low adsorption enthalpy which points to a physisorption process.

The result of this study gives great hope that carbonyl complexes might be well suited to study gas phase chemical properties of Sg, Bh, Hs, and Mt.
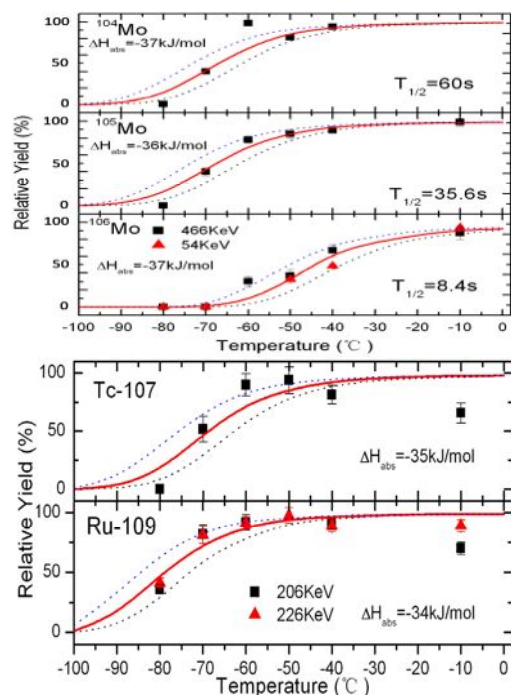
Fig. 1: Isothermal chromatography curves of different isotopes of Mo (upper part), of ^{107}Tc, and ^{109}Ru, respectively, on a quartz surface. The solid lines represent Monte Carlo simulations adapted to the experimental data.

REFERENCES

[1] Yang Wang et al., see this report, p. 12.
[2] A.C. Wahl, J. Radioanal. Nucl. Chem., **55** (1), 111 (1980).
[3] M.-S. Lin et al., Radiochim. Acta **98**, 321 (2010).

PRODUCTION AND DETECTION OF ^{13}N LABELED N_2O_5

G. Gržinić, A. Türler (Univ. Bern & PSI), T. Bartels-Rausch, M. Birrer, M. Ammann (PSI)

In order to investigate the uptake of N_2O_5 on aerosol particles the short-lived radioactive tracer ^{13}N provided by the PROTRAC facility (PSI) was used to produce ^{13}N labeled N_2O_5 to be used in the uptake experiments.

INTRODUCTION

N_2O_5 is an important reactive intermediate in the atmospheric chemistry of nitrogen oxides and plays a significant role in the nighttime tropospheric NO_x cycle [1]. The importance of N_2O_5 stems from its role as a NO_3 radical reservoir and a major sink for NO_x species thanks to the reaction of hydrolysis with water. N_2O_5 thus directly impacts the ozone level and in general the oxidative capacity of the atmosphere [1, 2].

EXPERIMENTAL

In our experiments the short-lived radioactive tracer ^{13}N technique [3] developed at the Paul Scherrer Institute was used in conjunction with a flow tube reactor. This method allows for the study of N_2O_5 uptake kinetics under realistic conditions, e.g., at ambient pressure, low trace gas concentrations and high relative humidity values. N_2O_5 gas-phase formation was modelled in Matlab in order to optimize N_2O_5 production, study concentration and temperature dependence and evaluate potential problems that might arise (e.g. N_2O_5 formation time vs. half-life of ^{13}N). Fig. 1 shows a schematic of the experimental setups used. The NO and O_3 gas flows are mixed in the reactor where N_2O_5 is formed. Additionally an aerosol flow can be injected via a movable aerosol inlet into the reactor. The feed from the reactor can be monitored via a Scanning Mobility Particle Sizer (SMPS) system, and is directed to a narrow parallel plate diffusion denuder setup that allows for selective separation of the gaseous species present. A particle filter is mounted at the exit to trap particles. Activity of the ^{13}N labeled species deposited on the denuder plates and the particle filter is monitored via scintillation counters.
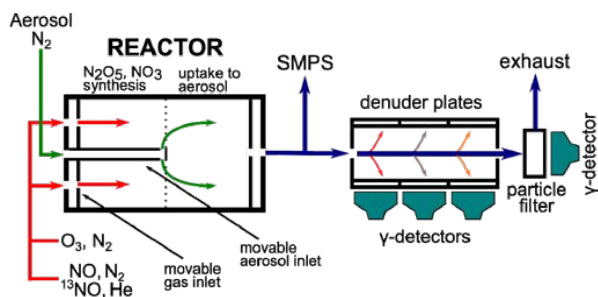
Fig. 1: A schematic representation of the experimental setup used.

RESULTS

Several denuder coatings for N_2O_5 were tested (Oleic Acid, Methyl Oleate, Gliceryl Trioleate, Citric Acid). Citric acid was selected because of lower interference from NO_2. A comparison of modelled vs. measured N_2O_5/NO_2 ratio has shown that the values differ by about a factor of two, but are of the same order of magnitude. This is an acceptable result taking into consideration the uncertainties and sources of errors like radioactive decay, wall uptake, calibration issues and activity deposition. A preliminary study using a citric acid aerosol at relative humidities of 50-80% RH has shown uptake of radioactively labeled N_2O_5 on the aerosol particles. Fig. 2 shows uptake of N_2O_5 onto citric acid aerosol when an aerosol flow is injected into the reactor. First results obtained from a limited data set show an uptake coefficient γ in the order of 10^{-3}.
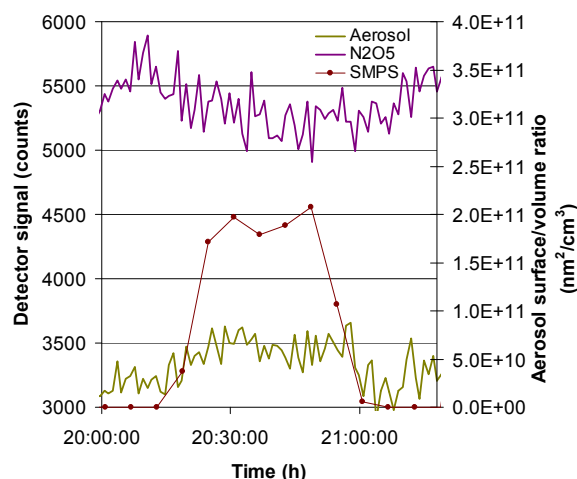
Fig. 2: Uptake of N_2O_5 on citric acid aerosol.

AKNOWLEDGEMENT

REFERENCES

[1] W.L. Chang et al., Aerosol Sci. Technol., **45**, 665 (2011).

[2] B.J. Finlayson-Pitts, J.N. Pitts, Jr. Academic Press, San Diego, CA (2000).

[3] M. Ammann, Radiochim. Acta, **89**, 831 (2001).

GAS UPTAKE AND CHEMICAL AGING OF AMORPHOUS SEMI-SOLID PARTICLES

M. Shiraiwa, U. Pöschl (MPI-CH), T. Koop (Univ. Bielefeld), S. Steimer (ETHZ & PSI), M. Ammann (PSI)

The humidity dependent kinetics of ozone uptake by an amorphous protein was measured using the coated wall flow tube technique. The results show that the properties of semi-solid phases influence gas uptake and chemical aging of aerosol particles.

INTRODUCTION

Organic substances can adopt an amorphous semi-solid state [1-2], influencing the rate of heterogeneous reactions and multiphase processes in atmospheric aerosols. Here, we demonstrate how molecular diffusion in the condensed phase affects the gas uptake and chemical transformation of semi-solid particles. Flow tube experiments show that the ozone uptake and oxidative aging of an amorphous protein is kinetically limited by bulk diffusion. The reaction rate depends on the diffusion coefficients of both the gaseous and the condensed phase reactants. Based on numerical simulations [3], we present first spatial and temporal profiles of the concentration and reaction rate of ozone and reactive amino acid residues in an amorphous protein matrix. The chemical lifetime of reactive compounds in atmospheric particles can increase from seconds to days and more as the diffusion coefficients decrease over ten orders of magnitude from the liquid to the solid state in response to changing relative humidity [4].

EXPERIMENTS

Measurements of ozone uptake by amorphous protein were conducted in a coated wall flow tube coated with a few hundred nm thick bovine serum albumin (BSA) film for a wide range of ozone concentrations and relative humidities (42–207 ppb O_3, 0–95% RH, 296 K, 1 atm). The measurement results are ozone uptake coefficients (γ_{O3}), which represent the probability that ozone molecules colliding with the surface are taken up by the condensed phase. Fig. 1 shows double-logarithmic plots of γ_{O3} plotted against reaction time (t), which exhibit a slope that is characteristic for diffusion-limited gas uptake (−0.5). It also shows that the uptake coefficients observed at a given ozone concentration level increased with increasing relative humidity. This behavior can be explained by a decrease of viscosity and increase of diffusivity with increasing RH, while the amorphous protein is transformed from a glassy to a semisolid state (moisture-induced phase transition) [4].

KINETIC MODELLING

We applied a kinetic multi-layer flux model (KMSUB)[3] to analyze the experimental results of ozone uptake by the amorphous BSA film. KM-SUB can reproduce the observed γ_{O3} very well, showing the steep concentration gradient of ozone and the BSA turnover rate in the bulk, which confirms the bulk diffusion limited uptake kinetics. The best fit values and humidity dependence of diffusion coefficients agree well with the estimates obtained from theoretical calculations using literature data of protein viscosity and hygroscopic growth [4]. The modeling results show that mass transport can have strong non-linear effects on the chemical aging of atmospheric aerosols, and that the amorphous solid state with high viscosity and low diffusion coefficients can effectively shield reactive organic compounds from degradation by atmospheric oxidants, such as O_3, OH, NO_3, N_2O_5 and halogen radicals.
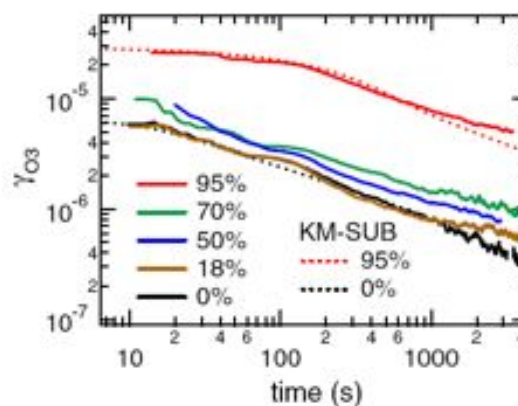
Fig. 1: Uptake coefficient of ozone on a 246 nm thick BSA film at 140 ppb O_3 at varying relative humidity (solid lines). The dotted lines are model results.

ACKNOWLEDGEMENTS

REFERENCES

[1]   A. Virtanen et al., Nature, 467: 824, 2010.
[2]   E. Mikhailov et al., Atmos. Chem. Phys., **9,** 9491 (2009).
[3]   M. Shiraiwa et al., Atmos. Chem. Phys., **10**, 3673 (2010).
[4]   M. Shiraiwa et al., Proc. Natl. Acad. Sci., **108**, 11003 (2011).

INFLUENCE OF HUMIDITY ON THE OZONE UPTAKE OF TANNIC ACID

S. Steimer (ETHZ & PSI), A. Huisman, U. Krieger, C. Marcolli, T. Peter (ETHZ), M. Ammann (PSI)

A coated wall flow tube system was used to investigate how the uptake kinetics of ozone on tannic acid depends on relative humidity. It was found that the uptake coefficient increases by nearly two orders of magnitude when raising humidity from 0% RH up to 95% RH.

INTRODUCTION

Recent findings show that organic particulate matter is capable of forming amorphous solids or semi-solids under atmospheric conditions [1]. Such particles are highly viscous, leading to low diffusivity within the bulk. This should slow down eventual chemical reactions in the bulk, thereby increasing the lifetime of the organic compounds involved. First indications of such behavior were recently shown for the reaction of thin protein films with ozone [2]. To investigate the influence of the physical state on reactivity, the uptake of ozone on tannic acid, a proxy for atmospheric polyphenolic materials, was measured in a coated wall flow tube. We assumed that the viscosity of tannic acid would be a function of relative humidity.

EXPERIMENTAL
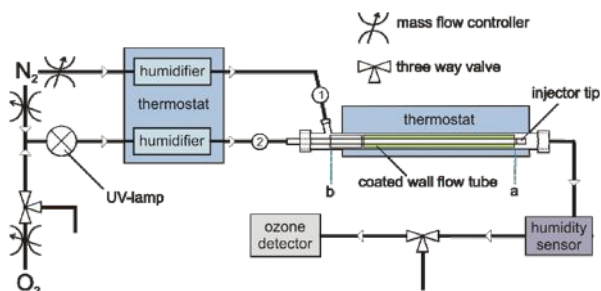
Fig. 1: Setup of the flow system. Flow (1) is the N_2 sheath flow. The O_3 containing flow (2) enters the flow tube casing through the injector tip. Injector tip in position (a): no O_3 flow through the coated wall flow tube. Injector tip in position (b): tannic acid film exposed to O_3.

An HF etched glass tube (l=48 cm, i.d.=1.2 cm) was coated with a solution of 5.0 mg tannic acid in 450 µL ethanol and the resulting film conditioned with a flow of humidified N_2 (85% RH). The tube was then inserted into the flow system (Fig. 1) while no O_3 is produced. After insertion of the tube, the injector was moved to position (a) where the tube is not exposed to the injector gas flow and O_3 production was resumed to passivate the system. After about 1 h of equilibrating the film to the set humidity, the injector was moved to position (b) which exposes the tannic acid film to O_3. The injector was moved back to position (a) once during the experiment and again at its end to control for an eventual drift in the baseline O_3 concentration. The experiment was then repeated at four additional humidities.

RESULTS

The uptake coefficient γ is the rate of uptake normalized to the gas kinetic collision rate [3] and is obtained from the measured loss of the gaseous species. Fig. 2 shows the uptake coefficient of O_3 on tannic acid over a time interval of 6 h at five different humidities.
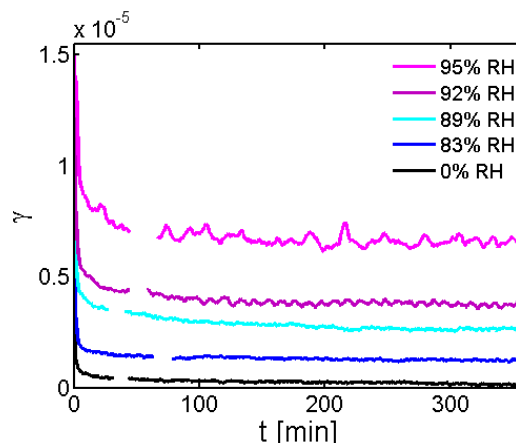
Fig. 2: Decrease of the uptake coefficient γ over 6 h at five different humidities. Breaks in the data are due to intermediate baseline O_3 measurements.

At all five humidities, a longterm uptake is observed. The uptake coefficient clearly increases with relative humidity. After 6 h, the uptake coefficient at 95% RH is $7 \cdot 10^{-6}$, while it is only $1 \cdot 10^{-7}$ at 0% RH, indicating a change close to two orders of magnitude between wettest and driest conditions. The current hypothesis is that the uptake coefficient is a strong function of the diffusion coefficient of O_3 in the tannic acid film. Rate limiting steps over the different time domains will be determined by kinetic modelling of an extended data set.

ACKNOWLEDGEMENT

REFERENCES

[1] A. Virtanen et al., Nature, **467**, 824 (2010).
[2] M. Shiraiwa et al., Proc. Natl. Acad. Sci., **108**, 11003 (2011).
[3] U. Pöschl et al., Atmos. Chem. Phys., **7,** 5989 (2007).

NEXAFS STUDY OF SHIKIMIC ACID PARTICLES: IN SITU OXIDATION UNDER HUMID CONDITIONS

S. Steimer (ETHZ & PSI), A. Huisman, U. Krieger, C. Marcolli, T. Peter (ETHZ), E. Coz (CIEMAT), G. Gržinić (Univ. Bern & PSI), M. Lampimäki, M. Ammann (PSI)

Scanning transmission X-ray microscopy and near edge X-ray absorption fine structure spectroscopy were used to monitor the reaction of shikimic acid and ozone under humid conditions.

INTRODUCTION

It has been shown that organic compounds may account for up to 90% of matter found in aerosols [1]. Their chemical aging changes the physical and chemical properties and therefore the environmental impact of the aerosols [2]. Shikimic acid is a plant metabolite which has been found to be present in biomass burning aerosol [3]. In the present study the aging of shikimic acid particles via reaction with ozone was investigated under humid conditions. The process was monitored in situ using scanning transmission X-ray microscopy (STXM) and near edge X-ray absorption fine structure spectroscopy (NEXAFS).

EXPERIMENTAL

Shikimic acid particles were generated from a 3.3 g/L solution of shikimic acid (≥99%, Sigma-Aldrich) in MilliQ water via ultrasonic nebulisation. The particles were dried with a diffusion drier, and a differential mobility analyzer (DMA) was used to select only particles of a specific electrical mobility. These were then impacted on a silicon nitride membrane. A temperature controlled environmental micro reactor [4] was used to keep the humidity at about 85% during the experiment and facilitate in situ exposure to ozone for up to 210 min. The STXM and NEXAFS experiments were conducted at the Pollux beamline at the SLS.
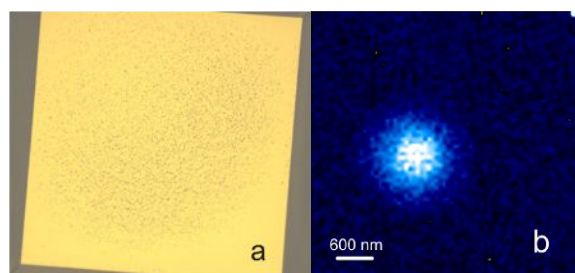
Fig. 1: (a) Size selected shikimic acid particles deposited on a silicon nitride window. (b) Background subtracted STXM absorption image of an unoxidized particle at 284.4 eV.

RESULTS

The carbon K-edge spectra for shikimic acid particles before and after oxidation are shown in figure 2. A strong change in features can be observed over the course of oxidation. The main distinguishing features are found at 284.5, 286.5 and 288.5 eV. The post oxidation spectra show a decrease in the double bond peak at 284.5 eV, which becomes more pronounced

after increased exposure time. The peak at 286.5 eV shows the opposite behaviour and increases with progressing oxidation. An additional change can be observed in the region of the carboxyl K 1 s→π* transition around 288.5 eV, where the absorption increases relatively to the post edge adsorption intensity. This could either be caused by an actual increase of the feature or a decrease in the absorption of total carbon which was used for normalization. The latter could be caused by eventual evaporation of volatile reaction products.
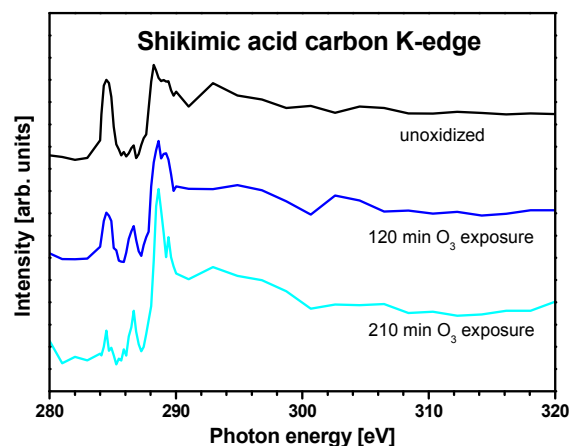
Fig. 2: Typical carbon K-edge spectra of an unoxidized shikimic acid particle and after exposure to ozone, measured at 85% RH. The spectra are linear background substracted and normalized to the mean intensity between 310 and 320 eV.

ACKNOWLEDGEMENT

REFERENCES

[1] M. Kanakidou et al., Atm. Chem. Phys., **5**, 1053 (2005).

[2] Y. Rudich et al., Chem. Rev., **103**, 5097 (2003).

[3] P. M. Medeiros et al., Environ. Sci. Technol., **42**, 8310 (2008).

[4] T. Huthwelker et al., Rev. Sci. Instrum., **81**, 113706 (2010).

HUMIDITY DRIVEN NANOSCALE CHEMICAL SEPARATION IN COMPLEX ORGANIC MATTER

V. Zelenay, T. Huthwelker, A. Křepelová (PSI), Y. Rudich (Weizmann Institute), M. Ammann (PSI)

X-ray Microspectroscopy at the PolLux beamline (SLS) was used to observe morphological changes as a function of humidity in fulvic acids, a proxy for atmospheric humic like substances (HULIS).

INTRODUCTION

Atmospheric humic like substances constitute a major fraction of organic material in atmospheric aerosol particles generated by oxidation of primary organic compounds. Such atmospheric aerosol particles have a substantial effect on our climate, both through direct and indirect effects [1]. Many questions are still open as e.g. the influence of the relative humidity on the morphology of atmospheric particles. We try to approach this question using x-ray absorption microspectroscopy in a new developed microreactor at the x-ray microscope at the PolLux beamline (SLS) [2,3]. We use Swannee River fulvic acids as a proxy for atmospheric humic like substances.

EXPERIMENTAL

The SRFA was purchased from the International Humic Substance Society (IHSS), product number 1S101F. Solutions of SRFA were prepared with a concentration of 2.6 g/l in MilliQ water (final pH 2.56). Additionally, SRFA was fractionated using ultrafiltration [4]. Fraction F2 having an estimated molecular weight ranging from 0.5-1.0 kDa with pH 2.4 and fraction F5 ranging from 10-30 kDa with pH 2.45 were used here. The fulvic acid samples were prepared by means of a piezo-driven microdispenser, which deposited about 30 μm large droplets of the solution on the sample holder. A temperature controlled environmental micro reactor [2,3] was used to vary the relative humidity during the experiment. The STXM and NEXAFS experiments were conducted at the Pollux beamline at the SLS.

RESULTS

The near edge X-ray absorption spectra at the C K-edge show characteristic peaks at 284.8, 286.5 288.4 eV to represent aromatic, phenolic and carboxylic functional groups, respectively. The fractions F2 and F5 show significant differences in the relative intensities of these peaks [5]. Parallel to that, at the O K-edge, features related to the oxygen functionalities can be used: at 532.5 eV for C=O double bonds, and the broad features around 542 eV to trace H_2O associated with the sample. The O:C ratios increased from 0.28 at 0 % to 0.75 at 90 % RH, respectively. This corresponds roughly to two water molecules per oxygen in dry SRFA at 90 % RH, respectively [5]. The swelling of the particles due to water uptake observed from images at the O-edge was consistent with volume growth measurements reported by Dinar et al. [4]. Images taken at the different individual energies mentioned above allow obtaining chemical contrast within the sample. The unfractioned SRFA sample exhibited substantial reorganization of the material when the dry droplet residue was humidified to 90%. The inhomogeneous mixture showed different features at the micro- and nanoscales that could be differentiated occording to the relative occurrence of the different functional groups meantioned above, as shown in Fig. 1.
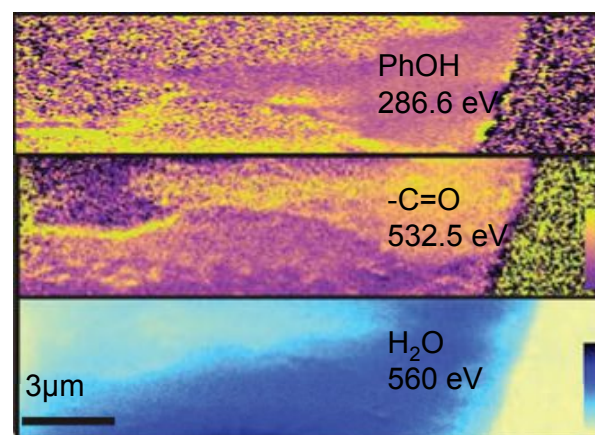
Fig. 1: Upper: absorption image measured at 286.6 eV representing the distribution of phenolic OH groups in the unfractionated SRFA sample after exposing to 90% relative humidity. Middle: absorption image measured at 532.5 eV to represent the distribution of C=O bonds. Lower: distribution of water within the sample determined from the absorption image measured at 560 eV.

ACKNOWLEDGEMENT

REFERENCES

[1] V. Ramanathan, et al., Science, 294, 2119 (2001).

[2] T. Huthwelker et al., Rev. Sci. Instrum., **81**, 113706 (2010).

[3] V. Zelenay et al., J. Aerosol Sci., 42, **38** (2011).

[4] E. Dinar et al., J Geophys. Res. 112, doi:10.1029/2006JD007442 (2007).

[5] V. Zelenay et al., Env. Chem., 8, 450 (2011).

EVOLUTION OF THE CARBON FUNCTIONAL GROUPS IN 2-STROKE SCOOTER EXHAUST PARTICLES WITH PHOTOCHEMICAL OXIDATION

E. Coz (CIEMAT), S. Platt, I. El Haddad, J.G. Slowik, A.S.H. Prévôt (PSI/LAC), S. Steimer (ETHZ & PSI), G. Gržinić, (Univ. Bern & PSI), M. Lampimäki, M. Ammann (PSI)

Changes in the carbon functional groups in individual particles from scooter exhaust experiments in the PSI smog chamber were characterized by scanning transmission X-ray microscopy and near edge X-ray absorption fine structure spectroscopy.

INTRODUCTION

Recent results suggest that the emissions of organic compounds from scooters are much higher than from other vehicles [1]. Secondary organic aerosol (SOA) from 2-stroke scooters can be distinguished by aerosol mass spectrometry from that of diesel vehicles, wood burning or alpha-pinene oxidations products [2]. Their evolution during atmospheric aging will determine the effects of these aerosols on the atmosphere and the climate [3]. In the present study, changes to the carbon functional groups in individual particles from 2-stroke scooter experiments at the PSI mobile smog chamber with different degrees of oxidation were investigated. Samples collected at different stages during an experiment were analyzed offline using scanning transmission X-ray microscopy (STXM) and near edge X-ray absorption fine structure spectroscopy (NEXAFS), which allow the retrieval of spatially resolved information about carbon functional group composition and the C/O ratio [4].

EXPERIMENTAL

The smog chamber experiments were performed in the new mobile smogchamber of the LAC under UV-light (http://www.psi.ch/lac/mobile-smog-chamber). Particle samples were collected by inertial impaction on silicon nitride membrane windows on Si wafers. The wafers were mounted into the standard sample holder fitting into the STXM at the PolLux beamline at SLS. Images and NEXAFS spectra were taken at the carbon and oxygen K-edges in the energy ranges 280 – 320 eV and 520 – 560 eV, respectively.

RESULTS

The carbon K-edge spectra for the 2-stroke scooter exhaust particles before and after photooxidation are shown in Figure 1. Clear changes in the features were observed at the carbon K-edge. The main distinguishing features are found at 285.2, 286.7, 288.3, and 292 eV, which correspond to the peak energies of the C 1 s→π* transitions of aromatic, phenolic or ketone carbon, the carboxylic carbon, and the aliphatic and/or aromatic carbon, respectively. The spectra show a pronounced decrease in the aromatic fraction and a corresponding gradual increase in the phenolic and carboxylic groups with processing. The spectra of the particles with 1.5 h of photoxidation show significant particle to particle variation, representing a vari-

ety of stages between the unprocessed and heavily processed spectra. These differences in the degree of processing seem to be size dependent. Similar spectral changes, but to a much lesser extent, were observed in a previous study with wood burning and diesel vehicle exhaust [5].
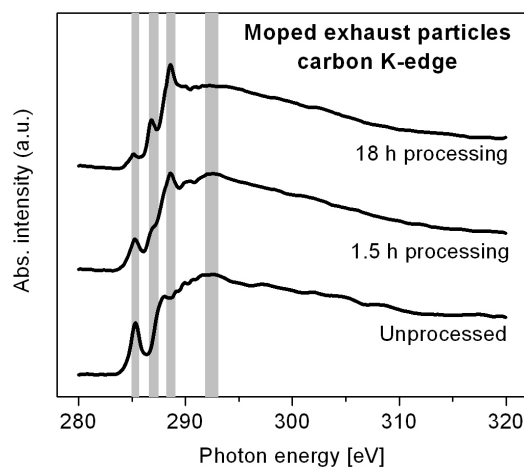
Fig. 1: Typical carbon K-edge spectra of particles from fresh 2-stroke scooter exhaust (unoxidised) and after 1.5 and 18 h of processing, respectively. The spectra are linear background subtracted and normalized to the intensity at 320 eV.

ACKNOWLEDGEMENT

REFERENCES

[1] R. Chirico, Thesis, ETH No. 19237, 2010.
[2] M. F. Heringa et al., Atmos. Chem. Phys. Discuss. **11**, 29091 (2011).
[3] P. M. Medeiros et al., Environ. Sci. Technol. **42**, 8310 (2008).
[4] M. G. C. Vernooij et al., Environ. Sci.Technol. **43**, 5339 (2009).
[5] V. Zelenay et al. Atmos. Chem. Phys. **11**, 11791 (2011).

MINERAL DUST AND IRON OXIDE PARTICLES STUDIED UNDER OXIDIZING AND ACIDIC CONDITIONS

M. Lampimäki, S. Steimer, V. Zelenay, A. Křepelová, G. Gržinić, M. Birrer, M. Ammann (PSI)
B. Watts, J. Raabe (PSI/SLS)

Mineral dust and iron oxide particles were characterized after exposure to O_3 and acidic gases by scanning transmission X-ray microscopy.

INTRODUCTION

Metal oxides as a common part of mineral dust have an important role in the heterogeneous reactions of dust particles with ozone or acidic gases. Furthermore, mineral dust particles serve as a primary external iron source to the open ocean and the bioavailability of iron from these particles is highly dependent on the oxidation state of the metal [1,2]. In the present study we have investigated both pure oxides and authentic mineral dust particles exposed to nitrogen oxide and ozone by Scanning transmission X-ray microscopy (STXM) and Near edge X-ray absorption fine structure (NEXAFS) techniques.

EXPERIMENTAL

Authentic mineral dust particles (Arizona test dust) were measured before and after exposure to ozone and nitrogen oxides. Characteristic features corresponding to different oxidation states of iron were monitored by following changes at oxygen K- and iron L-edges and compared to reference oxides (Fe_3O_4 and Fe_2O_3 powders, Sigma Aldrich) The humid and acidic conditions were facilitated in the environmental micro reactor described in ref [3]. The STXM and NEXAFS measurements were conducted at the PolLux beamline at SLS.

RESULTS
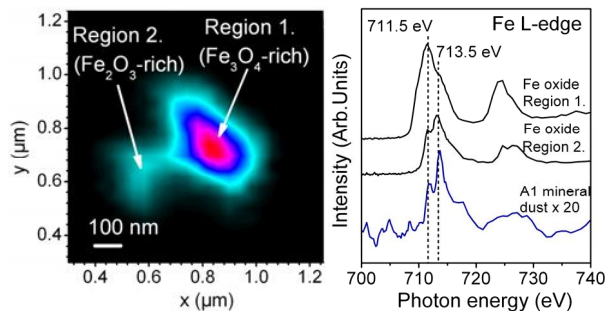
Fig. 1: STXM-image of a submicrometer iron oxide particle showing Fe_2O_3- and Fe_2O_3-enriched regions (left). Iron L-edge spectra from iron oxide and Arizona test dust (right).

Fig 1. shows a STXM image of submicrometer size iron oxide particles containing Fe_2O_3- and Fe_3O_4-enriched regions (left) and corresponding iron L-edge spectra, plotted as ratio of absorptions at 711.5 eV and 713.5 eV, with colors towards red indicating high ratios.

Fig 2. illustrates O K-edge NEXAFS spectra of Arizona test dust before (lower spectrum) and after NO and O_3 exposure (upper spectrum). On unexposed particles, the peak at ~532 eV corresponds to iron oxide, most likely hematite. Subsequent to NO_2- and O_3-exposure, absorption in this photon energy region (~532.5 eV) is increased, presumably due to formation of surface nitrite/nitrate. Furthermore, enhanced absorption at ~547 eV could represent the contribution from adsorbed HNO_3 [4] likely formed under these conditions. The next steps of the research include the analysis of the changes to the Fe distribution from the chemical maps obtained at the Fe L-edge.
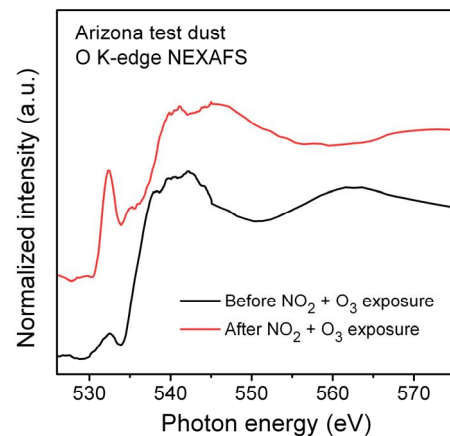
Fig. 2: O-edge NEXAFS spectra obtained from Arizona test dust, unexposed (black) and after exposure to NO_2 and O_3 (red).

ACKNOWLEDGEMENT

REFERENCES

[1] R. A. Duce et al. Limnol. Oceanogr. **36**, 1715 (1991).

[2] P. Falkowski et al., Science **281**, 200 (1998).

[3] T. Huthwelker et al., Rev. Sci. Instrum. **81**, 113706 (2010).

[4] A. Křepelová et al., Phys. Chem. Chem. Phys., **12**, 8870 (2010).

Fe- AND Ti-OXIDE SURFACES STUDIED BY AMBIENT PRESSURE XPS AND NEXAFS: EFFECT OF OZONE AND NITROGEN OXIDES

M. Lampimäki, V. Zelenay, A. Křepelová (PSI), Z. Liu, H. Bluhm (LBNL), M. Ammann (PSI)

Fe- and Ti-oxide surfaces were investigated by ambient pressure X-ray photoelectron spectroscopy (XPS) during exposure to O_2, ozone, NO and water vapor at beamline 9.3.2 at the Advanced Light Source.

INTRODUCTION

Metal oxides as part of mineral dust are important in heterogeneous chemical reactions of nitrogen oxides, e.g., NO_2, HNO_3, $HONO$, and N_2O_5 [1]. In the present study we have investigated $Fe_3O_4(100)$ and $TiO_2(110)$ single crystal surfaces during exposure to O_2, O_3, NO, and humidity. Oxygen, iron, and nitrogen core-level XPS-transitions were measured in situ at elevated pressures. Additionally, the surface chemical composition was monitored by Near Edge X-ray Absorption Fine Structure (NEXAFS) spectroscopy.

EXPERIMENTAL

The $Fe_3O_4(100)$ single crystal was cleaned by 1 kV Ar^+-ion sputtering in a 1×10^{-5} Torr background pressure of O_2 and annealed at ~830 K for 10 min. The $TiO_2(100)$ single crystal was cleaned by 1 kV Ar^+-ion sputtering in a 5×10^{-7} Torr background pressure of O_2 and annealed at 850 K for 10 min. Water purified by multiple freeze-pump-thaw cycles was introduced via a leak valve into the analysis chamber. Ozone was produced using a corona discharge device (Yanko Industries Ltd MKS Type 247). The photoelectron spectroscopic measurements were performed by employing the spectrometer described in ref. [2].

RESULTS
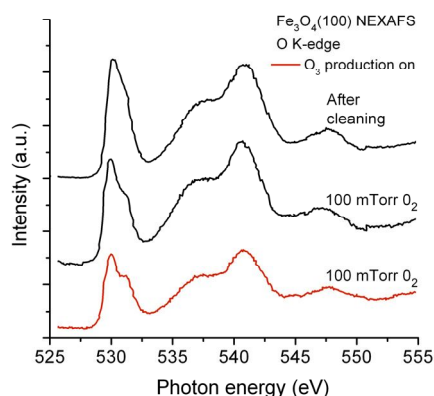
Fig. 1: O-edge Auger electron yield NEXAFS spectra of spectrum obtained on clean $Fe_3O_4(100)$ surface (black) and during exposure to O_2 and O_3.

Fig. 1 shows O-edge Auger electron yield NEXAFS spectra obtained on the $Fe_3O_4(100)$ surface during exposure to O_2 and O_3. On the clean surface, the t_{2g} peak characteristic of magnetite is clearly observed at 530.1 eV. As the O_2 pressure is increased and the O_3

flow to the chamber is established, a more pronounced split of the peak is observed at 531.4 eV and at 529.9 eV. This might indicate further oxidation of the sample surface and/or formation of surface species possibly due to decomposition of O_3. The formation of surface nitrogen oxide species after exposure to NO_2 have been previously investigated on TiO_2 and MgO surfaces by employing AP-XPS [3,4] In this study we used NO, O_2, O_3, and H_2O to observe different phases of surface NO_2^- and NO_3^- formation during a sequence of gas exposures (Fig. 2(a)). In Fig. 2(b) thermal decomposition of NO_3^- is observed in situ under elevated pressures of NO (3 mTorr) and O_2 (100 mTorr) over the temperature range 313 – 393 K and after chamber evacuation at 423 K.
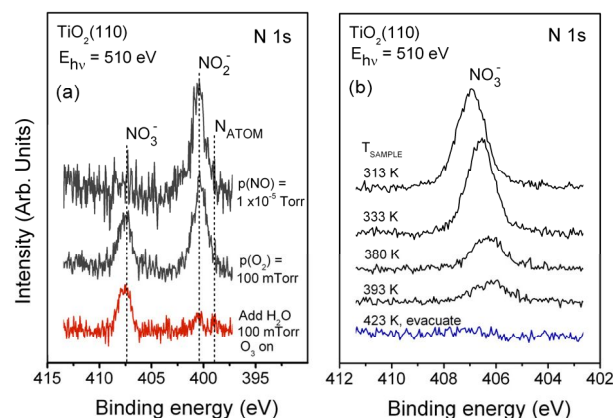
Fig. 2: (a) N 1s XPS spectra obtained on $TiO_2(110)$ surface after exposure to NO, O_2, and O_3 (b) Thermal decomposition of NO_3^- measured in situ at elevated pressure.

ACKNOWLEDGEMENT

REFERENCES

[1] Frinak et al., J. Phys. Chem. A, 108, 1560 (2004).
[2] M. E. Grass et al., Rev. Sci. Instrum., 81, 053106 (2010).
[3] Star et al., J. Phys. Chem. C, 113, 7355 (2009).
[4] J. Haubrich et al., Langmuir, 26, 2445 (2010).

CONTROLLING THE NUMBER OF GRAIN BOUNDARIES IN ICE

T. Ulrich (Univ. Bern & PSI), M. Ammann, M. Birrer (PSI), S. Leutwyler (Univ. Bern), T. Bartels-Rausch (PSI)

A new reactor that allows varying the grain boundary length in an ice sample by a factor of eight was designed and tested. The reactor with its planar ice sample will be used for kinetic uptake experiments of trace gases to ice.

INTRODUCTION

Snow and sea ice are polycrystalline materials. Grain boundaries, the interface where two ice grains meet, can host a variety of contaminants such as sulphuric acid, salts, and organics. They may impact the flux of contaminants between the ocean and sea ice [1] or between air and ice particles or snow [2]. A new experimental set-up is presented that allows to (i) control and to monitor the total number of grains in an ice sample and (ii) to investigate the kinetics of trace gas interactions with this well defined ice sample.

EXPERIMENTAL

Central to this new set-up is a flow reactor, where trace gases can be exposed to an ice surface and the kinetics of the uptake to this sample can be investigated. The ice is frozen from approximately 8 ml of water. The resulting ice is of planar geometry with a thickness of about 1 mm. The number of individual ice grains can be modified in a process known as *zone refining*. It has been used earlier for ice [3], but never with a planar geometry. During the zone refining a melting unit, a heated copper sheet 1 mm above the ice surface, is moved very slowly over the ice bed. The ice melts in a small area across the entire width of the ice bed. Recrystallization starts as soon as the melting unit has moved down the ice plate.

The planar geometry of the ice bed allows analyzing the ice surface before and after each experiment. The number of ice grains and the length of the grain boundaries are observed with a microscope and crossed polarization filters.

RESULTS

The ice initially formed has a high number of needle shaped ice grains, typically 100 grains per cm^2 (Fig. 1, left side). The zone refining was optimized with respect to the temperature and forward speed of the melting unit. A temperature of 160 °C and a velocity of 50 mm/h were found to be optimal to produce ice with significant less individual grains (Fig. 1, right side).

Figure 2 compares the total length of the grain boundaries on the surface. This length was measured manually in the microscope images of the ice (Fig. 1, blue lines). A reduction in grain boundary length by a factor of eight was achieved with this optimized zone refining (Fig. 2).
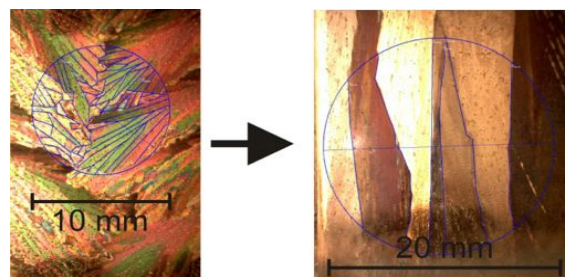
Fig. 1: Pictures of ice samples as seen under the polarized light in a microscope (12x magnification) before (left) and after zone refining (right). Also shown is the area in which the grains were counted (blue circle). The black dots are gas bubbles.

This method allows for the first time to vary and to measure the length of grain boundaries on the surface of ice samples. This is a significant improvement, as in earlier studies this quantity was not directly accessible [4]. The untreated ice showed some surface roughness, reducing this is work in progress. Kinetic experiments that analyze the trace gas uptake to the two different kinds of ices are planned.
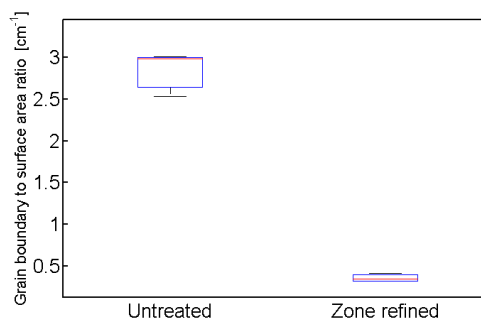
Fig. 2: Quantified results of grain boundary length normalized to the surface area of untreated and zone refined ice.

ACKNOWLEDGEMENT

REFERENCES

[1] E.C. Hunke et al., Cryosphere Disc., 5 4 (2011).

[2] T. Huthwelker et al., Chem. Rev., 106 4 (2006).

[3] J. Bilgram et al., J. Cryst. Growth, 20, 4 (1973)

[4] F. Riche et al., Ann. Rep. Lab. of Radio- & Environ. Chemistry, Uni Bern & PSI (2010), p. 17.

THE ADSORPTION OF PEROXYNITRIC ACID ON ICE

T. Ulrich (Univ. Bern & PSI), M. Ammann (PSI), S. Leutwyler (Univ. Bern), T. Bartels-Rausch (PSI)

The adsorption of peroxynitric acid on ice surfaces has been investigated with a coated wall flow tube. Its adsorption to ice is orders of magnitude lower than previously thought. This finding implies that, for example in the upper troposphere, only dense ice clouds at cold temperatures take up a significant fraction of peroxynitric acid.

INTRODUCTION

Ozone in the upper troposphere affects the radiative balance at the Earth's surface. Measurements in the upper troposphere have shown that the ozone production increases with the concentration of nitrogen oxides [1]. Therefore, sources and sinks of nitrogen oxides are expected to affect the ozone budget. The uptake of nitric acid (HNO_3) to ice clouds has long been discussed to be a strong sink. Recently it was suggested that the uptake of peroxynitric acid (HNO_4) to ice is as important, because its concentration in the upper troposphere is high [2], and a strong uptake to ice was observed in an early laboratory study [3].

Here we show results of a first study of the uptake of HNO_4 to ice at low concentrations.

RESULTS

The uptake experiments were done in a coated wall flow tube coupled to a chemical ionization mass spectrometer. Direct observable of the experiments is the distribution of HNO_4 between air and the ice surface.
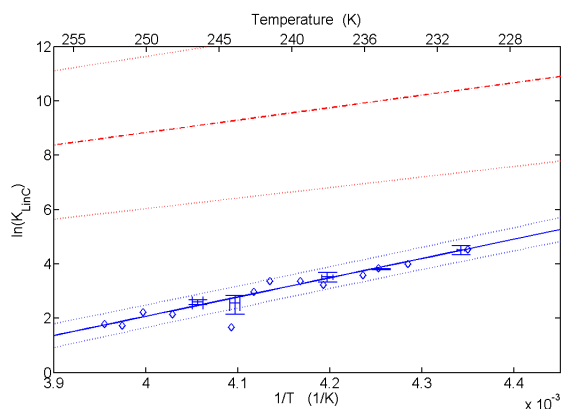
Fig. 1: Temperature dependence of K_{LinC} of HNO_3 (red) and HNO_4 (blue). The data for HNO_4 are from this study, while for HNO_3 the current IUPAC recommendation is used [4]. Errors are given by 95 % confidence bonds of the fit for HNO_4 and the uncertainty of the IUPAC data for HNO_3.

Figure 1 shows the temperature dependence of this distribution, where the partitioning coefficient (K_{LinC}) is simply the ratio of the number of adsorbed molecules to the number of molecules in the gas phase. Figure 1 clearly shows that the partitioning of HNO_4 is orders of magnitude smaller than the one of HNO_3 for the whole temperature range covered in this study.

This result suggests that the interaction of HNO_4 with ice is less pronounced than currently thought.

This low tendency to stick to ice surfaces has significant environmental implications. Figure 2 shows the amount of HNO_3 and HNO_4 taken up by cirrus clouds, calculated based on our experimental results. The higher the uptake, the more of the nitrogen oxides are lost from the gas-phase and thus are no longer available for ozone production. While HNO_3 is strongly taken up by both cloud types at the largest part of the temperature range, the uptake of HNO_4 is only important for dense clouds at cold temperatures. The snow cover on the ground adsorbs HNO_4 almost completely at temperatures up to 273 K, because it is much denser than the ice in cirrus clouds, and snow is thus an important sink for this nitrogen oxide.
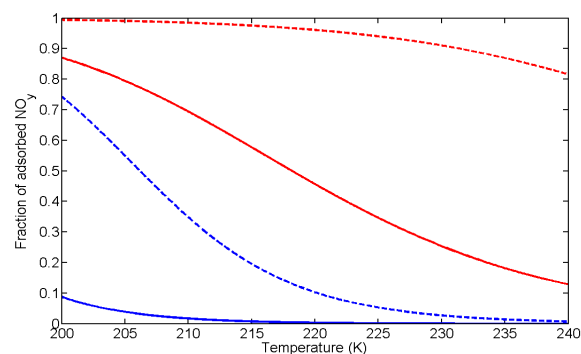
Fig. 2: Fraction of adsorbed HNO_3 (red) and HNO_4 (blue) on cirrus clouds for environmentally relevant temperatures. The dashed lines represent dense clouds with 3×10^{-4} particles per cm^{-3} and the solid lines represent sparse clouds with 1×10^{-5} particles per cm.

ACKNOWLEDGEMENT

REFERENCES

[1] P.O. Wennberg et al., Science, **279** 5347 (1998).
[2] S. Kim et al., J. Geophys. Res., **112**, D12S01 (2007).
[3] Z.J. Li et al., J. Geophys. Res.-Atmos., **101**, D3 (1996).
[4] J.N. Crowley et al., Atmos. Chem. Phys., **10**, 18 (2010).

NUMERICAL SIMULATION OF SNOW DIFFUSION CHAMBER (SDC) EXPERIMENTS

S. Schreiber (ETHZ & PSI), T. Bartels-Rausch (PSI), F. Riche, M. Schneebeli (SLF), M. Ammann (PSI)

The diffusive flux of an adsorbing gas into porous snow was calculated numerically. This allows to test whether a Langmuir adsorption model can be applied for the modelling of transport processes in snow.

INTRODUCTION

The complex interplay of snow microphysics, heterogeneous photochemistry and transport out of the snow is not understood is important in our understanding of air-ice chemical interactions [1]. A lab study at PSI could show that NO and NO_2 diffuse in snow like inert gases within a porous medium, while the diffusion of HONO is significantly slowed due to interaction with the ice [2]. The basic principle of the experiment is given in Fig. 1: For HONO, an effective diffusion constant D_{eff} was measured directly via the migration profile into the snow by detecting the decay of tracer molecules labelled with [13]N [3]. In case of NO and NO_2, the analytical solution of the diffusion equation with a constant gas phase concentration in the head space as boundary condition was calculated and fitted to the experimental data. This data analysis was limited to either labelled or weakly interacting molecules. The interesting question, whether diffusion through snow can be modelled for a wide class of species by assuming simple Langmuir adsorption requires a full numerical simulation of the diffusion process and the fluxes in the headspace.

NUMERICAL SIMULATION

The basic 1D diffusion equation for the gas phase concentration within the snow pores $c(x,t)$ reads

$$\nabla c(x,t) = D_{eff} c(x,t)$$

where D_{eff} is an effective diffusion constant given by

$$D_{eff} = D/\kappa$$

D is the gas phase diffusion including corrections for the snow structure. The dimensionless parameter κ is a function of the snow surface to volume ratio and the adsorption equilibrium. In case of strong adsorption, κ can become much larger than 1. The flux balance in the headspace is drawn in fig. 1:

$$J_{in} = J_{out} + J_{diff}$$

Assuming ideal mixing in the headspace, the concentration of the outgoing flow c_{out} is similar to that at the top of the snow column $c(0,t)$. The flux balance determines the boundary condition

$$c(0,t) = c_0 - (AD/F)\nabla c(0,t)$$

The numerical solution was computed with MATLAB.

APPLICATION

Experiments with acetone were conducted and analyzed for D_{eff} by comparing the experimentally obtained concentration trend to the simulations based on tabulated values for the adsorption. Results for different temperatures are shown in Fig. 2. Simulation and experiment agree fairly well within uncertainties.
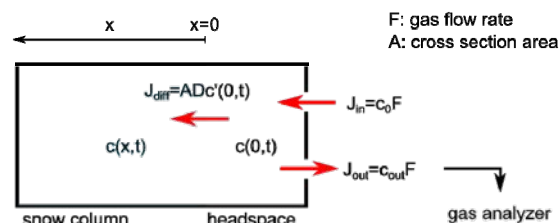
Fig. 1: Schematic of the experiment: The humidified carrier gas enters the headspace of the SDC with a flow rate F and a constant concentration c_0 of the species of interest. The diffusive flux J_{diff} into the snow reduces the concentration $c(0,t)$ in the headspace. The exit flow with $c_{out}=c(0,t)$ is analyzed by mass spectrometry.
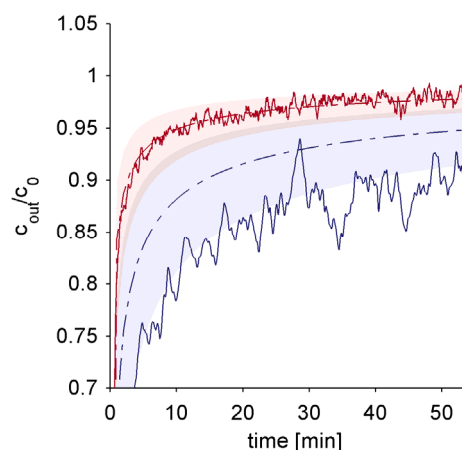
Fig. 2: Measured and simulated signal (dash-dotted line) for acetone at -30°C (red) and -50°C (blue). The shaded area represents the uncertainty of the tabulated adsorption equilibrium constants.

ACKNOWLEDGEMENT

REFERENCES

[1] F. Domine et al., Atmos. Chem. Phys., **8,** 171 (2008).

[2] B. R. Pinzer et al., J. Geophys. Res., **115**, D03304 (2010).

[3] M. Ammann, Radiochim. Acta, **89**, 831 (2001).

DETERMINING ADSORPTION KINETICS WITH A KNUDSEN CELL

S. Schreiber (ETHZ & PSI), M. Birrer, M. Ammann (PSI)

Kinetic data for Langmuir adsorption can be obtained with a Knudsen cell flow reactor that is operated with radioactive tracer atoms by using a pulsed flow and analysing the response of the system.

INTRODUCTION

The Knudsen cell reactor (KC) is a well established tool for studying heterogeneous reactions [1]. At PSI, a KC is operated with radioactively labelled tracer atoms ^{13}N, provided by the PROTRAC facility [2]. This allows studying the interaction of relevant nitrogen oxides (HONO, HNO_3) on ice at atmospherically relevant low concentrations below surface saturation. The uptake on the ice can be seen directly by the gamma radiation emitted during the decay of the tracer.

When run in continuous mode with a constant flow of tracer to the cell, it is not possible to distinguish whether the detected counts origin from weakly bound molecules at the surface with a short desorption lifetime or from molecules that were irreversibly taken up, e.g., into the bulk ice or grain boundaries.

However, the response of the detected signal to changes of the ^{13}N flow is sensitive to this: in case of irreversible uptake, the response is always given by the radioactive decay rate λ of the ^{13}N tracer ($t_{1/2}$ =10min.); in case of reversible Langmuir adsorption, the response is a single exponential decay with a faster rate constant λ_{eff}, which is also a function of adsorption, desorption and effusion kinetics:

$$\lambda_{eff} = \lambda + k_{des} \times k_{esc} / (k_{esc}+k_{ads}).$$

CONCENTRATOR

The labelled molecules are supplied by PROTRAC as NO. The species of interest is produced in an online synthesis step. The gas flow trough the KC is small, so the concentration of tracer atoms provides a lower limit for the sensitivity of the setup. Therefore, the NO concentration in the primary gas flow is increased with the device show in fig. 1. Two tubes contain a chemical trap for NO and cycle between a loading phase at high flow rates and room temperature and a subsequent release of the deposited NO at small flow rates by heating. The increase in concentration is theoretically given by the ratio of the flow rates.

Rapid heating leads to a quick release of the stored NO and results in a pulsed flow with pulse widths of 30s as shown in the upper panel of fig. 2a. These pulses allow to probe the response time of the uptake signal in the Knudsen cell.

NUMERICAL SIMULATION AND RESULTS

A typical signal as detected for HONO on vapour deposited ice at 205K is given in figure 2b. A convolution of the ^{13}N flow into the KC with exp(-$\lambda \times t$), shown as green line, does not reproduce the experimental data. HONO partitioning on ice at 205K is therefore a mostly reversible process, as reported earlier. The best fit for λ_{eff} is shown as red line. With a simple Langmuir adsorption model, the kinetic parameters are estimated from λ_{eff} to be k_{des}=0.01 s^{-1} for desorption and α_s <10^{-3} for the surface accommodation coefficient.
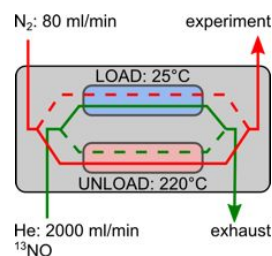
Fig. 1: Schematic of the concentrator. Trap 1 (blue box) is loaded with NO at high flow rates at room temperature. Trap 2 is heated to 220C and flushed with a small flow, thereby releasing previously deposited NO. After 2 minutes, the flows are switched (dotted lines).
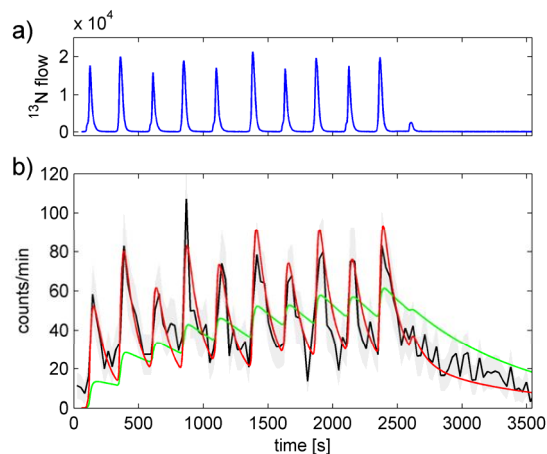
Fig. 2: a) The pulsed ^{13}N flow into the cell is given in blue. b) HONO uptake on ice at 205 K:. The resulting count rate at the KC given in black (gray shaded area: statistical error) can not be fitted with the assumption of a continuous uptake (green). The best fit with λ_{eff} =9λ is given in red.

REFERENCES

[1] F. Caloz et al., Review of Scientific Instr., **68(8),** (1997).

[2] M. Ammann, Radiochim. Acta, **89**, 831 (2001).

[3] S. Schreiber et al., Ann. Rep. Lab. of Radio- & Environ. Chemistry, Uni Bern & PSI (2011), p. 23.

THREE CENTURIES OF EASTERN EUROPEAN AND ALTAI LEAD EMISSIONS RECORDED IN BELUKHA ICE CORE

A. Eichler, L. Tobler (PSI), S. Eyrikh, N. Malygina, T. Papina (IWEP), G. Gramlich (PSI), M. Schwikowski (PSI & Univ. Bern)

A 300 year ice core Pb concentration record from Belukha glacier in the Siberian Altai is presented. Until 1935 Pb concentrations reflected the local history of mining and metallurgical processing, whereas enhanced values during 1935-1995 were caused by the use of Pb additives in Russian gasoline. Various regions in the world experienced distinct timing of anthropogenic Pb emissions, reflecting significant differences in industrialization.

The biogeochemical Pb cycle introduced by anthropogenic activities is much more extended than the natural Pb cycle and has caused Pb pollution to be a worldwide issue for humans and the environment. While historical Pb emissions from Western Europe, North America, and Asia are well documented, there is no equivalent data for Eastern Europe.

Here we present ice-core Pb concentrations from Belukha glacier in the Siberian Altai, assumed to be representative for emissions in Eastern Europe and the Altai for the period 1680-1995.
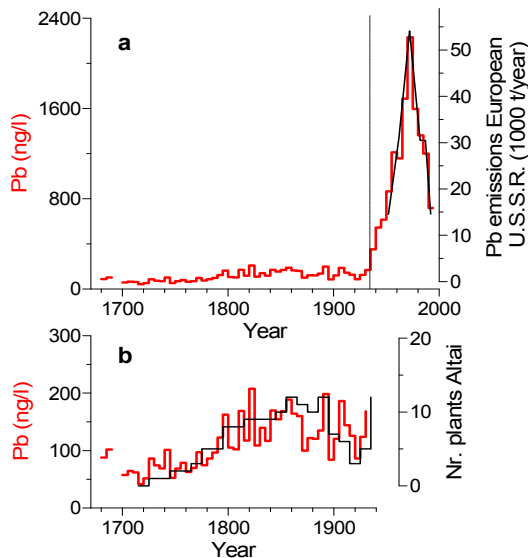
Fig. 1: (a) 5-year Pb concentrations in the period 1680-1995 and **(b)** preindustrial period 1680-1935 together with historical Pb-emission estimates for the European U.S.S.R. (1955-1995) and the number of smelters and metallurgical plants in the ore Altai [1].

The Pb concentration record in the period 1680-1935 reflects the history of local emissions from Rudny Altai (Russian for "ore Altai") mining and related metallurgical processing primarily for the production of Russian coins (Fig. 1b) [1]. After 1935, Pb concentrations were strongly enhanced, following the use of Pb additives in Russian gasoline (Fig. 1a). During the period 1955-1995 the Pb concentration record shows the same trend as the Pb-emission estimates in the European part of the U.S.S.R. The history of Pb pollution in Western Europe and North America as derived from Alpine and Greenland/Devon Island ice-core records [2-4] (Fig. 2) is characterized by increased emissions already from the mid of the 19th century on, indicating an earlier industrialization compared to Eastern Europe. Comparable to Western Europe and North America, Eastern European Pb emissions peaked in the 1970s. However, the subsequent down-

ward trend in Eastern Europe was mainly caused by the economic crisis in the U.S.S.R. and not by a widespread phase-out of leaded gasoline. Pb emissions in Asia, reconstructed from Mt. Logan, Himalayan, and Pamir ice cores [5-7] (Fig. 2), show a totally different trend. They remained on a low level until 1960-1970, increased considerably afterwards and are still rising, due to the later industrialization, the ongoing use of leaded gasoline in some parts of Asia, and significant contributions from coal combustion and metallurgical processes.
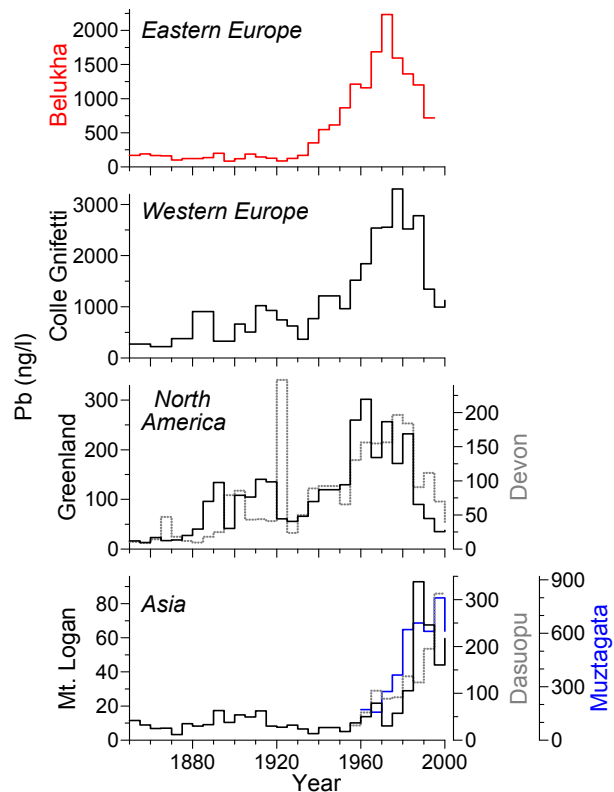
Fig. 2: Comparison of ice core Pb-concentration records from different Northern Hemisphere sites in the period 1850-2000, representing anthropogenic Pb emissions from Eastern Europe (Belukha, this study), Western Europe, North America, and Asia [2-7].

REFERENCES
[1] N. Malygina et al., this report, p. 27.
[2] M. Schwikowski et al., ES&T, **38**, 957-964 (2004).
[3] J.R. McConnell et al., GRL, **29**, 2130 (2002).
[4] W. Shotyk et al., Geophys. Res. Lett, **32**, L21814 (2005).
[5] E. C. Osterberg et al., Geophys. Res. Lett., **35**, doi: 10.1029/2007GL032680 (2008).
[6] Z. Li et al., Chin. Sci. Bull., **51**, 1996 (2006).
[7] W. Huo et al., Chin. Sci. Bull., **44**, 1309 (1999).

HISTORICAL DEVELOPMENT OF MINING AND METALLURGICAL PROCESSING IN THE ALTAI REGION

N. Malygina, S. Eyrikh, T. Papina (IWEP), A. Eichler (PSI)

The history of mining and related metallurgical processing in the Altai region is investigated for the validation of ice-core heavy metal records from Belukha glacier. The Altai region had been subject to mining activities already in the Bronze Age. In the 18th-19th century increasing raw material industry in the Rudny Altai was associated primarily with the production of Russian silver and copper coins.

Here we report on a comprehensive literature search to obtain data about historical mining and metallurgical processing in the region of the Rudny Altai (Russian for "ore Altai"). These data are used for the validation of ice-core heavy metal records obtained from Belukha glacier in the Siberian Altai [1] (Fig. 1).

The Altai region was subject to mining activities already in the Bronze Age. In the Rudny Altai, located in East Kazakhstan and the Altai region of Russia, vast polymetallic deposits containing e.g. massive sulfide ores of Pb, Cu, Zn, Au, Ag, and Fe were found within an area of about 500 km length and 60-100 km width. Extensive metal mining began in the beginning of the 18th century. In 1726 the first Altai metallurgy plant (Kolyvano-Voskresensk) started working. The extended Zmeinogorsk deposit in the north of the Rudny Altai was discovered in 1732. By the end of the 18th century eight mining and metallurgical plants operated in the region (Fig.1).
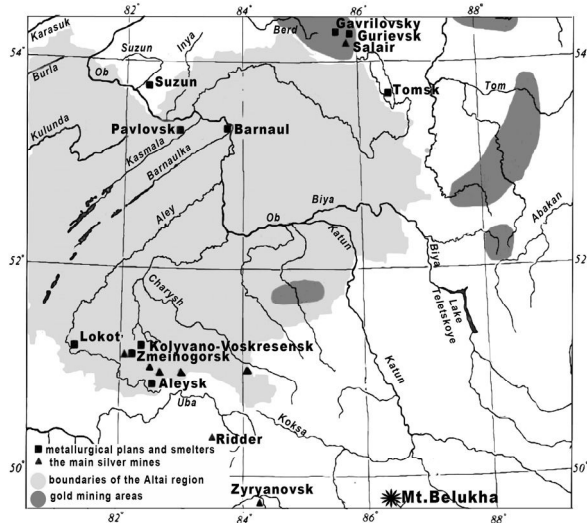
Fig. 1: Mines, metallurgical plants and smelteries in the Altai during the 18th-19th century and the location of the Belukha ice-core site (adapted from [2]).

"Goldish silver" (silver with gold impurities) was one of the most important products of mining and metallurgical industry of Altai. In the 18th and early 19th centuries, 90% of Russian silver was produced in the Altai region. Between 1766 and 1781 Siberian copper coins and later from 1781 to 1847 all Russian silver and gold coins were manufactured in Suzun. At the end of the 18th century the richest deposits of the Zmeinogorsk mine were exhausted and in the first half of the 19th century the ore base of the Altai mining industry was displaced mainly to the south (Zyryanovsk and Ridder deposits, discovered in 1794 and 1791, respectively) and the northeast (Salair deposits).

The Zyryanovsk and Ridder mines became the main supplier of raw materials (95% of the ore) for the smelteries in Zmeinogorsk, Barnaul, Lokot' and Pavlovsk. The number of smelters and metallurgical plants in the Altai region grew rapidly during the first half of the 19th century (Fig. 2). In this time, Altai was the main producer of silver and lead in Russia, the second in production of copper, and the third in production of gold [3]. After 1861 the mining industry being the major economic sector of the region entered a period of economic crisis. Depletion of rich ores, the fall in silver prices, and industrial crisis caused a considerable reduction of mining and smelting activities. At the end of the 19th century industry slowed down and gradually agriculture became the basis of Altai economy throughout the 1920-30s despite the industrialization in the U.S.S.R.
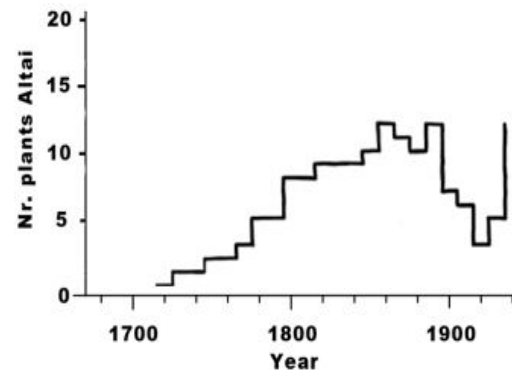
Fig. 2: The number of smelters and metallurgical plants in the Altai region (period 1725-1935).

Documents of the history of industrial development in the Altai region were gathered in a rare fund of the Altai Regional Shishkov's Scientific Library, in the State Archives of the Altai Territory and in the Department of archives of the Altai. More than 200 primary sources of archival material have been analyzed, also in free access [4,5].

REFERENCES

[1] A. Eichler et al., this report, p. 26.

[2] V.B. Borodaev, A.V. Kontev The historical atlas of the Altai region, Barnaul, "Azbuka" Publishers, 215 (2007).

[3] http://www.altairegion22.ru/en/

[4] Z.G. Karpenko, Mining and metallurgical industry of Western Siberia in 1700-1860. Novosibirsk, the Publishing House of the SBAS of the URSS, 216 (1963).

[5] Encyclopedia of the Altai region (in 2 volumes), Barnaul, Altai Book Publishers, **1**, 366 (1995) ; **2**, 488 (1996).

LEAD (Pb) SOURCE CONTRIBUTIONS DERIVED FROM LEAD ISOTOPE RATIOS IN AN ICE CORE FROM BELUKHA GLACIER

L. Tobler, A. Eichler, G. Gramlich (PSI), S. Eyrikh, N. Malygina, T. Papina (IWEP),
M. Schwikowski (PSI & Univ. Bern)

Pb isotope ratios were determined by Inductively Coupled Plasma Sector Field Mass Spectrometry (ICP-SFMS) in an ice core from Belukha glacier in the Siberian Altai for the time period 1680–1995. Pb isotope ratios were compared to values from Russian leaded gasoline, Altai ore lead, coal, and mineral dust. A binary mixing model was used to estimate the time dependent contribution of ores from the Rudny Altai region to the total Pb concentration, based on Pb isotope ratios

Determination of the Pb isotopic composition is a valuable tool to derive information of the origin of Pb in environmental samples.

Pb isotope ratios were determined by ICP-SFMS in an ice core from the Belukha glacier in the Siberian Altai in order to infer different Pb sources. The comparison of the Belukha Pb isotope ratios with values of mineral dust, coal combustion, Rudny Altai ores, and Russian leaded gasoline is presented in a three-isotope plot (Fig. 1).
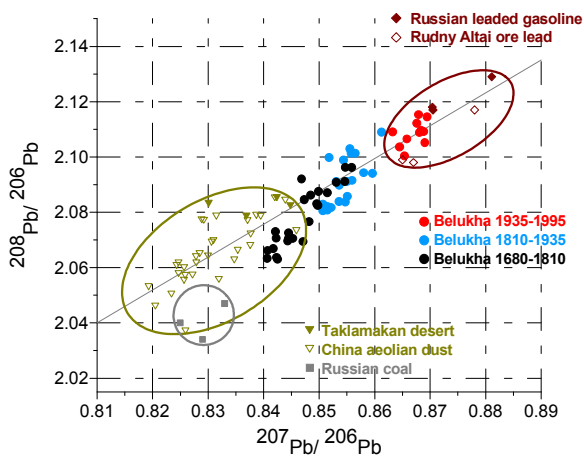
Fig. 1: 5-year means of Pb-isotope ratios in the Belukha ice core during three time periods are shown together with Pb-isotope ratios from different sources [1]. The three circles indicate the range of background dust (olive), Russian coal (grey), and Altai ore Pb (brown). The Pb growth curve is illustrated in grey [2].

^{207}Pb/^{206}Pb ratios in the industrial period 1935-1995 agree well with values for Russian leaded gasoline (0.87-0.88) and with those of ore Pb in the Rudny Altai (Fig. 1). During the time period 1680-1935, 75% of the data points are outside the range 0.82-0.847 (^{207}Pb/^{206}Pb) of mineral dust and coal combustion, suggesting that already in pre-industrial times emissions from mining activities and related metallurgical processing in Rudny Altai significantly influenced the Pb isotopic composition at the Belukha glacier. To estimate the contribution of ore Pb from Rudny Altai to the overall Pb concentration, a binary mixing model was applied, assuming two major Pb-emission sources during the investigated period 1680-1995 (Eq. 1) [1].

Source 1 represents Pb emissions from Rudny Altai ores and source 2 represents Pb emissions from mineral dust and coal combustion, which can not be sepa-

rated due to their similar Pb isotopic composition. The lower and upper limit of the ^{207}Pb/^{206}Pb ratios for the two sources were set to 0.87 (mean Rudny Altai ore Pb), 0.875 (Russian leaded gasoline) and 0.83 (mean coal combustion and mineral dust), 0.842 (Taklamakan desert) respectively.

$$\text{ore Pb} [\%] = 100 \cdot \frac{[(^{207}\text{Pb}/^{206}\text{Pb})_{sample} - (^{207}\text{Pb}/^{206}\text{Pb})_{dust+coal}]}{[(^{207}\text{Pb}/^{206}\text{Pb})_{ore} - (^{207}\text{Pb}/^{206}\text{Pb})_{dust+coal}]} \quad (1)$$

The mean contribution of ore Pb, given by the lower and upper limit, changed from (38±16)% in the time period 1680-1935 to (86±6)% during the industrial period 1935-1995 (Fig. 2). As a result of the increased mining and smelting activities for the production of Russian coins [3], there is also a significant increase in the ore Pb contribution from (28±13)% in the period 1680-1810 to (50±8)% from 1810-1935. After 1935, ore Pb from Rudny Altai used in Russian gasoline was the major contribution with peak values up to 98%.
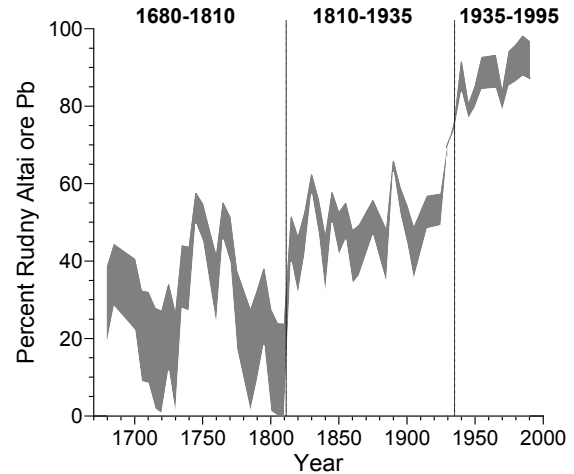
Fig. 2: Range of percentage contributions of the Rudny Altai ore Pb to the atmospheric Pb concentrations for the time period 1680-1995. For the definition of upper and lower limits see the text. Periods 1680-1810, 1810-1935, and 1935-1995 are indicated.

REFERENCES

[1] A. Eichler et al., submitted to Environ. Sci. Technol., (2011).

[2] G.L. Cumming and J.R. Richards, Earth Planet. Sci. Lett., **28**, 155-171, (1975).

[3] N. Malygina et al., this report, p. 27.

DATING OF THE TSAMBAGARAV ICE CORE INDICATES MILLENNIAL ICE IN THE MONGOLIAN ALTAI

P.A. Herren, A. Zapf (PSI & Univ. Bern), A. Eichler (PSI), T. Papina (IWEP), M. Schwikowski (PSI & Univ. Bern)

Precise dating of the upper 36 m weq ice core from Tsambagarav glacier using a combination of methods gives an age range of 200 years. ^{14}C ages as well as glacier flow models indicate that ice close to bedrock at 58 m weq is several thousand years old. Between 36 and 58 m weq ^{14}C ages suggest strong changes in accumulation rates, precluding a fit with conventional glacier thinning equations. The obtained age-depth relation confirms that the ice core contains at least a millennium of high-resolution climate and environmental signals.

In 2009 an ice core was collected from the Tsambagarav ice cap in the Mongolian Altai. Preliminary work on the ice core and measurements in the field has shown the feasibility to use the ice core as climate archive [1]. After completing the analyses of climate proxies such as major ions and stable isotopes (δ^{18}O) a precise depth-age relation had to be established. The upper 36 m weq contain climate information of the past 200 years. The methods applied were: identifying horizons, annual layer counting and nuclear dating with ^{210}Pb decay [2].

Strong thinning of the annual layers in the lower part of the ice core leads to a smoothing of the excess-sulphate peaks from volcanic eruptions. Additional dating techniques such as ^{14}C and glacier flow models are thus required. Details about the methods and their limitations are given in [3, 4]. Fifteen ^{14}C samples were analyzed within the lower 20 m weq. The results are given in Figure 1.
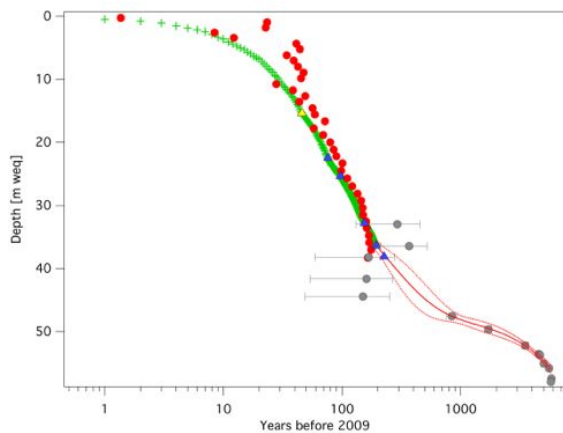
Fig. 1: Depth-age relation for the Tsambagarav ice core. Annual layer counting (green crosses), tritium peak (yellow triangle), ^{210}Pb activity (red circles), exponential equation with 2σ-range (red line) and ^{14}C values with the 1σ-range (grey circles).

The ages of the four youngest ^{14}C samples are in the upper application range of the ^{14}C method. A broad calibration curve for this period leads to large uncertainties and explains the inconsistent age increase with depth. The samples were analyzed to exclude an age offset between the methods applied for the last 200 years and the ^{14}C values. The older ^{14}C results suggest a strong thinning starting slightly below 36 m weq and leading to an abrupt change in the depth-age relation. Close to bedrock at 58 m weq the thinning becomes less pronounced. According to the ^{14}C values, the last meter of ice above bedrock contains a smaller time

interval than between 48 and 49 m weq. The age close to bedrock is consistently reproduced by multiple samples at about 5800 years before 2009.

Different hypotheses exist to explain the variable thinning suggested by the ^{14}C results: varying accumulation or changing flow lines due to a shift of the ice dome shape with time. A combination of the two processes may have changed the thickness of the glacier and can thereby be an additional reason of the observed thinning. A hiatus in the depth-age relation (no accumulation over a certain time period) can be excluded since no significant increase in the calcium concentration as tracer for mineral dust input indicates such phenomenon. A combination of ^{14}C values with a glacier flow model is not possible. The changed thinning cannot be fitted in a reasonable way by conventional glacier thinning equations. As useful fit a double exponential equation was applied with $R^2 = 0.999$. Although the equation has no physical significance, it provides a smooth transition between the last horizon and youngest ^{14}C value. The fit interpolates discrete dating by ^{14}C values to a continuous depth-age relation (Fig. 1).

The combination and correct interpretation of the different methods is the key for a precise dating of the ice core. The initial goal of the project to find an archive containing one millennium of climate information is achieved. Future work will be the implementation of the depth-age relation to the already measured climate proxies for regional climate reconstruction.

ACKNOWLEDGMENTS

REFERENCES

[1] P.A. Herren et al., Ann. Rep. Lab. of Radio- & Environ. Chemistry, Uni Bern & PSI (2009) p. 32.
[2] P.A. Herren et al., Ann. Rep. Lab. of Radio- & Environ. Chemistry, Uni Bern & PSI (2010) p. 21.
[3] M. Sigl et al., J. Glaciol., **55**, 194 (2009).
[4] L. Thompson et al., A. Glaciol., **14**, (1990).

ICE CORE BASED δ^{18}O AS TEMPERATURE PROXY IN WESTERN MONGOLIA

P.A. Herren (PSI & Univ. Bern), A. Eichler (PSI), T. Papina (IWEP), M. Schwikowski (PSI & Univ. Bern)

The δ^{18}O ice core record of Tsambagarav glacier was calibrated with instrumental temperatures from the station in Hovd, validating δ^{18}O as a temperature proxy for Western Mongolia. The best correlation was obtained with temperatures in the months June, July and August, suggesting a strong concentration of the annual precipitation in the summer season.

An ice core from Belukha glacier in the Siberian Altai (49°48'N, 86°35'E) showed an exceptionally high correlation of the temperature proxy δ^{18}O with reconstructed solar activity during the pre-industrial period 1250-1850 AD [1]. This finding initiated an intense discussion about the importance of solar radiation on the Southern Siberian climate. For a better understanding of the correlation and its spatial and temporal importance, a new ice core was collected in the Tsambagarav mountain range. The site is situated around 350 km to the south of Belukha [2]. The suitability of the ice core as climate archive was shown in previous work [3] and the dating is presented in this issue [4].

The stable isotope ratio δ^{18}O was analysed in the entire ice core. To use the δ^{18}O values as temperature proxy for the region, a calibration with local instrumental temperatures is required. Data from four weather stations close to Tsambagarav are available from National Oceanic and Atmospheric Administration (NOAA). The station in Hovd (48°0'N, 91 38'E) is the only one having a continuous record from 1936 to 2009 with a monthly resolution. The station is situated around 90 km away from the glacier at an altitude of 1400 m a.s.l. Temperatures from Hovd were therefore used to calibrate the δ^{18}O record.
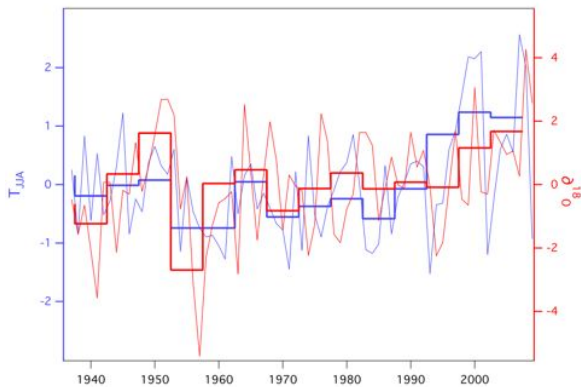
Fig. 1: Yearly June-July-August temperature in Hovd (thin blue line) and five-year averages (thick blue line), combined with yearly δ^{18}O (thin red line) and five-year averages (thick red line). All values are given as anomalies.

In Mongolia the climate is extremely continental with a strong seasonal distribution of precipitation. The summer months (June to August) contribute up to 70% of the total precipitation, while the winter months (December to February) account for only 4%. This suggests that the δ^{18}O represents almost exclusively spring-summer-fall temperature. Since different sea-

sons show diverse temperature trends over time it is essential to identify when snow accumulates at the glacier. A correlation analysis between temperature and δ^{18}O was performed by changing the amount of months in the temperature record and the number of years averaged. The best correlation with the highest significance was obtained for five-year averages of the temperature of the months June, July and August (R-value = 0.74, p-value $\leq$ 0.001, Fig. 1). Time averaging corrects for possible dating errors in the δ^{18}O record. The relation is given by

$$\delta^{18}O = (1.10 \pm 0.42) \, T_{JJA} - (32.00 \pm 6.82 \, ‰).$$

Very negative δ^{18}O-values could represent rare events of winter snowfall. The δ^{18}O frequency distribution is skewed towards negative values. To correct a potential seasonal bias of the temperature signal δ^{18}O values below the 200 points moving average minus two standard deviations were removed. However this procedure did not improve the correlation coefficient between temperature and δ^{18}O. This suggests that negative δ^{18}O values represent indeed cold summer conditions and that precipitation in the mountains is stronger concentrated towards the summer months than in the lowlands of western Mongolia.

The significant correlation between temperature at the nearby Hovd station and the stable isotope ice core record validates δ^{18}O as temperature proxy. This result enables further research about the role of solar activity on the climate, helping to put the findings of the Belukha ice core in a larger perspective.

REFERENCES

[1] A. Eichler et al., 2009 Geophys. Res. Lett. **36** doi: doi:10.1029/2008GL035930.

[2] M. Schwikowski et al., Ann. Rep. Lab. of Radio- & Environ. Chemistry, Uni Bern & PSI (2009), p. 31.

[3] P.A. Herren et al., Ann. Rep. Lab. of Radio- & Environ. Chemistry, Uni Bern & PSI (2009) p. 32.

[4] P.A. Herren et al., this report, p. 29.

BIOLOGICAL SPECIES RECORDED IN BELUKHA (SIBERIAN ALTAI) AND TSAMBAGARAV (MONGOLIAN ALTAI) ICE CORES

E. Mitrofanova, N. Malygina, T. Papina (IWEP), A. Eichler (PSI), P.A. Herren, M. Schwikowski (PSI & Univ. Bern)

Diatom algae, cysts of chrysophycean algae, spores of inferior plants, and pollen grains of high plants (coniferous trees, hardwoods and herbs) were analyzed in two Altai ice cores. The results indicate a stronger steppe environment at the Mongolian Altai site compared to the Siberian site. Records differ in concentration and trend of the biological species between the two sites, indicating differences in source regions.

Analyses of biological species in ice cores provide a valuable tool for the reconstruction of regional vegetation, climate dynamics, and the forest fires history [e.g. 1, 2]. However, the extremely low concentration of pollen, algae or cysts in ice cores hinders a broad application of biological analyses. Plants and algae are characterized by specific seasonal growth and pollen production. Diatoms and cysts grow during spring and autumn months, coniferous trees flower mainly in spring, hardwoods and herbs at the end of spring beginning of summer. This seasonal occurrence of different species can be used as additional dating tool to conventional dating methods [3].

Here we report on the investigation of pollen, cysts, and diatoms in two ice cores from the Altai, 350 km distant. The ice core from Belukha glacier in the Siberian Altai drilled in 2001 (4062 m a.s.l., 49°48'N, 86°34'E) was analyzed with annual resolution in the period 1963-2000 (Fig. 1). The ice core from the Tsambagarav summit in the Mongolian Altai drilled in 2009 (4140 m.a.s.l., 48°39'N, 90°51'E) was sampled with a resolution of approximately three years between 1935 and 2009 (Fig. 2). The climate at both sites is strongly influenced by Westerlies [4, 5].
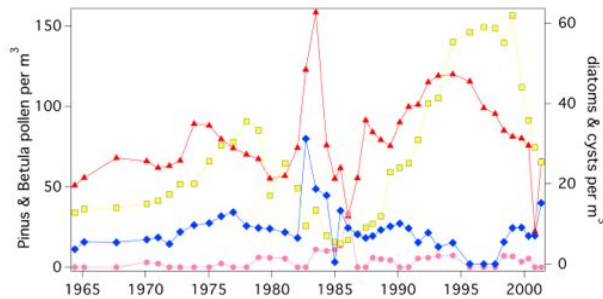
Fig. 1: Concentration of diatoms (blue diamonds), chrysophycean cysts and spores of inferior plants (yellow squares), pollen grains of coniferous trees (*Pinus*, red-triangle), hardwoods and herbs (*Betula*, pink circles) in the Belukha ice core.

In general, concentrations of all species are higher at the Tsambagarav site. This was not expected for the *Pinus* pollen record, considering the larger distance of the Mongolian Altai site to the extended Siberian forests. Possible reasons for the higher values at this site could be the smaller accumulation rate (being a factor of 2-3 lower compared to the Belukha site), a stronger dry deposition, and differences in the origin of the air masses arriving at both sites.

The abundance of the different biological species can provide information about the dominant vegetation types. While diatoms are more important in the high mountain steppe zone, pollen of coniferous trees is more abundant in the mountain forest zone. The mean ratio between concentrations of *Pinus* pollen and diatoms is significantly higher at the Belukha site, confirming a stronger influence of the mountain forest on the Siberian Altai site, whereas the Mongolian Altai site is stronger determined by a mountain steppe ecosystem. However, the investigated ratio is strongly changing with time, suggesting varying influence of the different vegetation types.
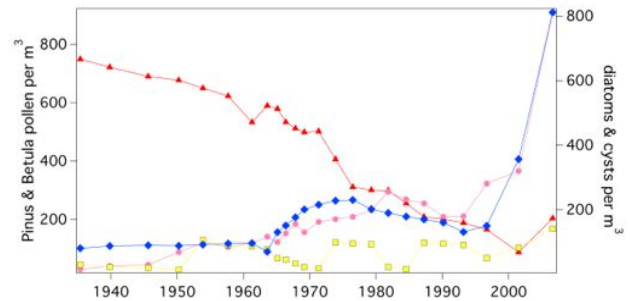
Fig. 2: Concentration of diatoms (blue diamonds), chrysophycean cysts and spores of inferior plants (yellow squares), pollen grains of coniferous trees (*Pinus*, red-triangle), hardwoods and herbs (*Betula*, pink circles) in the Tsambagarav ice core.

At the Tsambagarav site, the record of the diatoms and *Betula* pollen is anticorrelated with the *Pinus* pollen record. Strong increasing steppe elements and decreasing concentrations of coniferous tree pollen during the period 1935-2001 suggest a decreasing input of mountain forest and an increasing influence of mountain steppe. This is different at the Belukha, where diatoms, *Betula* and *Pinus* pollen do not show a significant trend. These results indicate differences in the origin of the air masses arriving at the two sites. Further research is needed to confirm our findings.

REFERENCES

[1] A. Eichler et al., Quartenary Science Reviews, **30**, 1027 (2011).

[2] J. Uetake et al., Ann. Glaciology, **43**, 70 (2006).

[3] F. Nakazawa et al., J. Glaciology, **51** (174), 483 (2005).

[4] V. B. Aizen et al., Ann. Glaciology, **43,** 49 (2006).

[5] V.S. Sheinkman, Developments in Quaternary Science, **Vol. 15**, 883 (2011).

SUTAI UUL MOUNTAIN (4210 M A.S.L.) - A POTENTIAL SECOND ICE CORE DRILLING SITE IN THE MONGOLIAN ALTAI?

H. Machguth (Univ. Zürich), P.A. Herren (Univ. Bern & PSI), B. Rufibach (PSI), T. Papina, E. Mitrofanova, T. Uskov (IWEP), O. Demberel (Hovd University), N.M. Nurlanbek (MAS), M. Schwikowski (PSI & Univ. Bern)

In June 2011 Sutai Uul mountain in the western Mongolian Altai was explored in search for an ice core drilling site. The topography of the glacier has proven to be nearly ideal for the retrieval of an ice core record. However, in a snow pit traces from distinct melt events were found and logistics in the area are extremely challenging.

In July 2009 PSI and IWEP successfully drilled an ice core on Tsambagarav mountain [1, 2]. Retrieving a second ice core from the Mongolian Altai would allow cross validating the first record and opens up new scientific perspectives, e.g. reconstruction of desertification history.

Starting 15th of June 2011, PSI and IWEP (Barnaul, Russia) performed a two weeks expedition to explore a second potential ice core drilling site in the Mongolian Altai. The expedition aimed at Sutai Uul Mountain (46°37' N, 93°36' E, 4210 m a.s.l.), located nearby Gobi desert and being the second highest peak in Mongolia [cf. 3, 4]. It was planned to assess the suitability of Sutai Uul for retrieval of an ice core from (1) measurements of the ice thickness using Ground Penetrating Radar (GPR), (2) surveying of the exact glacier topography by means of high precision GPS and (3) digging of snow pits to analyse the frequency of melt events (ice lenses) at the potential drill site.

Despite of being shipped one month in advance, GPR and GPS devices arrived with a delay of six weeks in western Mongolia and could not be deployed during the expedition. The reasons for the delay were Li-Ion batteries that were (erroneously) considered dangerous goods. While waiting, a part of the expedition team drove to Sutai Uul, climbed the mountain twice and dug a snow pit (Fig. 1).

The expedition revealed a controversial picture of Sutai Uul as a potential drilling site: On the one hand the topography of the summit was confirmed to be excellent for drilling: Sutai Uul features a large (~2 x 2 km) and almost concentrical ice cap. From the analysis of satellite imagery, digital elevation models and own observations, ice thickness is estimated to be in the range of 80 to 120 m and very likely exceeds the 72 m drilled at Tsambagarav [1]. Furthermore the location of Sutai Uul nearby Gobi desert and observed accumu-

lation rates in the snow pit point to a slightly drier climate than on Tsambagarav [2]. This assumption is supported by the concentrations of major ions in the snow pit which are generally higher than concentrations during the last 10 years at Tsambagarav. Thus the glacier might contain a climate record reaching further back in time. On the other hand the ice thickness could not be measured directly by means of GPR and massive ice lenses were found in the snow pit. The latter indicates melt events that are stronger than on the more northerly Tsambagarav. Finally, logistics are challenging in the area: GPR and GPS arrived with a large delay and roads in western Mongolia are not suitable for the transport of ice cores. Helicopter support from Russia similar to the Tsambagarav expedition [1] would be a prerequisite for a potential drilling expedition. However, Sutai Uul is located further away from the Russian border making it difficult and expensive to organize helicopter flights.

REFERENCES

[1] M. Schwikowski et al., Ann. Rep. Lab. of Radio- & Environ. Chemistry, Uni Bern & PSI (2010).
[2] P.A. Herren et al., Ann. Rep. Labor Radio- & & Environ. Chemistry, Uni Bern & PSI (2010).
[3] A. Jarvis et al., http://srtm.csi.cgiar.org (2008).
[4] Aster GDEM terrain model, METI and NASA, http://asterweb.jpl.nasa.gov/gdem.asp.
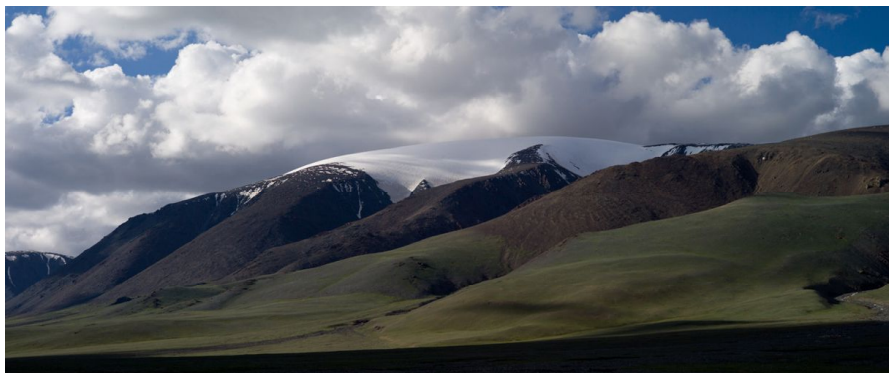
Fig. 1: Sutai Uul (4210 m a.s.l.) seen from the base camp at ~2900 m a.s.l.

^{14}C MEASUREMENTS OF SAMPLES FROM "JUVFONNE ICE TUNNEL", NORWAY – TOWARDS FURTHER METHOD VALIDATION

A. Zapf (Univ. Bern & PSI), A. Nesje (Univ. Bergen), S. Szidat (Univ. Bern), L. Wacker (ETHZ),
M. Schwikowski (PSI & Univ. Bern)

Ice samples from the Norwegian Juvfonne ice patch retrieved from previously well-dated adjacencies were dated with our ^{14}C-method in order to further validate this dating approach for glacier ice.

SETTING

Juvfonne is a small ice patch in the Jotunheimen Mountains in central southern Norway (61.676°N, 8.354°E). The ice patch (0.2 km^2) is situated at 1850 to 2000 m a.s.l. with a maximum ice thickness of 17-19 meters as revealed by Ground Penetrating Radar (GPR) soundings in 2009. Increased focus in those ice patches arose as a result of the extreme melting this region experienced in 2006 when numerous historical artefacts had been uncovered by the retreating ice. In 2010, a 30 meter long ice tunnel was established in the Juvfonne ice patch for scientific as well as educational and touristic purposes [1, 2].

Stratigraphic examination of the ice patch from inside the ice tunnel yields two distinct features: while upper horizons are nearly parallel to the present glacier surface, the deepest ice layers form "a distinct angular unconformity with the surface" probably caused by deformation when the ice patch grew during the Little Ice Age or earlier [1]. Several organic rich layers can be identified in the ice patch (Fig. 1), which were used by Norwegian scientists to confine the age of the ice by means of conventional radiocarbon dating [2].

Fig. 1: Inside the Juvfonna ice tunnel. Dark organic-rich layers are clearly visible at the walls and within the illuminated column (photo courtesy of A. Nesje).

In order to further test and validate our method to date glacial ice based on carbonaceous aerosols incorporated in the ice matrix [3] we were provided with ice blocks retrieved from three different locations in the ice patch where adjacent spots were already dated and estimations of the expected ages exist (Tab. 1).

RESULTS

Multiple measurements were performed for each sampling location.

Tab. 1: Samples with their estimated ages [2].

Location	Estimated age
JUV 1	1535 ± 30 to 2960 ± 30 yr BP
JUV 2	≈ 1480 ± 30 yr BP
JUV 3	modern or 2960 ± 30 yr BP

Two out of three values for JUV 1 (green) lie within the age range given. The third value is regarded an outlier due to probable sample contamination during preparation (extremely high OC/EC ratio). Results for JUV 2 (blue) slightly scatter around a quite narrow age range. The unconformity in the deeper ice layers might be an explanation for this. More detailed information about the stratigraphy around this sample would help to put the results in perspective. JUV 3 (red) measurements clearly confirm one of the two estimated ages. All values show modern ^{14}C-ratios.
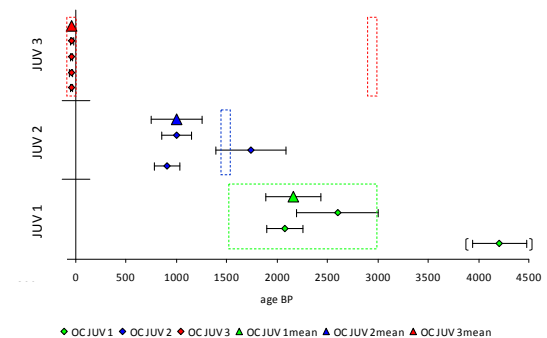
Fig. 2: Calibrated radiocarbon ages (based on OC, organic carbon) of the three ice samples (diamonds). The triangles show the weighted mean of the respective series. Error bars indicate the 1σ-range. Dashed boxes represent the estimated ages as specified in Tab.1. Considered outlier shown in brackets.

Results for all three ice samples are very reasonable with respect to the age estimates given [2]. Thus, this is a further validation for our radiocarbon method to provide the true age of the ice.

REFERENCES

[1] R. S. Oedegaard et al., Geophys. Res. Abstr., **13**, EGU2011-12027 (2011).

[2] A. Nesje et al., The Holocene DOI: 10.1177/0959683611425552 (2011).

[3] M. Sigl et al., J. Glaciol., **55**, 194 (2009).

SAMPLING THE VERTICAL ICE CLIFFS ON MOUNT KILIMANJARO, TANZANIA

A. Zapf, P.A. Herren (Univ. Bern & PSI), B. Rufibach (PSI), D. R. Hardy (UMass),
M. Schwikowski (PSI & Univ. Bern)

During September/October this year the vertical ice cliffs of the Northern Ice Field on Kibo (Kilimanjaro massif, Tanzania) were sampled. Horizontal ice cores were extracted from 22 discrete ice layers by means of a new battery driven hand drill. Samples are being analyzed in our group for ^{14}C with a view to constrain the age of the glaciers on Kilimanjaro by an independent dating effort.

The age of the plateau glaciers on Kibo, Kilimanjaro's highest summit, is currently a matter of discussion. Paleoclimate reconstructions based on six ice cores, extracted from the ice fields on Kilimanjaro in 2000, assigned a basal age of 11'700 years [1]. Another study claims that plateau glaciers on Kilimanjaro are subject to recurring cycles of waxing and waning with estimated decay time periods of 165±10 years. An absence of the ice bodies was reconstructed for the period around 850 years ago [2]. Near basal ice samples from Kibo's Northern Ice Field (NIF), collected by our collaborator Douglas Hardy from UMass during a field campaign in 2009, were already analyzed in our group by means of ^{14}C-dating. The obtained results led to an expedition to recover more sample material in a stratigraphic sequence in order to come up with a firm conclusion on the age of the ice fields.

A joint expedition of University of Massachusetts and Paul Scherrer Institut to Kilimanjaro took place from 22 September to 7 October 2011. The ascent was done on the Umbwe route via the Western Breach in a total of six days passing four intermediate camps. Equipment and food was carried by some 30 porters. On the crater plateau the high camp was established just in front of the southern margin of the NIF (Fig. 1).

Fig. 1: High camp at 5800 m a.s.l. with the Northern Ice Field in the background.

Potential sampling sites were selected during a reconnaissance hike round the NIF. Logistics limited the sample capacity to a maximum of 48 short cores. The extraction of the ice cores was done with a newly constructed battery driven hand drill, which can be operated by one person while rappelling down the cliff (insert Fig. 2). Short cores obtained are 50 cm long with a diameter of 8 cm. By means of a simple pulley the samples were lowered for on-site processing, documentation and packing. At the main sampling site the entire height of the ice cliff (35 m) was discretely sampled at characteristic horizons (Fig. 2). As previously analyzed ice samples from the NIF contained rather low amounts of carbon two parallel cores were retrieved from each sampled layer to obtain sufficient material for analysis. Furthermore basal ice was also sampled at the centre of the NIF, which is now accessible due to the recent break-up of the ice field. In order to investigate for potential age offsets which might be intrinsic to the results, samples were additionally collected from the glacier's surface.

Fig. 2: View from south to the NIF with the sampled cliff section indicated by the red box. The insert shows the drilling process while belayed by top-rope.

Prior to descent the ice cores were stored in a small ice cave close to camp, eventually carried down the mountain by porters within a few hours and stored in a freezer in Moshi, Tanzania until being shipped to PSI. Radiocarbon analysis of the ice is on-going and first results are expected soon.

REFERENCES

[1]   L. Thompson et al., Science, **298**, 589 (2002).
[2]   G. Kaser et al., The Holocene **20**, 1079 (2010).

RADIOCARBON ANALYSIS OF ORGANIC CARBON AND ELEMENTAL CARBON IN FIRN SAMPLES

F. Cao (PSI & GIG CAS), S. Szidat (Univ. Bern & PSI), M. Schwikowski (PSI & Univ. Bern)

We have developed a new decontamination method for firn cores, which could be applied on the upper parts of Fiescherhorn cores, covering the time period 1940-2002. Radiocarbon in the OC and EC fractions of carbonaceous particles contained in firn cores will be analysed for source apportionment studies of past anthropogenic and biogenic emissions.

INTRODUCTION

A first long-term record of organic carbon (OC) and elemental carbon (EC) concentrations along with the corresponding fraction of modern (f_M) carbon derived from radiocarbon (^{14}C) analysis in ice was published by our group [1]. The f_M allows a distinction and quantification of natural (biogenic) and anthropogenic (fossil) sources of carbonaceous particles in the past. OC and EC were extracted from the ice samples, with resulting carbon quantities in the microgram range [2]. Analysis of ^{14}C by accelerator mass spectrometry (AMS) was therefore highly demanding. ^{14}C analysis offers a unique potential for unambiguous source apportionment of aerosol particles due to the possibility of a direct distinction of contemporary and fossil carbon [3]. Samples were taken from bedrock up to the firn/ice transition, covering the time period 1650-1940 and thus the transition from the pre-industrial to the industrial era. For the upper part of the core, we have to develop a new decontamination technique for firn sample, which has lower density and higher porosity.

METHODS

Cutting of the firn samples and removal of possibly contaminated outer layers was performed in a cold room ($-20°C$) using a pre-cleaned stainless-steel band saw. After cutting, all parts were cleaned by chiselling to remove surface contamination. Afterwards, samples were preserved in pre-cleaned containers which were closed for melting at room temperature. Detailed procedures on sample preparation, separation of the two fractions and applied analytical methods (AMS) can be found in [2].

PRELIMINARY RESULTS

The concentrations of OC/EC and the fraction of modern carbon (f_M) obtained for processing blanks, Jungfraujoch artificial firn and Fiescherhorn ice core samples are presented in Tab. 1. OC concentrations for chiselled blank ice are higher than the value reported by [1], but they contribute less than 10% OC in our target samples. The value for f_M is comparable to the reported value. OC and EC of the artificial firn samples from a natural archive (Jungfraujoch) were also determined, which were decontaminated by present method. Result show OC, EC concentrations and their f_M in the chiselled Jungfraujoch artificial firn are comparable with values for Jungfraujoch reference snow (supplied by A. Zapf).

To test this decontamination method, ^{14}C in the OC/EC fractions of five samples collected from 15 Fiescherhorn ice cores representing the years 1912-1934 were conducted, showing a good agreement with the values previously reported [1].

The above results demonstrate that the present pretreatment method is suitable for firn cores with a relative high concentration of carbonaceous particles, including Fiescherhorn firn cores.

Tab. 1: OC, EC concentrations and ^{14}C derived from ultrapure water ice, Jungfraujoch artificial firn, and Fiescherhorn ice core samples.

Sample	OC($\mu g\ l^{-1}$)	EC ($\mu g\ l^{-1}$)	f_M OC	f_M EC
Blank ice, chiselled (this study)	2.85±0.13	0.33±0.05	0.67±0.23	-
Blank ice, rinsed [1]	1.30±0.60	0.30±0.10	0.60±0.10	0.30±0.30
Jungfraujoch, chiselled (this study)	24.69±2.80	3.61±1.39	0.85±0.05	0.69±0.01
Jungfraujoch Ref (A. Zapf, 2010)	31.20±1.39	6.20±3.01	0.80±0.02	0.61±0.02
Fiescherhorn 1912-1934, chiselled (this study)	39.61±6.88	28.72±7.98	0.82±0.03	0.33±0.04
Fiescherhorn 1912-1934, rinsed [1]	31.52±8.47	34.33±18.72	0.76±0.09	0.32±0.04

OUTLOOK

This chiselling decontamination method will be applied on the upper part of Fiescherhorn core. In order to minimize positive and negative artefacts on the ^{14}C content of OC and EC, a thermo-optical OC/EC Analyzer will be used to separate OC and EC [4].

ACKNOWLEDGEMENT

REFERENCES

[1] T.M. Jenk et al., Atmos. Chem. Phys., **6**, 5381 (2006).

[2] T.M. Jenk et al., Nucl. Instrum. Methods B, **259**, 518, doi:10.1016 (2007).

[3] S. Szidat et al., Nucl. Instrum. Meth. Phys. Res. B, **829,** 223(2004).

[4] Y.L. Zhang et al., this report, p. 65.

PRECIPITATION AND TEMPERATURE SIGNAL FROM TWO ALPINE ICE CORES

I. Mariani (Univ. Bern & PSI), A. Eichler (PSI), T. Jenk (CIC), M. Schwikowski (PSI & Univ. Bern)

Ice cores are natural archives to study the past climate. The stable isotope ratio $\delta^{18}O$ and the annual accumulation are typically used as temperature and precipitation proxy, respectively. High resolution, well-dated ice core records for the period 1960-2000 allow to verify the validity of the proxies.

INTRODUCTION

$\delta^{18}O$ in ice cores is often used as a proxy for temperature, with a seasonally varying signal. However, its values intrinsically depend on the precipitated snow that in turn may exhibit seasonality. It was found, for example, that the Colle Gnifetti record is mainly a summer signal, because of winter snow erosion at that site [1]. High resolution records from two other Alpine ice cores offer the opportunity to test whether the atmospheric signal is preserved in the two glaciers (Fig. 1): Fiescherhorn ~3900 m asl, Northern Alps [2], and Grenzgletscher, ~4200 m asl, Southern Alps [3]. Their $\delta^{18}O$ and accumulation records are compared with gridded meteorological data over the period 1960-2000.

Fig. 1: Location of the Fiescherhorn and Grenzgletscher ice core drilling sites.

ACCUMULATION/PRECIPITATION

Reconstructed annual accumulation in the uppermost part of the cores was obtained by taking into account ice thinning with depth, using the Nye model. Monthly, high resolution gridded precipitation data (~2.2 km, 1961-present), provided by Meteoswiss, were correlated with Fiescherhorn (1962-2001) and Grenzgletscher (1962-1993, 1968-1970 excluded because of missing data) reconstructed accumulation.
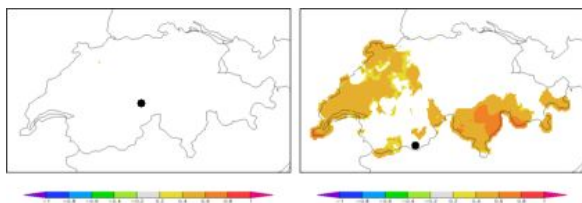
Fig. 2: Spatial rank correlation of annual precipitation (Meteoswiss gridded data) with Fiescherhorn (left) and Grenzgletscher (right) annual accumulation. p<5% values shown. Black dots indicate the glacier locations. Correlations performed with KNMI Climate Explorer (http://climeexp.knmi.nl).

Whereas Fiescherhorn accumulation has no correlation with precipitation, presumably due to local and sporadic conditions (e.g. precipitation at the upwind side of the mountain during Föhn situations), Grenzgletscher is significantly correlated with precipitation in Tessin and Jura mountains (Fig. 2). In order to check whether accumulation is mainly concentrated in a particular season, correlations with seasonal precipitations were performed (not shown). In this case, the highest correlations were found in spring, whereas nothing significant for Fiescherhorn was obtained.

TEMPERATURE/$\delta^{18}O$

$\delta^{18}O$ was correlated with fields from the Twentieth Century Reanalysis Project dataset [4]. 700 hPa (~3000 m) temperature was used. Fig. 3, left, shows that Fiescherhorn $\delta^{18}O$ is correlated with annual temperature. When seasonal fields are considered, no correlation with a particular season was found. Thus, the $\delta^{18}O$ signal is probably uniformly deposited throughout the year. The interpretation is more complicated for Grenzgletscher, where no correlation was found (Fig. 3, right). When looking at seasonal means, correlations were found in spring, as for precipitation. However, when compared to autumn values, $\delta^{18}O$ exhibits anticorrelated behaviour with temperature (not shown). A possible explanation is the high variability of the annual accumulation (1σ=0.8 mweq/y, a factor 2 higher than at Fiescherhorn), that could affect the $\delta^{18}O$ signal.
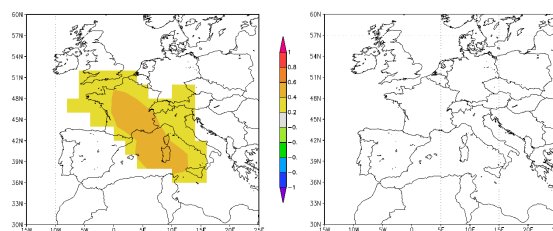
Fig. 3: Spatial rank correlations as in Fig.1, $\delta^{18}O$ versus 700 hPa temperature.

ACKNOWLEDGEMENT

REFERENCES

[1] M. Sigl, PhD thesis, University of Bern (2009).
[2] T. Jenk, PhD thesis, University of Bern (2006).
[3] A. Eichler et al., J. Glaciol. **46**, 507 (2000).
[4] G.P. Compo et al., Quart. J. Royal Met. Soc., **137**, 1 (2011).

DEUTERIUM EXCESS AS ATMOSPHERIC CIRCULATION PROXY?

I. Mariani (Univ. Bern & PSI), T. Jenk (CIC), M. Schwikowski (PSI & Univ. Bern)

Stable isotopes in ice cores may provide information about atmospheric circulation. In order to better characterize different air regimes affecting precipitation over the Alps, a study involving deuterium excess from the Fiescherhorn ice core along with weather type frequencies was conducted.

Deuterium excess in ice cores is a proxy for air moisture in the source region (high values corresponding to dry air, the opposite for low values), and may therefore provide information about air masses leading to precipitation at the glacier. A challenge is to interpret this proxy for Alpine climate, where different sources (Atlantic, Mediterranean, continental...) have different contributions to precipitation during the year [1]. Here a study correlating seasonal deuterium excess from the Fiescherhorn ice core, Northern Alps [2], and weather types over the period 1959-2001 was conducted.

Seasonal averages of deuterium excess were obtained with the following procedure: Fiescherhorn $\delta^{18}O$ minimum (temperature proxy) was aligned with the coldest month at the Jungfraujoch station, about 5 km west (for which a correlation coefficient r=0.38, p<0.05, between annual $\delta^{18}O$ and temperature, was found over the period 1959-2001). Monthly values of deuterium excess were obtained by subdivision of the interpolated data into 12 equidistant values. Seasonal averages were then taken in order to reduce dating uncertainties. Deuterium excess shows a different seasonality compared to $\delta^{18}O$. The moisture proxy shows minima in summer and maxima in winter, probably related to the warmer, wetter air masses affecting precipitation in summer and the colder, drier ones (Atlantic, North Sea) in winter.

Weather types are recurring patterns in atmospheric circulation. Their frequencies are defined as the number of days per season in which a particular type occurred [3]. A new classification scheme (GWT, GrossWetter Types), based on predefined patterns, is provided by Meteoswiss. GWT classification is available in 10, 18, 26 types covering the period 1959-2001. Skills in reproducing a parameter (temperature, precipitation) vary with season and region. For the Northern Alpine sector the GWT classification based on sea level pressure with 26 types proved to be the most suitable to explain precipitation variability, especially in spring-summer [3]. The seasonal frequency of each type is usually not higher than 11-12%, because of the high number of types.

Since stable isotope ice core proxies are intrinsic parameters of precipitation, significant rank correlations are presumably related to patterns that lead to precipitation at Fiescherhorn. Results are shown in Tab. 1. In winter, deuterium excess is positively correlated with the NorthEastern cyclonic pattern, consisting in low pressure over Central Italy and cold, dry easterlies advected toward the Alps (not shown). In spring, typical northern Föhn situations (e.g. NorthWestern, cyclonic type, Fig. 1, top, and the North, cyclonic pattern) advect air masses from the Northern quadrants, resulting in higher excess values. No significant correlations

were found in summer. In fall the Southern anticyclonic type brings more precipitation over Western Europe and slightly higher temperatures over the Northern Alps (+1° C, Fig. 1, bottom). Negative correlations with the deuterium excess could be explained in terms of wetter air masses coming from the Mediterranean. More difficult is the interpretation of the East anticyclonic (winter) and the East indifferent, (spring): no significant precipitation over the Alps occurs during these situations (not shown). Possible reasons for this result could be the lower skill of the classification in reproducing these patterns, and/or the dating uncertainties in the ice core.
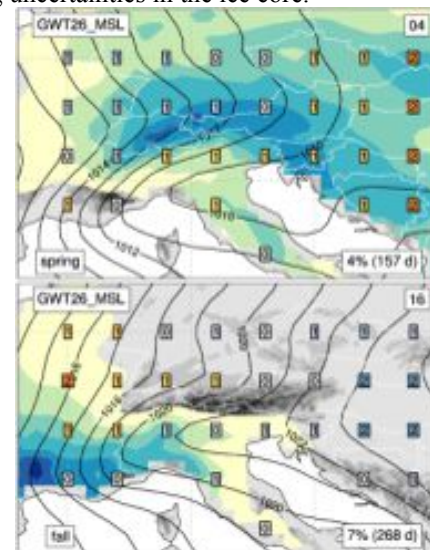
Fig. 1: NorthWest, cyclonic type in spring (top), and South, anticyclonic type in fall (bottom). Isobars are shown together with temperature anomalies (squares) and precipitation patterns (coloured contours) [3].

Tab. 1: Weather types showing a significant rank correlation (p<5%) with Fiescherhorn deuterium excess, 1959-2001.

exc	Positive	Negative
DJF	• NorthEast, cyclonic (+0.404)	• East, anticyclonic (-0.323)
MAM	• NorthWest, cyclonic (+0.316) • North, cyclonic (+0.358)	• East, indifferent (-0.339)
JJA		
SON		• South, anticyclonic (-0.414)

ACKNOWLEDGEMENT

REFERENCES
[1] H. Sodemann et al., Int. J. Clim. **30**, 947 (2009).
[2] T. Jenk, PhD Thesis, University of Bern (2006).
[3] T. Weusthoff, Meteoschweiz Arbeitsbericht Nr. 235 (2011).

ANALYZING TEMPERED ICE: RESEARCH CHALLENGES

P.A. Pavlova (PSI, Empa & Univ. Bern), P. Schmid (Empa), C. Bogdal (ETHZ), M. Schwikowski (PSI & Univ. Bern)

The first surface-to-bedrock temperate ice core was drilled on the Silvretta glacier. Dating and analyzing this ice core introduces a completely new research field and, thus, a major scientific challenge.

The main goal of the SNSF project „Accelerated release of persistent organic pollutants (POPs) from Alpine glaciers" aims at understanding the role of melting glaciers as secondary source of organic contaminants. Therefore, reliable data about ice core profiles of POPs are required. This task represents major scientific challenges as most Alpine glaciers are temperate glaciers. Temperate ice contains 0.1% to 2% liquid water, mostly at grain boundaries, which is expected to affect the signal of the conventional ice core proxies.

From 20 to 25 April 2011 a 101 meter long surface-to-bedrock ice core was collected from Silvretta glacier (46°51'N, 10°06'E, 2927 m a.s.l.). The drilling site was chosen on the col of the glacier, where the lateral flow of the glacier ice is expected to have a negligible influence and the flat smooth surface of the glacier facilitates the positioning of the drilling equipment (Fig. 1). Silvretta glacier is a temperate glacier with ice temperatures near the melting point from 10 m below surface down to the bedrock. Therefore, a modified version of the thermal drill had to be developed and was used here for the first time [1]. This new equipment includes a heavier upper barrel instead of the usual fluid containers to ensure higher melting speed. Power supply for the energy consuming thermal drilling was ensured by two gasoline generators with a capacity of 2 kW each. Because of the unusually high temperatures during daytime, the collected ice cores were stored in insulating boxes covered with snow to assure a temperature below -1º C.
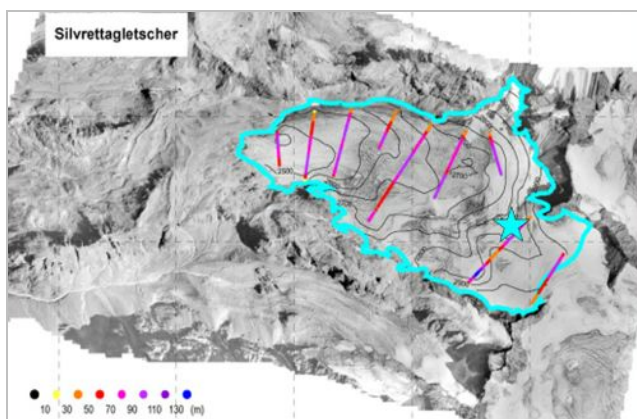
Fig. 1: Silvretta glacier thickness obtained by ground penetrating radar. Drilling site marked by a star [2].

Already at the drill site it was possible to observe some characteristics in the structure of the Silvretta ice core. Particularly impressing was to notice that the glacier is strongly affected by melting, consisting of alternating layers of superimposed ice and normal glacier ice containing air bubbles. The superimposed ice layers are sometimes almost 1 meter thick, containing macro

and micro deposits (Fig. 2). This Silvretta ice core will be used to examine POPs' contamination in pristine areas of the Swiss Alps with a particular focus on the effect of melting and percolating water on their concentration in glacier environments. In order to fulfil this aim and to better understand the processes occurring in the glacier ice matrix, further measurements next to POP quantification are necessary. Independent dating techniques using radioactive isotopes (^{3}H and ^{210}Pb) and the methane concentration in air bubbles will be compared with existing glacier mass balances to obtain a reliable age-depth relationship for the Silvretta ice core. Black carbon will be analysed to examine adsorptive effects of soot particles on POPs.

Fig. 2: M. Schwikowski with the bottom most segment of the Silvretta ice core with embedded pieces of rock.

Measuring ultra-traces of POPs in glacier ice represents a difficult task. The expected concentrations in the range of pg/g ice demand the use of specific and highly sensitive detection methods, which is accomplished by gas chromatography coupled to high resolution mass spectrometry. The conventional methods for sample preparation include fluid or solid extraction using large amounts of solvents. Since the target POPs are ubiquitous contaminants, minimization of background concentrations is the ultimate objective of a suitable method. According to this, an alternative preparation method based on minimal contact of the sample with ambient air and any surfaces is being developed and tested. To do so, we are currently working on an extraction through a thin coated quartz capillary. The target substances are eluted with very small amounts of solvent. In order to optimize the method efficiency and the handling procedure, different performance tests are carried out.

REFERENCES

[1] M. Schwikowski et al., Ann. Rep. Lab. of Radio- & Environ. Chemistry, Uni Bern & PSI (2010), p. 33.

[2] A. Bauder VAW/ETHZ, Pers. Communication.

INFLUENCE OF PARTICULATE MATTER ON THE ALBEDO
OF PLAINE MORTE GLACIER, SWISS ALPS

E. Bühlmann (Univ. Bern), P.A. Herren (Univ. Bern & PSI), S. Brütsch (PSI), M. Hoelzle (Univ. Fribourg)
M. Schwikowski (PSI & Univ. Bern)

Natural fluctuations of a glaciers albedo can be substantially altered by the accumulation of surface deposits containing soot, mineral dust, algae and decomposing organic matter. This pilot study was an attempt to identify the most relevant biogeochemical components contributing to the observed albedo reduction on Plaine Morte glacier

INTRODUCTION

Particulate matter deposits were found to reduce a glaciers surface albedo and therefore enhance melting and contribute to global warming by additional light-absorption [1]. In this regard, soot from fossil fuel combustion was so far most emphasised due to its strong absorption properties and its anthropogenic origin [2]. However, supra-glacial particulate deposits, generally termed cryoconite, have been shown to contain a diversity of additional absorbing components, including mineral dust, algae and decomposing organic matter [3]. The present study aimed to investigate the biogeochemical composition of cryoconite and to determine the relative contribution of its different components to observed estival albedo reductions on an Alpine glacier. The study site at Plaine Morte glacier (46°23'N, 7°29'E) is situated in the western Swiss Alps and has been previously reported to be characterised by exceptional sensitivity towards changes in the energy budget (e.g. albedo) due to its small inclination [4].

METHODS

In the course of the ablation season in 2010, broadband albedo and spectral reflectance were measured and snow samples, particulate matter and ice samples were collected for biogeochemical analyses. Major ions and trace elements were used to identify impurity sources within the snowpack. The composition of cryoconite was analysed by determining the bulk mineralogy, the organic fraction and the elemental carbon (EC) content. Biogenic matter and microorganisms were additionally assessed qualitatively by microscopic techniques. The obtained cryoconite composition was then related to the observed albedo reduction between June and August 2010 (from 0.74 to 0.16) to quantify the relative contribution of each of the cryoconite compounds.

Tab. 1: Relative biogeochemical composition of cryoconite samples (IS1 and IS4-7).

Cryoconite composition	IS1	IS4	IS5	IS6	IS7
Cryoconite load (g/m²)	124.2	102.1	423.5	385.1	221.2
Mineral dust (%)	39.5	40.8	46.1	43.2	40.6
Organic matter (%)	6.4	8.5	9.2	9.2	9.2
EC (%)	0.4	1.1	0.9	1.5	0.9
Unexplained fraction (%)	53.8	49.6	43.8	46.1	49.3

Fig. 1: Picture of a glacial moulin illustrating layers of annual particulate matter deposits within the ice on Plaine Morte glacier.

RESULTS

Cryoconite deposits were found to be heterogeneously distributed on the glacier surface, but showed comparable biogeochemical composition with predominant contribution from mineral dust of local origin (Tab. 1). Due to a lack in accurate albedo models, the relative contribution of cryoconite components to the albedo reduction could only be roughly estimated. However, the results stressed the importance of both EC and humic substances for the absorption properties of cryoconite and indicated a feedback-mechanism involving liquid water. Cryoconite was enriched in organic matter and EC compared to local loose rock, indicating slow removal processes, high biological activity and multiannual accumulation by outcropping dust layers from melting glacier ice (Fig. 1). Therefore, the overall-effect of cryoconite might increase in the course of glacier retreat.

REFERENCES

[1]   J. Hansen et al., PNAS, **101**, 2 (2003).
[2]   S.G. Warren et al., J. Atmos. Sc., **37** (1980).
[3]   N. Takeuchi, J. Glac., **55**, 192 (2009).
[4]   F. Paul et al., EARSeL eProceedings, **4** (2005).

BLACK CARBON ANALYSIS IN ICE CORES

I. Wendl (Univ. Bern & PSI), M. Gysel, M. Laborde (PSI/LAC), A. Eichler (PSI), M. Schwikowski (PSI & Univ. Bern)

Here, the optimization of a method for measuring Black Carbon in ice is presented. The new set-up, containing an Apex Q nebulizing system and a single soot particle photometer, is capable of transporting larger particles than the previous one. Furthermore, sample treatment could be optimized, the best treatment being no acidification, sonication for at least 30 min and no stirring.

INTRODUCTION

Black Carbon (BC) is generated by incomplete combustion of biomass and fossil fuels. Due to its light-absorbing properties it affects climate. On the one hand, it has a direct warming effect in the atmosphere; on the other hand, when deposited on the earth's surface, it changes the albedo. In case of snow and ice this means that it accelerates melting.

METHOD DEVELOPMENT

In order to determine the BC concentration in ice a single particle soot photometer (SP2, Droplet Measurement Technologies, DMT, Boulder, USA) is used. Within this instrument, single BC particles are heated to their boiling point (~4000 K) by a Nd:YAG-laser. At that temperature the BC particles emit incandescent light which then is detected by two photomultiplier tubes (PMT). The intensity of that light beam is proportional to the BC mass in the particle (for further details see [1]).

Previous measurements with an ultrasonic nebulizer (U5000AT[+], CETAC Technologies, Nebraska, USA) indicated a loss of particles on their way from the liquid sample to the SP2, thus pointing at a nebulizer issue (e.g. [2]). Therefore, a new set-up, including a jet nebulizer (Apex Q, Elemental Scientific Inc., ESI, Omaha, USA), was tested and shown to be more effective, especially in transporting larger particles (Fig. 1). Since large particles contain most of the mass, those are particularly important in climate concerns.
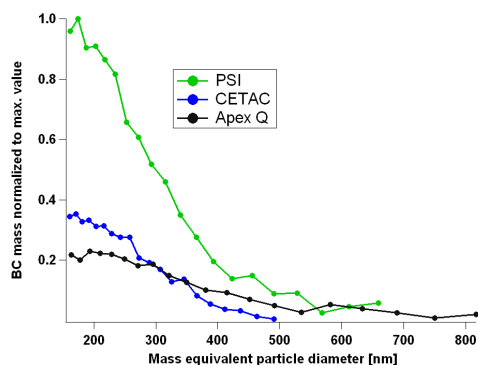
Fig. 1: Size distribution of a BC standard material (Aquadag[®], Henkel Corporation, Madison Heights, Michigan, USA) measured with different nebulizers. PSI: custom-built "Collison-type" nebulizer by the Laboratory of Atmospheric Chemistry, PSI; CETAC: ultrasonic; Apex Q: jet.

First tests concerning sample treatment (acidification to 0.5M HNO_3, sonication for different time spans and stirring) indicate the optimal treatment to be no acidification, sonication for at least 30 min and, due to no great additional effect and potential source for cross-contamination or dilution, no stirring (Fig. 2 & 3).
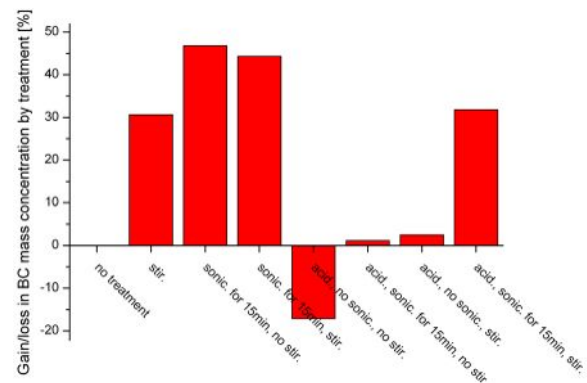
Fig. 2: Gain/loss in BC mass concentration by different treatment of snow from the Jungfraujoch, Switzerland.
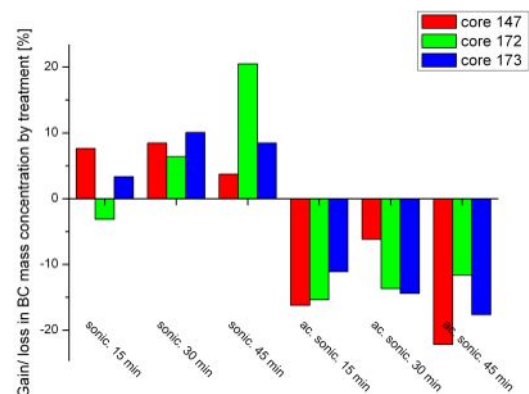
Fig. 3: Gain/loss in BC mass concentration by different treatment of samples of the 2009 Lomonosovfonna ice core from Svalbard.

Further optimization, also regarding material of sample containers, is planned. Finally, BC will be analyzed in several ice cores retrieved by PSI.

REFERENCES

[1] J. P. Schwarz et al., J. Geophys. Res., **111**, D16207 (2006).
[2] M. Schläppi, PhD thesis, Univ. Bern (2010).

FIRST DATING ATTEMPT FOR THE 2009 ICE CORE FROM LOMONOSOVONNA, SVALBARD

I. Wendl (Univ. Bern & PSI), A. Eichler, L. Tobler (PSI), J. Eikenberg (PSI/ASI), T. Martma (Univ. Tallinn), E. Isaksson (NPI), E. Vogel (Univ. Bern), M. Schwikowski (PSI & Univ. Bern)

A first dating attempt has been conducted on the uppermost 23.6 m weq of the Lomonosovfonna ice core. The three independent methods applied include identification of the tritium horizon, ^{210}Pb decay and annual layer counting along the $\delta^{18}O$ record. They show that the 1963 tritium peak is detectable and seasonal variations in the $\delta^{18}O$ record permit annual layer counting.

In March 2009 a 149.5 m long ice core was drilled on Lomonosovfonna, Svalbard, Norway (1202 m asl; 78°49`24``N, 17°25`59``E). In spite of melt, this glacier was proven to be feasible as climate archive, containing a seasonal signal for major ions as well as stable isotopes (e.g. [1]).

Here, a first attempt for dating the uppermost 23.6 m weq of the core is shown. Three different methods have been used, including identification of reference horizons, annual layer counting and nuclear dating with ^{210}Pb decay.

The first method applied is the identification of the horizon with the highest tritium values attributed to the year 1963, resulting from preceding nuclear weapon tests. The tritium activity in samples with a resolution of about 60 cm was determined by liquid scintillation counting (Fig. 1). The tritium maximum of 1400 TU was observed at a depth of ~23 m weq which is in general agreement with the high-resolution tritium profile from the Lomonosovfonna 1997 core [2].
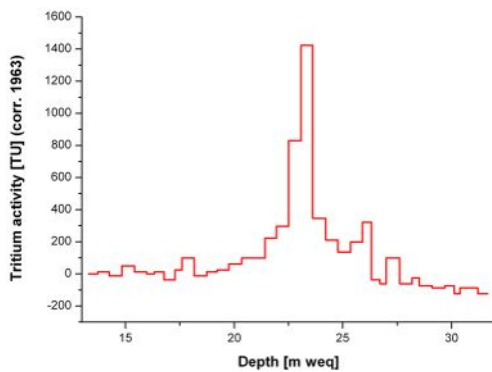
Fig. 1: Tritium activity in samples of the Lomonosovfonna ice core.

The second dating technique is the determination of the ^{210}Pb activity with depth. Assuming a constant input to the glacier, the decrease in ^{210}Pb activity gives an approximate age (preliminary results given in Fig. 2). The low ^{210}Pb surface activity of about 40 mBq/kg is consistent with values expected for maritime air masses and with data from a previous core from Lomonosovfonna [3]. Up to date, the ^{210}Pb analysis is not finished yet. A constant background activity is expected to be reached in the deeper part of the core. According to this value a background correction will be conducted which will probably result in a better agreement with the tritium horizon.
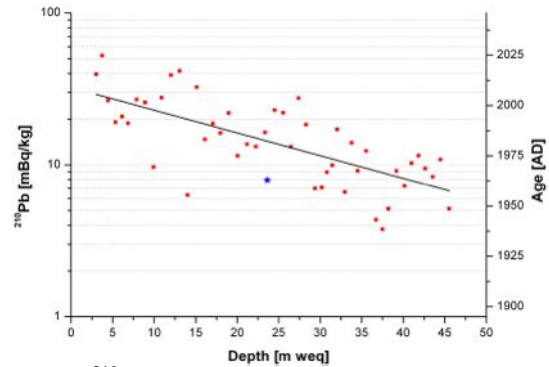
Fig. 2: ^{210}Pb activity (red squares) and linear fit (black line) with corresponding age vs. depth of the Lomonosovfonna ice core. The tritium peak is displayed by a blue asterisk.

Additionally, dating was conducted down to the tritium horizon by annual layer counting along the $\delta^{18}O$ record. Since $\delta^{18}O$ functions as a sort of thermometer, indicating higher (lower) temperatures for higher (lower) $\delta^{18}O$ values, its seasonal variations can be used for counting years. Thus, in combination with the tritium horizon at a depth of ~23.6 m weq, 46 annual cycles can be counted down to that depth (Fig. 3). The preliminary dating results in an average net accumulation of ~0.51 m weq/yr which is slightly higher than the values of the 1997 Lomonosovfonna core [4].
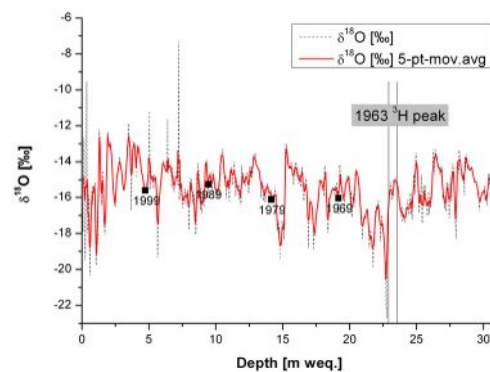
Fig. 3: $\delta^{18}O$ record with the tritium peak indicated. Preliminary annual layer counting resulted in the age displayed.

REFERENCES

[1]   V. Pohjola et al., J. Geophys. Res., **107** (2002).
[2]   L.G. Van der Wel et al., J. Glac. **57**, 1087 (2011).
[3]   J. F. Pinglot et al., J. Glac. **49**, 149 (2003).
[4]   T. Kekonen et al., J. Geophys. Res., **110**, D07304 (2005).

TRACE ELEMENT ANALYSIS IN A FIRN CORE FROM ILLIMANI, BOLIVIA BY CIM-ICP-SF-MS

G. Gramlich (PSI & Univ. Bern), L. Tobler (PSI), T. Kellerhals (KUP), M. Schwikowski (PSI & Univ. Bern)

Trace element analysis by Continuous Ice Melting (CIM) Inductively Coupled Plasma Sector Field Mass Spectrometry (ICP-SF-MS) was applied to the upper 27 m of firn of an ice core retrieved from the Illimani glacier, Bolivia. The applicability of the CIM device with its ice melting head for the less dense firn was assessed. Concentration records were extended to the uppermost part of the core.

Trace element analysis in ice cores from glaciers and ice sheets provide valuable time resolved information on the concentration of key elements in the past. Especially, highly-resolved trace element records of the last hundred years allow for a detailed insight into anthropogenic pollution history as well as into geochemical events e.g. volcanic eruptions or outstanding long-range dust transport from the Sahara. While trace element records have been obtained for the ice section of the 138.7 m long ice core retrieved from Nevado Illimani glacier by continuous ICP-SF-MS analysis [1, 2, 3], the firn section, i.e. the part younger than 1962, remained unexamined by this method up to now.

Of special interest is information on the historical evolution of Pb, an anthropogenically influenced element, which is only sparsely documented for South America [4]. Furthermore due to the geographical location of the Illimani glacier at the eastern edge of the Cordillera Mountains, the source for precipitation and therefore also pollutants derive mainly from the Amazon basin by tropical north-eastern winds.

To verify the applicability of the Continuous Ice-Melting (CIM) device with its melting head which is normally used for the more compact ice of deeper glacier layers, the concentrations of Mg were compared with values independently analysed by ICP-OES from discrete samples. For the firn section between 12 and 23 m, equivalent to the period between 1979 and 1990, equal concentrations for both methods with no indication for smearing or contamination were found (Fig. 1). Thus the CIM set-up is in principal suitable for the analysis of firn cores from Illimani.
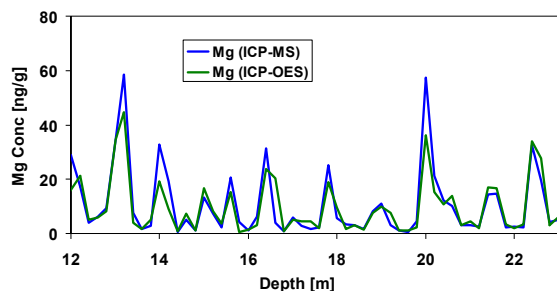
Fig. 1: Comparison of ICP-SF-MS (blue curve) and ICP-OES (green curve) Mg records.

The record for the trace element Pb could be complemented beyond the year 1963. The data suggest a moderate rise in Pb concentration after a period of lower abundance following the end of World War II (Fig. 2).
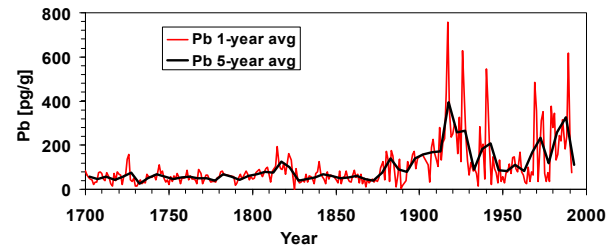
Fig. 2: Ice core record of Pb concentrations extended by data of the firn section after 1963.

A mean annual layer thickness of 0.8 m for Illimani firn combined with highly resolved CIM-ICP-MS analysis allow for an insight into seasonal variations of minor and trace element concentrations. As an example shown in Fig. 3a, the dust related, geogenic elements Al and Ce display nearly parallel concentration curves and maxima, that can be attributed to the dry period around June [1]. On the other hand Pb exhibits, beside similar higher concentrations during the dry period, a deviating behaviour which might be attributed to anthropogenic activity (Fig. 3b).
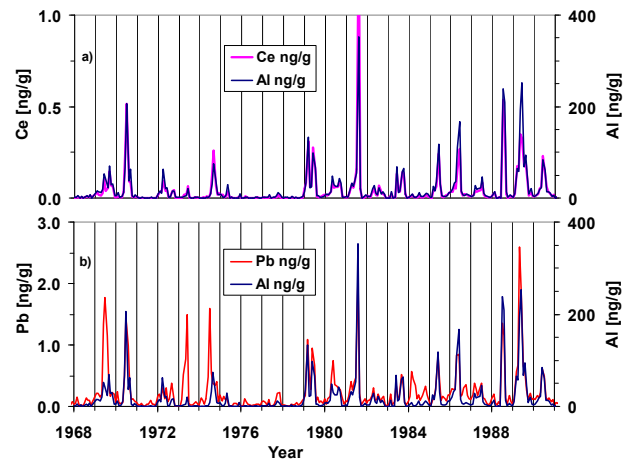
Fig. 3: a) Concentration records (monthly average) of the two geogenic elements Al (blue line) and Ce (magenta). b) Anthropogenically influenced element Pb (red) is included instead of Ce for comparison. The black vertical gridlines mark the turn of the year.

REFERENCES
[1] S. Knüsel, PhD thesis, Univ. of Bern (2003).
[2] T. Kellerhals, PhD thesis, Univ. of Bern (2008).
[3] T. Kellerhals et al., Environ. Sci. Tech. **44**, 888 (2010).
[4] M. E. Kylander et al., Earth Planet. Sci. Lett. **290** (2010).

ISOTOPICAL AND HYDROCHEMICAL ANALISYS IN THE MENDOZA RIVER BASIN, CENTRAL ANDES OF ARGENTINA

S. Crespo (PSI & IANIGLA-Conicet), L. Gomez, J. Aranibar (IANIGLA-Conicet), S. Brütsch (PSI), M. Schwikowski (PSI & Univ. Bern)

The stable isotope composition and major ion concentration in samples of stream water, precipitation, groundwater, glacier ice, and snow was used to distinguish different water sources feeding the rivers of the Mendoza river basin.

Water from the Mendoza River, in the North of Mendoza province (Argentina), derives mainly from glacier and snow melt. This river provides water for domestic use, irrigation, industry and hydroelectric energy generation [1]. In these latitudes (32ºS), there are three mountain ranges with direction North-South. From East to West: Precordillera, Cordillera Frontal and Cordillera Principal.

Given these features, it is possible to infer that geology, precipitation systems, and altitude differences in recharge areas have an influence on the chemical and isotope composition of the water in the different basin areas. With a temperature increase scenario and changes in the precipitation regimes [2], it is important to differentiate and quantify the recharge sources in the different areas in order to plan adaptation policies.

The objective of this work is to obtain isotope and chemical tracers that allow us to distinguish different water sources which feed the different rivers of the Mendoza river basin. We expected to find a characteristic stable isotope composition of the water originating from the Cordillera Principal, Cordillera Frontal and Precordillera, based on the different altitudes, temperatures and moisture sources (Atlantic vs Pacific) of precipitation. We also expected to find a different chemical fingerprint of the water originating from snow, glacier melting and groundwater.

For this purpose, we collected water from streams, precipitation, groundwater, glacier ice, and snow in different time periods (February, May, and August 2011), with a total of 121 samples. The study area is located in the high basin area from the Mendoza River, from 1370 m a.s.l. in the entrance of the Potrerillos dam, to 4700 m a.s.l. in the Parque Provincial Aconcagua region. The chemical analyses to determine major ion concentrations and the stable isotope ratio $\delta^{18}O$ were carried out in the Paul Scherrer Institut (PSI), Switzerland.

According to the expectations, we found isotopic differences of streams originating in the different mountain ranges. $\delta^{18}O$ values decreased from East to West, showing the lowest values in the Cordillera Principal region and the highest values in the Precordillera region (Figure 1).

The chemical composition of surface waters showed a distinct trend from West to East, from calcium and magnesium sulphate waters in the Cordillera Principal to calcium bicarbonate in the Frontal Cordillera (Figure 2). This evolution is assumed to reflect the geological features of the different mountain ranges.

This study allows us to propose that it is possible to identify the contributions of different hydrologic components (glacier, snow, groundwater) and geographic areas (Cordillera Principal, Cordillera Frontal and Precordillera) to the streams of the Mendoza river basin.
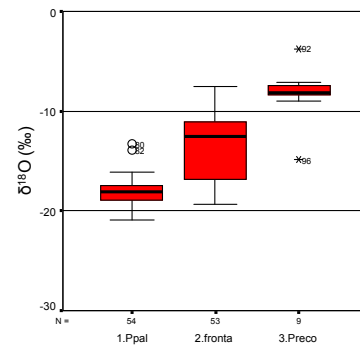
Fig. 1: Box-Plot diagram showing $\delta^{18}O$ values in streams and groundwater from North of Mendoza. 1Ppal: Cordillera Principal; 2fronta: Cordillera Frontal; 3Preco: Precordillera.
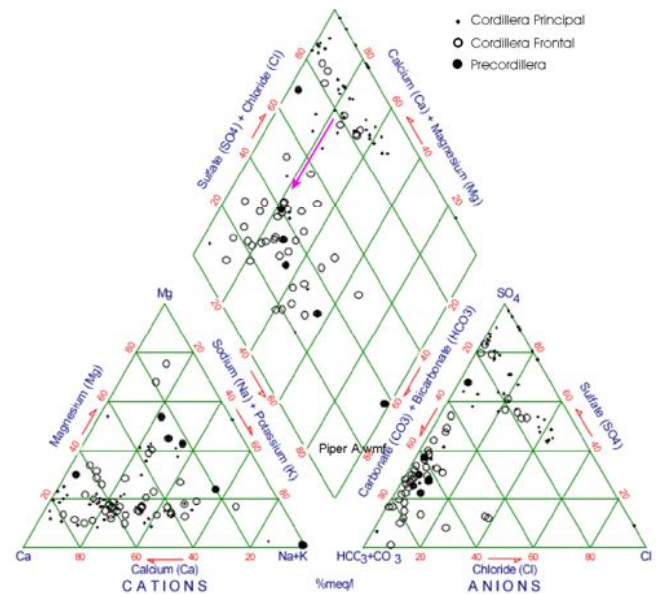
Fig. 2: Piper diagram showing the chemical composition of water from streams and groundwater from North of Mendoza.

REFERENCES
[1] M. Masiokas et al., J. Clim. **19**, 6334 (2006).
[2] R.S. Bradley et al., Geophys. Res. Lett., **31**, doi:10.1029/2004GL020229 (2004).

INFORMATION DEDUCED FROM ^{210}Pb ACTIVITY CONCENTRATIONS MEASURED ALONG AN ICE CORE FROM EASTERN TIEN SHAN

W. Chaomin, S. Hou (Nanjing Univ. & State Key Lab. of Cryospheric Sciences, Lanzhou, China),
H.W. Gäggeler, L. Tobler (PSI), S. Szidat, E. Vogel (Univ. Bern)

An ice core drilled to bedrock in 2005 in the Eastern Tien Shan (43°03'19"N, 94°19'21"E, 4512 m a.s.l.) was dated with ^{210}Pb. The lowermost samples showed background values for the ^{210}Pb activity concentrations, hence were older than about 150 years. The surface activity concentration of ^{210}Pb was about 400 mBq/L and the net annual accumulation rate 21 cm w.eq./y. No indication for thinning nor for melting was observed for the analysed part of the ice core.

In 2005, two ice cores to bedrock (58.7 m and 57.6 m in length for Core 1 and Core 2, respectively) were recovered from a dome on the Miaoergou glacier (43°03'19''N, 94°19'21''E, 4512 m a.s.l.) [1]. There is no modern glacier to the East of the Miaoergou glacier in the eastern Tien Shan. The low borehole temperature at the drilling site (−7.2°C at 10 m depth and −8.2°C at the bottom, respectively [2]) is beneficial for the preservation of ice core records. Therefore, a first study of trace elements contained in Core 2 was already performed down to 17 m (= 14 m w.eq.) [1]. Besides some heavy metals also the bomb peak assigned to the year 1963 was found at about 12.5 m depth (= 10.0 m w.eq.) based on total β-counting [1]. The analysis was stopped at a depth of 17 m depth (assigned to the year 1953) due to lack of dating of the deeper part of the core.

An attempt was therefore made to date Core 2 down to bedrock with ^{210}Pb using the technique described in [3]. The sample size was about 300 g. A thin slice of the outermost part of the core was taken for analysis to get a continuous record of ^{210}Pb.

The data are depicted in figure 1. The activity concentrations between 35.2 m w.eq. and bedrock at 47.9 m w.eq. stayed constant with a value of 5.5 mBq/L. This value was considered as background and was subtracted from all ^{210}Pb values above 35.2 m. Hence, the data depicted in figure 1 represent the net ^{210}Pb activity concentrations.

The ^{210}Pb dating agrees within uncertainty well with the bomb horizon in 1963 at 10.0 m w.eq.

The surface activity of about 400 mBq/L is very high, even higher than those observed at other continental sites such as at Belukha, Russia with 280 mBq/L [4] or nearby Tsambagarav, Mongolia [5] with the same surface activity concentration. This means that the ^{222}Rn concentration in air and, thus, the ^{238}U concentration in nearby soil must be high, as this is the source of ^{210}Pb.

The average annual net accumulation rate that emerges from figure 1 is 21 cm w.eq./y.

It is interesting to note that until a depth of about 35 m w.eq., which is 73 % of the total length, no significant indication for thinning of the glacier is observed.

From the continuous decrease of the ^{210}Pb activity concentration with depth it also follows that negligible melt processes seem to influence this glacier site. Otherwise a high fluctuation of the activity profile is expected (see e.g. a ^{210}Pb activity profile from the Vernagtferner in the Austrian Alps [6], where percolating

melt water displaced ^{210}Pb downwards to the next layer of mineral dust at which ^{210}Pb was adsorbed.)
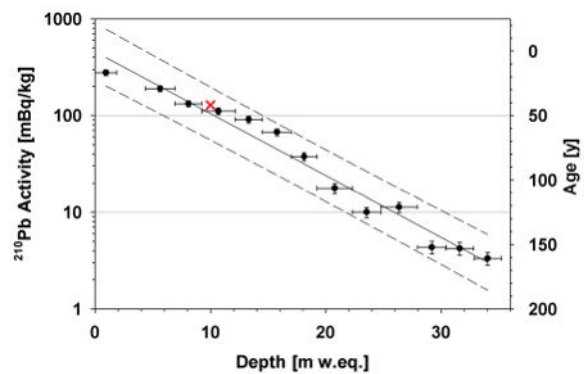
Fig. 1: Net ^{210}Pb activity concentrations representing the measured values after subtracting a background value of 5.5 mBq/L. The right axis depicts the resulting ^{210}Pb age normalized to the year 2005. The cross indicates the bomb horizon deduced from β-counting assigned to the year 1963 [1].

ACKNOWLEDGEMENT

REFERENCES

[1] Y. Liu et al., J. Geophys. Res. **116**, D12307 (2011).

[2] Y. Liu et al., J. Mt. Sci., **6**, 221 (2009).

[3] H.W. Gäggeler et al., Ann. Rep. Lab. of Radio- & Environ. Chemistry, Uni Bern & PSI (2010), p. 64.

[4] S. Olivier et al., J. Geophys. Res. **111**, D05309 (2006).

[5] P.A. Herren et al., Ann. Rep. Lab. of Radio- & Environ. Chemistry, Uni Bern & PSI (2010) p. 21.

[6] H.R. von Gunten et al., Z. für Gletscherkunde und Glazialgeol., **18 (1)**, 37 (1982).

EXOTIC RADIONUCLIDES FROM ACCELERATOR WASTE FOR SCIENCE AND TECHNOLOGY
NUCLEAR CHEMISTRY FOR NUCLEAR SCIENCES

D. Schumann (PSI) for the ERAWAST collaboration

The second workshop on Exotic Radionuclides from Accelerator Waste for Science and Technology (ERAWAST II) was held from 29.8.-2.9.2011 at PSI. 36 participants from Europe, America and Australia came together to present recent achievements and discuss planned future experiments.

INTRODUCTION

Five years ago, the first ESF-sponsored Exploratory ERAWAST workshop was organised at PSI. ERAWAST means: Exotic Radionuclides from Accelerator Waste for Science and Technology. The initiative was aimed to explore the possibilities to isolate rare exotic radionuclides from existing accelerator waste of high-power accelerator facilities like that at PSI on the one side and identify potential users for those isotopes on the other side.

The 36 participants of the present workshop presented first encouraging results and decided to continue the successful international collaboration. In total, 34 talks were given addressing mainly topics from the nuclear astrophysics field and basic nuclear physics.

ISOTOPES AND THEIR SOURCES

Exotic isotopes can be chemically separated from exposed components of the high-power accelerator facilities of PSI and/or from other sources (reactors, other accelerator facilities). Since the components are hit with protons and secondary particles up to 590 MeV, the entire spectrum of radionuclides with mass numbers up to one unit higher than the target mass, have to be expected.

The following sources containing some examples for rare exotic isotopes are currently available at PSI:

SINQ cooling water	^{7}Be, ^{22}Na, ^{54}Mn
Copper beam dump	^{44}Ti, ^{53}Mn, ^{26}Al, ^{60}Fe
Graphite targets	^{7}Be, ^{10}Be
Steel samples from STIP	^{44}Ti, ^{53}Mn, ^{26}Al
Lead samples from SINQ	^{207}Bi, ^{182}Hf, ^{148}Gd

SELECTED ACHIEVEMENTS

- Determination of the neutron capture cross section of ^{60}Fe at stellar energies [1]
- Re-measurements of the half-life of ^{60}Fe [2]
- Determination of the neutron capture cross section of ^{63}Ni and ^{62}Ni at n_TOF [3]

PLANNED EXPERIMENTS

- ^{44}Ti(α,p) (target) at HZDR, Germany
- ^{44}Ti(α,γ); ^{44}Ti(α,p); ^{44}Ti(p,γ) (beam) at CERN ISOLDE, Switzerland and TRIUMF, Canada
- ^{26}Al(n,p) (target) at CERN n_TOF , Switzerland
- ^{7}Be(n;α) (target) at SARAF, Israel
- ^{53}Mn(n,γ) (target) at PSI and n_TOF CERN, Switzerland
- ^{53}Mn half-life measurement at PSI, Switzerland
- ^{10}Be halo nuclei studies (beam) at INFN Catania, Italy

REFERENCES

[1] E. Uberseder et al., PRL 102, 151101 (2009).
[2] G. Rugel et al., PRL 103, 072502 (2009).
[3] C. Lederer et al., 2nd ERAWAST workshop, 29.8.-2.9.2011, Villigen, Switzerland, abstracts, p. 17.

Fig. 1: Participants of the ERAWAST II workshop 2011 at PSI

PREPARATION OF A $^{62/63}$Ni TARGET FOR MEASUREMENT OF NEUTRON CAPTURE CROSS SECTIONS AT n_TOF CERN

D. Schumann, M. Ayranov, S. Köchli (PSI), C. Lederer (Univ. Vienna), C. Massimi (INFN Bologna),
F. Käppeler (KIT) and the n_TOF collaboration

Two $^{62/63}$Ni samples, foreseen as target material for studies of neutron capture cross sections at the n_TOF facility at CERN, were purified from the decay product ^{63}Cu using wet chemistry. A decontamination factor of 2000 for the copper fraction could be achieved.

INTRODUCTION

About half of the overall abundances of elements heavier than Fe are produced by the slow neutron capture process (s-process). This process occurs during He burning stages of stellar evolution and is characterized by small reaction rates, thus the reaction flow takes place close to the valley of stability - if a radioactive nuclide is produced, its decay happens faster than a subsequent neutron capture. An exception are long-lived radionuclides, where neutron capture competes with radioactive decay and the reaction path at these so-called branching points is very sensitive to the neutron capture cross section. Despite the importance of neutron capture cross sections at branching points for investigating physical conditions of s-process sites and calculating s-abundances, few experimental data are available since samples are hard to obtain and measurements are often complicated by additional background due to sample activity.

^{63}Ni, with a laboratory half-life of 100.1 years, represents such an example. It is produced in the weak s-process taking place in massive stars during two different burning stages: during He Core burning (at temperatures of kT = 26 keV), where neutron densities are too small to bypass the decay channel and ^{63}Ni entirely decays to ^{63}Cu, and later during C shell burning (kT = 91 keV) where subsequent neutron capture on ^{63}Ni becomes the dominant reaction. Network calculations showed that e.g. the final $^{63/65}$Cu abundances strongly depend on the ^{63}Ni(n,γ) cross section [1]. However, no experimental data are available above thermal neutron energies and all estimates for stellar environments are based on either calculations or extrapolations of the thermal cross section. Therefore, the n_TOF collaboration proposed to measure the neutron capture cross section of ^{63}Ni at the n_TOF facility from thermal up to energies of hundreds of keV [2].

SAMPLE DESCRIPTION AND PREPARATION

The material available for the experiment originated from two metallic nickel targets: one from LANL with 347 mg and one from KIT Karlsruhe with 661 mg. Both consist of enriched ^{62}Ni with 98% and were produced for Mössbauer spectroscopy at TU Munich by irradiation in high flux reactors about 30 years ago to a final content of around 11% ^{63}Ni. Since the history of the material is not exactly known, and, moreover, the decay product ^{63}Cu disturbs the measurement due to neutron resonances, chemical separation of the Copper was mandatory.

CHEMICAL SEPARATION OF ^{63}Cu

The Ni metal was dissolved in 7 M HNO_3, evaporated to dryness and again dissolved in 1 M HCl. From this solution, CuS was precipitated by adding gaseous H_2S. In model experiments with natural Ni it could be demonstrated using ICP-OES, that a decontamination factor of 2000 for Cu could be obtained.

The precipitate was removed and $Ni(OH)_2$ was precipitated from the remaining solution by adding 5 M NaOH. The hydroxide was dried at 80°C and afterwards calcinated at 800°C to produce NiO. We obtained a total amount of 1147 mg NiO, corresponding to a chemical yield of 91%. The material was packed into a PEEK capsule, as can be seen in Fig.1.
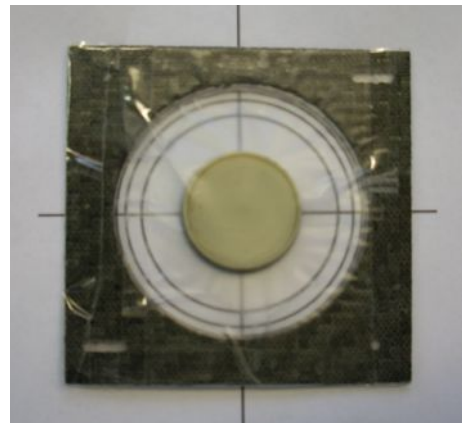
Fig. 1: Photo of the final $^{62/63}$Ni target

The neutron capture experiment took place in March/April 2011 at n_TOF CERN with extraordinary success. The data processing and the final isotopic characterisation of the target are currently underway, first results were presented at the second ERAWAST workshop [3] and the Annual n_TOF meeting [4].

REFERENCES

[1] M. Pignatari et al., Ap. J. 710, 1557-1577 (2010).

[2] C. Lederer, C. Massimi, et al., n_TOF proposal to the INTC committee INTC-P-283, (2010).

[3] C. Lederer et al., 2nd ERAWAST workshop, 30.8.-2.9.2011, Villigen.

[4] C. Lederer et al., n_TOF Annual meeting, 13.-16.12.2011, Lisbon.

PURIFICATION OF THE [53]Mn FRACTION FROM STABLE CHROMIUM – STIP I STAINLESS STEEL SAMPLES

M. Frei (PSI & ETH Zürich), M. Ayranov (PSI), M. Bunka (Univ. Bern & PSI), D. Schumann (PSI), R. Dressler (PSI)

STIP I originating stainless steel samples irradiated with high energy protons are a source of significant amounts of [53]Mn. In order to use the material for nuclear astrophysics experiments, a radiochemical procedure for the selective separation from isobarically interfering Cr has been developed.

INTRODUCTION

The radionuclide chronometer system ^{53}Mn–^{53}Cr (half-life ($t_{1/2}$): 3.7 ±0.4 Ma) is particularly suited for the study of the first ~20 million years of the solar system [1]. However, a more precise half-life determination will improve the accuracy of the dating method. An amount of ca. $3 \cdot 10^{14}$ atoms, sufficient for such an experiment, can be separated from proton-irradiated stainless steel samples [2]. The main expected interference is the isobar of stable ^{53}Cr which is present in the sample matrix. Therefore, a prerequisite for the successful half-life re-determination of ^{53}Mn is the selective chemical separation of Cr with a high decontamination factor. The separation was performed by solvent extraction with trioctylamine from hydrochloric acid media. The separation efficiency was controlled by ^{51}Cr and ^{54}Mn as radio-tracers.

EXPERIMENTAL

The stock solution containing ^{54}Mn and 20 mg/ml of stable chromium originates from the STIP I ^{44}Ti separation procedure [2]. ^{51}Cr was produced by irradiation of Cr_2O_3 with thermal neutrons in the Swiss Spallation Neutron Source (SINQ). Irradiated Cr_2O_3 was dissolved in 5 ml 6 M HCl. Extraction had been performed with 0.2 M trioctylamine (TOA) in cyclohexane [3]. The study of the extraction profile was performed with hydrochloric acid solutions in concentrations ranging from 1 M to 12 M, containing 20 kBq/ml ^{54}Mn and ^{51}Cr and 5 mg/ml stable carrier of both metals. 5 ml of the aqueous phase were shaken with an equal volume of 0.2 M TOA for 5 minutes in a 25 ml separation funnel. After the phase separation 1 ml aliquots from aqueous and organic phase were taken and the distribution of ^{54}Mn and ^{51}Cr was determined by gamma spectrometry.

The efficiency and selectivity of the separation was examined by extraction from 9 M HCl solution containing 100 mg of both Mn and Cr. Manganese is back extracted from TOA solution by equilibration with 0.5 M HCl.

RESULTS AND DISCUSSION

The pattern of the extraction profile for Cr and Mn is presented in figure 1. The maximum of the Mn extraction is found at 9 M HCl. Over the whole acid concentration region the Cr present in the organic phase is 1% to 3%. Since TOA is not extracting Cr(III), the presence of Cr is attributed to the contamination and a non-precise phase separation.
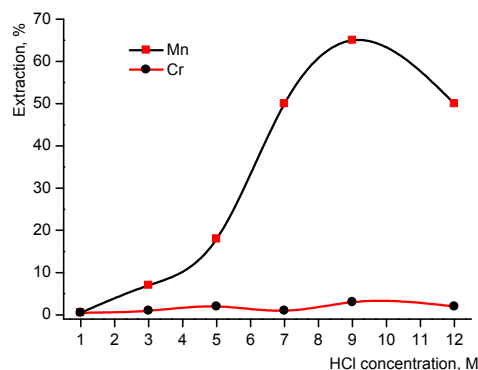
Fig. 1: Extraction of Mn and Cr with 0.2 M TOA as a function of HCl concentration.

In figure 2 the extraction efficiency of 200 mg Cr/Mn by multiple extraction steps is presented. After the fourth extraction Mn is quantitatively separated. In order to improve decontamination from Cr, all Mn fractions are collected and back extracted with 0.5 M HCl. The solution was conditioned in 9 M HCl and the extraction with 0.2 M TOA was repeated. The overall chemical yield of Mn separation is 81% and the decontamination factor of chromium is ca 9000.
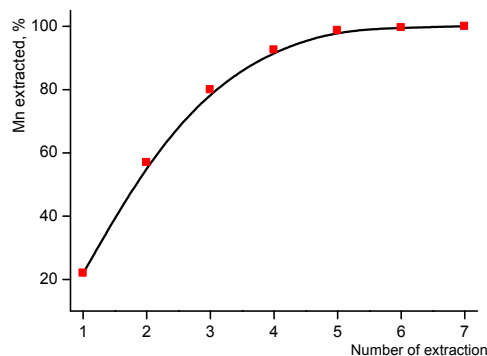
Fig. 2: Efficiency of Mn extraction from Cr with 0.2 M TOA as function of the number of extraction steps.

REFERENCES

[1] K. Yamashita et al., The Astrophys. J., **723**, 20 (2010).

[2] M. Bunka et al., Ann. Rep. Lab. of Radio- & Environ. Chemistry, Uni Bern & PSI (2011), p. 49

[3] S. Lahiri et al., Anal. Chem., **78**, 7517 (2006).

RE-DETERMINATION OF THE ^{60}Fe HALF-LIFE:
COMPARISON OF THE EXPERIMENTALLY DETERMINED AND CALCULATED ISOTOPIC COMPOSITION OF IRON

R. Dressler (PSI), I. Günther-Leopold, N. Kivel (PSI/NES), D. Schumann, M. Wohlmuther (PSI)

The isotopic composition of all stable iron isotopes as well as of ^{60}Fe in an aliquot of the sample used for the re-determination of the ^{60}Fe half-life were measured using MC-ICP-MS and compared with theoretical predictions.

SAMPLE & MC-ICP-MS MEASUREMENT

The authors reported in [1] about an ongoing experiment for the re-determination of the half-life of ^{60}Fe. In a previously conducted experiment [2] a significant deviation of the measured isotopic ratios of Fe isotopes from the natural abundance was observed although a total amount of about 5 mg stable iron was added during the chemical processing steps. The ^{60}Fe sample for the experiment discussed in this report was prepared from a copper beam dump as described in Uberseder et al. [3, 4]. Special care was taken to avoid additional contribution of stable iron during the separation, purification, and target preparation as well as during the reuse of the material for the present experiment [1].

The measurements of the isotopic composition were performed using the Neptune MC-ICP-MS (Thermo Fisher Scientific, Germany) at the PSI Hotlab using an APEX high efficient desolvating system with a PFA-ST micro flow nebulizer (65 µL/min) for sample introduction. Custom made cones out of Al were used to avoid elevated Ni background. The resolution of the mass spectrometer was about 2500. In total 25 individual measurements of the sample material and 50 of the IRMM-014 reference material were performed. The acquisition time for each measurement was 4.194 s. The measured isotopic ratios of mass 54, 57, 58, and 60 according to mass 56 were corrected for mass fractionation effects using the Russel law based on the isotopic ratio of mass 57 to 56. The isotopic ratios may also be influenced by an unknown amount of nickel in the sample. In a first test measurement it was found that the contribution of ^{60}Ni to the mass 60 is less then 10%. Unfortunately, the composition of nickel in the sample is also not natural
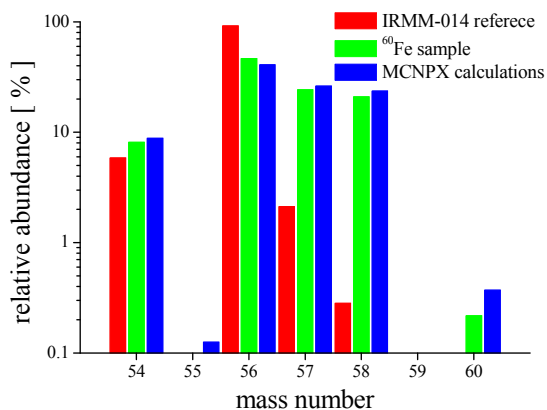
and a correction of the mass 60 value using other stable nickel isotopes is not possible. Therefore, an amount of 20 µg stable nickel was added to the MC-ICP-MS sample and afterwards chemical separated to re-establish a natural isotopic ratio of nickel isotopes. The total contribution of ^{60}Fe to the mass 60 signal was determined to be 35.92(38)% after this treatment. The abundances of iron (mass fractionation and nickel corrected) are shown in Fig. 1. The combined standard uncertainties of all values are smaller then 0.005.

MCNPX CALCULATIONS & DISCUSSION

The production of stable iron isotopes during the proton irradiation both from the copper itself, from impurities as well as via reactions of these materials with secondary particles will contribute to the final content of iron isotopes in the sample. Especially neutron activation of impurities in the copper can alter the resulting isotopic ratios essentially. Therefore, theoretical calculations were performed in order to predict the isotopic composition of iron in the copper beam-dump after the irradiation.

The data given in [4] were used to estimate the impurities in the copper material. The activation calculations have been performed with a patched version of MCNPX 2.5.0 [5] and the newly developed activation script as a driver for the calculation with SP-FISPACT [6] which allows treating residuals produced by high energy particles besides the activation of neutrons below 20 MeV. The results of the calculations are illustrated in Fig. 1 together with the MC-ICP-MS measurements.

The enhanced amount of heavier iron isotopes compared with the reference material is well reproduced by the calculations. Moreover, the remaining differences indicate that during the sample preparation less than 10% of the total iron content results from contaminations with natural iron.

Fig. 1: Abundance of iron isotopes according to MCNPX calculations, in IRMM-014 reference material, and in the present sample.

REFERENCES

[1] M. Ayranov et al., Ann. Rep. Lab. of Radio- & Environ. Chemistry, Uni Bern & PSI (2011), p. 51.

[2] G. Rugel et al., PRL **103**, 072502 (2009).

[3] E. Uberseder et al., PRL **102**, 151101 (2009).

[4] D. Schumann et al., Radiochim. Acta **97**, 123 (2009).

[5] F. Gallmeier (2007), private communication.

[6] R. A. Forrest, FISPACT-2003: User manual (2002).

SEPARATION OF ^{44}Ti, ^{26}Al, AND ^{53}Mn FROM IRRADIATED STEELS

M. Bunka, A. Türler (Univ. Bern & PSI), M. Ayranov (PSI), Y. Dai (PSI/GFA), D. Schumann (PSI)

High energy proton irradiated martensitic steel samples from the STIP I program were processed for the isolation of ^{44}T,. ^{26}Al, and ^{53}Mn isotopes being of interest for nuclear astrophysics experiments.

INTRODUCTION

^{44}Ti, ^{53}Mn, ^{26}Al, and others are attractive for applications in the field of nuclear astrophysics. Several proton-irradiated steels at PSI contain those isotopes and were taken into consideration for a preparative isolation. The in [1] envisaged material was a part of the PIREX gas chamber with a total content of about 100 MBq ^{44}Ti and a weight of 12 kg. First model studies were carried out and a chemical separation system could be developed aimed to isolate the two isotopes ^{44}Ti and ^{53}Mn [1]. Since the specific activities of the desired isotopes in this selected material were relatively low and, therefore, the processing would be time-consuming and cost-intensive, we switched now to another suitable source, the SINQ target-irradiation program (STIP), created more the 10 years ago to study radiation damage effects induced by high-energy protons and spallation neutrons, providing samples with specific activities of several magnitudes higher [2].

Additionally, after the second ERAWAST-workshop [3] it turned out, that the radionuclide ^{26}Al has a high priority for astrophysics experiments as well, and therefore, was also taken into account in the chemical separation system.

EXPERIMENTAL

The available materials for our purposes – martensitic steels (Optifer, Optimax A, and Optimax C) originate from the STIP I experiment, which was performed from July 1998 till December 1999 [2]. Typical shapes of the (tested) samples are shown in Figure 1.

Fig. 1: Samples of the OPTIMAX A type.

The elemental composition of the three steels is given in Table 1.

Tab. 1: Elemental composition of the 3 martensitic steels ; in wt%.

Steel	Fe	Cr	Ni	Mo	Mn	Ti	V	W
Optifer	bal.	9.48	0.06	0.002	0.55		0.245	0.985
Optimax A	bal.	9.3	< 0.01	0.09	0.60	< 0.01	0.24	0.97
Optimax C	bal.	9.5	< 0.01	0.15	0.40	< 0.01	0.25	1.9

In total, 38 samples with weights from 1 to 2 grams contain in total 300 MBq ^{44}Ti, 70 MBq ^{54}Mn (as a measure for the long-lived ^{53}Mn, which cannot be measured by γ-spectrometry), 70 MBq ^{60}Co and ~300 Bq ^{26}Al. The dose rates of the specimens vary from 1 - 9 mSv/h and are low enough to perform the separation in a fume hood with 10 cm lead shielding.

RESULTS AND DISCUSSION

The chemical separations were carried out following the procedures described in [1] with slight modifications concerning the element aluminium, whose behaviour being similar to that of chromium in all separation steps [4]. The Mn fraction had to be purified from traces of chromium, details of which are described in [5]. The Al fraction requires a complete separation from the macroamount of Cr present in the steel. The development of this chemical separation procedure using ion exchange is currently ongoing.

Up to now, 20 steel samples have been already processed. The overall yield of ^{44}Ti is 88 %, corresponding to 135 MBq. The decontamination factor of ^{60}Co in this fraction reached about 150. The separation of $^{54/53}$Mn was performed till now for eleven samples, resulting in 11 MBq ^{54}Mn, with ^{60}Co being quantitatively removed. ^{26}Al fractions from all 20 processed steel samples are currently prepared for the final purification.

By continuous evaporation, the volume of the generated liquid wastes could be reduced by a factor of ~ 100 to some ml, which is sufficient for disposal.

REFERENCES

[1] M. Ayranov, D. Schumann, Ann. Rep. Lab. of Radio- & Environ. Chemistry, Uni Bern & PSI (2011), p. 48.
[2] Y. Dai et al., J. Nucl. Mater., **296**, (2001).
[3] http://lch.web.psi.ch/webcontent/research/rad-waste/Erawast2/index.html.
[4] M. Bunka et. al., ERAWAST II 2011, abstracts p. 3.
[5] M. Frei et.al., this report, p. 47.

MEGAPIE SAMPLING, PART I:
ESTIMATION OF THE VOLATILIZATION OF POLONIUM AND MERCURY IN THE MELTING DEVICE

J. Neuhausen (PSI), M. Wohlmuther, V. Boutellier (PSI/GFA), D. Schumann (PSI)

The MEGAPIE project is currently in its Post Irradiation Examination phase. For these investigations, lead bismuth eutectic is going to be molten out of parts cut from the target. This report describes the process of melting and safety assessments that were performed concerning the volatilization of hazardous radionuclides within this process.

INTRODUCTION

As a prerequisite for the Post Irradiation Examination (PIE) of the MEGAPIE Target, material samples have to be retrieved from sections of the irradiated target that have been previously cut in ZWILAG [1]. For this purpose, lead bismuth eutectic (LBE) has to be removed from the construction materials by melting the sections in a specially developed furnace. These operations involve heating of the target material to temperatures of about 200 °C and thus enhance the volatilization of hazardous radionuclides. This report describes the process of melting and the safety assessments that were performed in order to make sure that the process can be performed in a safe manner.

MELTING PROCESS AND FURNACE

The sections retrieved from the MEGAPIE target are disks of 20 to 40 cm diameter and thicknesses ranging from 4.5 to 10 cm, made mainly from steel and filled to a large extent with solidified LBE. To remove this LBE, the disks will be heated to about 180°C under argon atmosphere in a specially designed furnace (Fig.1) operated in a hot cell. The LBE (melting point 125 °C) will flow out of the target disks and will be collected in the lower part of the furnace. After the furnace has cooled to room temperature, the argon will be vented through a filter system consisting of 2 HEPA and 2 activated carbon filters that should remove both particulate matter and molecular species.
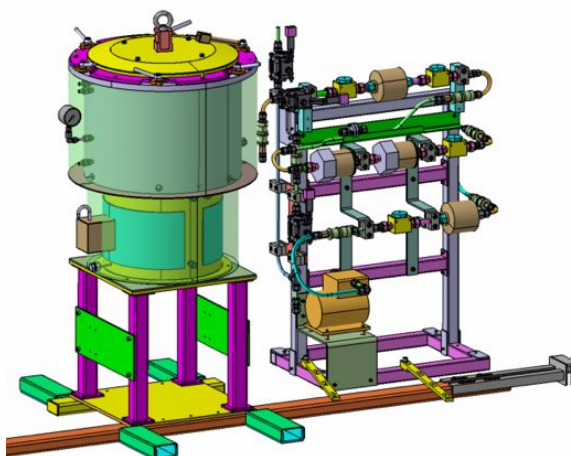
Fig. 1: Drawing of the furnace and filtering system constructed for the melting of sections from the MEGAPIE target.

More details on the furnace and filtering system as well as the melting procedure can be found in Ref.[2].

ASSESSMENT OF VOLATILIZATION

The licensing of the melting procedure required an assessment of the possible volatilization of hazardous radionuclides. For the evaporation of mercury and polonium during the melting in the closed surface, assessments of their gas phase concentrations were based on recommended relations for their equilibrium vapour pressure over LBE that were previously derived in this lab [3] using the operating parameters foreseen for the furnace and predictions on the concentrations of mercury and polonium present in the LBE obtained by nuclear calculations [4]. The resulting gas phase activities for one single melting procedure are compiled in Tab. 1. For the less volatile Po, very low gas phase activities are estimated, while for the highly volatile mercury substantial gas phase activities are predicted. However, mercury should be efficiently trapped on the charcoal filters. For more information on the assessment of volatilization see Ref. [2].

Tab. 1: Half life, estimated equilibrium gas phase activity for one single melting process and limits of allowance for relevant mercury and polonium nuclides.

Nuclide	$t_{1/2}$ [days]	Equilibrium gas phase activity [Bq]	LA [Bq]
^{208}Po	1059	5.71×10^{-4}	2×10^3
^{209}Po	37230	5.85×10^{-6}	2×10^3
^{210}Po	138	2.46×10^{-4}	2×10^3
Sum Po		$\mathbf{8.23\times10^{-4}}$	
^{194}Hg	189800	2.39×10^6	3×10^5
^{203}Hg	46.6	8.35	3×10^6
Sum Hg		$\mathbf{2.39\times10^6}$	

REFERENCES

[1] M. Wohlmuther, W. Wagner, J. Nucl. Mater. (2011), doi:1016/j.jnucmat.2011.11.024.

[2] P. Suter, Ch. Zumbach, M. Wohlmuther, J. Neuhausen, D. Schumann; V. Boutellier, MPR-1-WM85-019/2, PSI (2011).

[3] Environmental compliance report concerning the target material, EC-FP7 Project ESS-PP Deliverable D 8.1, PSI, Villigen, Switzerland, 2010.

[4] L. Zanini, J.-C. David, A.Yu. Konobeyev, S. Panebianco, N. Thiolliere, PSI-Report Nr. 08-04, PSI, Switzerland, December 2008.

MEGAPIE SAMPLING, PART II:
ESTIMATION OF THE VOLATILIZATION OF POLONIUM AND MERCURY DURING MEGAPIE SAMPLE CUTTING

J. Neuhausen (PSI), V. Boutellier, M. Wohlmuther (PSI/GFA)

Following melting-off the LBE, the steel parts retrieved from MEGAPIE have to be cut to pieces suitable for mechanical testing and surface analysis. This cutting will heat the samples that have still a layer of LBE adhering to their surfaces to high temperatures. For an assessment of polonium and mercury evaporation during this cutting procedure, a mass transfer model was employed that was previously validated using experimental evaporation data.

INTRODUCTION

The preparation of materials samples from the steel parts of MEGAPIE that have been crudely cleaned by melting-off the LBE involves cutting using a fast rotating disc that will heat the samples to temperatures up to 800 °C close to the cut. It is expected that after melting-off, a thin layer of LBE with a maximum thickness of 100 μm will still adhere to the surface of the material. This LBE will be heated up and radionuclides will evaporate at high temperatures in the air flow generated by the rotating disk. The evaporation of polonium and mercury in this process was estimated using a mass transfer model that was validated by comparison with experimental evaporation data.

VALIDATION OF MASS TRANSFER MODEL

According to film theory [1], the convective mass transfer of a species a at a liquid/ideal gas boundary can be expressed as

$$\frac{dw_a}{dt} = Ah_D \frac{M_a}{RT} p_a$$

when the concentration of a is zero at infinite distance from the surface (w_a: mass, t: time, A: surface area, h_d: convective mass transfer coefficient, M_a: molar mass, R: universal gas constant, T: absolute temperature, p_a: vapour pressure of a above melt). For a flat surface of length L and laminar flow, h_d can be expressed as

$$h_{D\,lam} = \frac{D}{L} \cdot 0.664 \cdot \sqrt{Re} \cdot Sc^{1/3}$$

with Re: Reynolds number, Sc: Schmidt number and D: diffusion coefficient of the gas phase species [1].

To validate this model, calculations of the mass transfer of polonium from liquid LBE samples were performed for a wide range of gas flow conditions, using recommended vapour pressure data from [2], a diffusion coefficient for gaseous PbPo estimated using the empirical correlation of Gilliland [1] and geometry and temperatures that were used in polonium evaporation experiments previously performed at PSI [3]. A comparison of the results of mass transfer calculations with experimental data from [3] and with calculations based on the Langmuir evaporation model [4] is presented in Fig. 1. The comparison shows that the mass transfer model yields reasonable agreement with the experimental data at low gas flow rates. It was concluded that the model gives physically sensible

results and can be used to estimate the evaporation during cutting.
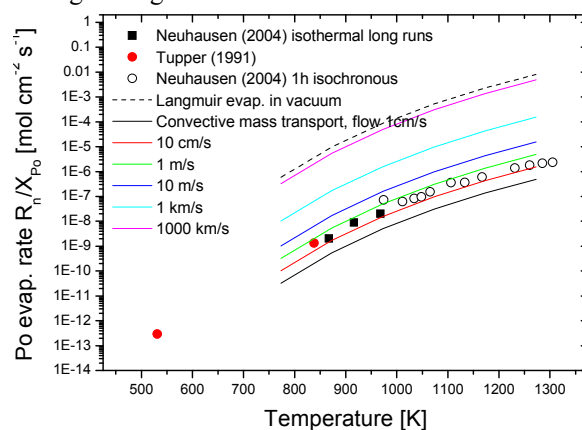
Fig. 1: Comparison of mass transfer calculations with experimental data obtained at a flow of approx. 1 cm/s.

ESTIMATIONS FOR SAMPLE CUTTING

To conservatively estimate the evaporation during sample cutting, a relatively large circular area of the sample was considered to be heated to a range of temperatures for the complete cutting time while being exposed to a flow of gas of the same temperature. The results of the calculations indicate that for the maximum temperature expected during cutting (800 °C) and a gas flow conservatively estimated as 2 m/s, approx. 3 % of the polonium contained in an LBE layer of 100 μm thickness adhering to the samples would be evaporated, corresponding to activities of $5.5 \cdot 10^5$ Bq, $5.7 \cdot 10^3$ Bq, and $2.4 \cdot 10^5$ Bq for ^{208}Po, ^{209}Po, and ^{210}Po, respectively. Similar calculations for mercury indicate that this element will be completely evaporated from the adhering LBE layer under the same conditions. For more information on these estimations see Ref. [5].

REFERENCES

[1] W. M Rohsenow, H. Y. Choi, Heat, Mass and Momentum Transfer, Prentice-Hall, New Jersey (1961).

[2] Environmental compliance report concerning the target material, EC-FP7 Project ESS-PP Deliverable D 8.1, PSI, Villigen, Switzerland, 2010.

[3] J. Neuhausen, U. Köster, B. Eichler, Radiochim. Acta, **92**, 917 (2004).

[4] I. Langmuir, Phys. Rev. 2nd Ser., **2**, 329 (1913).

[5] J. Neuhausen, M. Wohlmuther, TM24-11-01/0, MPR-11-NJ24-001/0, PSI (2011).

DISTRIBUTION OF RADIONUCLIDES IN A PROTON IRRADIATED LBE TARGET FROM MEGAPIE. SAMPLE CUTTING AND γ-SPECTROMETRY

B. Hammer, A. Türler (Univ. Bern & PSI), D. Schumann, J. Neuhausen (PSI), V. Boutellier, H.P. Linder, N. Shcherbina (PSI/Hotlab)

The distribution of radionuclides in a proton irradiated lead bismuth eutectic target from MEGAPIE was analyzed using -spectrometry.

INTRODUCTION

The prototype target MEGAPIE (MEGAwatt PIlot Experiment) was operated in the spallation source SINQ at PSI in 2006 [1]. It was the first spallation target close to the megawatt range using a liquid metal target (lead bismuth eutectic, LBE). The aim of the project was to prove the feasibility of designing, building and safely operating high power liquid spallation targets as a step towards the demonstration of the ADS concept and high power liquid metal targets in general [2, 3]. So far there are no experimental data concerning the amount and behavior of radionuclides formed within such a target. However, these data are important with respect to the licensing, safe operation and disposal of such a facility. The analysis of samples from the irradiated MEGAPIE target is a unique source of information with regard to these topics. In this report we present first results on the radionuclide content and the distribution in the MEGAPIE target. We chose ^{207}Bi, ^{194}Au, and ^{173}Lu as leading nuclides to be able to assess the target material itself as well as noble and reactive impurities.

SAMPLE PREPARATION AND ANALYSIS

After a cooling period of about 5 years the MEGAPIE target was cut into segments in the ZWILAG that were transferred to the Hotlab at PSI. From the segments H02 to H08 about 50 LBE samples from different locations of the target were taken using a special drilling device [4], comprising both "pure" LBE as well as samples including the LBE/steel interface and the free surface (LBE/covergas interface). For more details of the cutting procedure see [5]. All samples were analyzed by γ-spectroscopy.
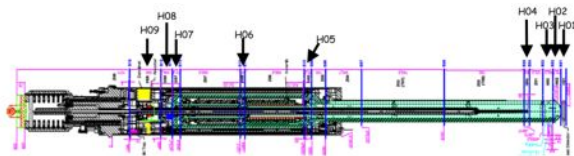
Fig. 1: Cutting plan of the MEGAPIE target [5], from the right to the left side flowed the beam.

RESULTS

Fig. 2 shows segment H07 with different sampling regions. In the inner ring, after shut down only some LBE drops remained, contaminated with a dark layer. The middle ring contained LBE that formed the free surface, also covered by a dark layer. According to the results obtained by γ-spectrometry (Tab. 1), this dark layer is highly enriched in lanthanides, here represented by ^{173}Lu. Samples containing the LBE

steel interface also contain lanthanide nuclides. On the other hand, ^{173}Lu is not detected in samples containing only bulk LBE. Apparently, lanthanides have deposited at the steel interface and at the free surface of LBE. The distribution of ^{207}Bi in the MEGAPIE target is homogeneous, as expected. Soluble noble metals such as Au are found throughout the target, however, ^{194}Au, also shows enrichment in a few samples. The origin of this behaviour will be analysed within more detailed studies, which are still ongoing.
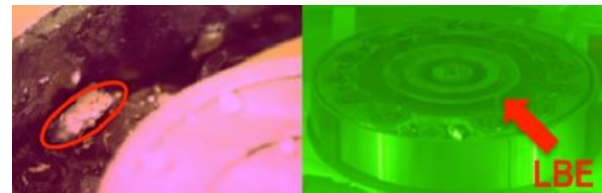
Fig. 2: Part of the inner mantle of segment H07. LBE drop of sample H07-U3 is red marked (left), and segment H07 (right).

Tab. 1: Measured activities of some samples.

Sample	Position	m [mg]	A [kBq/g]		
			^{194}Au	^{173}Lu	^{207}Bi
H08-U1-b	LBE/steel interface	159.3	88	12663	3595
H08-U2-b	across from H08-U1-b, LBE/steel interface	288.2	80	8740	3851
H07-S7	LBE free surface	104.00	43	7	3575
H07-U2	LBE/steel interface	226.10	73	2266	3725
H07-U3	LBE/steel interface	571.50	40	290	3497
H07-S9	LBE free surface	95.90	34	164	3576
H07-S-b	LBE	99.20	59	0	3559
H05-D4-b	LBE	95.60	2091	0	3510
H03-U1	LBE	40.60	969	0	3904
H03-D2	LBE	93.10	75	0	3544

REFERENCES

[1] G. S. Bauer, Nuclear Instruments and Methods in Physics Research Section A: Accelerators, Spectrometers, Detectors and Associated Equipment, **463**, 505 (2001).

[2] G. S. Bauer et al., Journal of Nuclear Materials, **296**, 17 (2001).

[3] W. Wagner et al., Journal of Nuclear Materials, **377**, 12 (2008).

[4] M. Wohlmuther et al., J. Nucl. Mater. (2011), doi:1016/j.jnucmat.2011.11.024.

[5] V. Boutellier, TM-43-11-15, PSI (2011).

SURFACE ENRICHMENT OF POLONIUM IN SOLIDIFIED LEAD BISMUTH ALLOY: IMPROVED SAMPLE PREPARATION

S. Heinitz, A. Türler (Univ. Bern & PSI), J. Neuhausen, R. Dressler, D. Schumann (PSI)

The enrichment of polonium at the surface of solidified lead-bismuth eutectic was studied by alpha spectroscopy. In order to ensure reproducible sample preparation and geometry, a procedure was developed to obtain cylindrically shaped LBE ingots. It was found that the dynamics of the diffusion process differs from sample to sample and the quantification of the underlying processes is not straightforward.

INTRODUCTION

The diffusion of polonium toward surfaces of solidified LBE was already studied some years ago by [1]. During this investigation, a steady increase of the surface activity with time was found using a sample without a specific regular shape.

A more thorough study of diffusion phenomena and their mathematical description requires samples with defined geometry. Therefore, a method was devised to prepare regularly shaped cylindrical samples of LBE containing ^{210}Po. The diffusion behaviour of ^{210}Po in these samples was subsequently studied by counting the surface activities as a function of time.

EXPERIMENTAL

Cylindrical samples with a height of approx. 10 mm and a diameter of 7 mm were prepared by the following procedure: a glass tube, closed at one end, was placed in a vertical furnace and heated to 500 °C. 50 g of neutron activated LBE with a specific activity of 1 kBq/g was heated in a beaker under nitrogen atmosphere and transferred into the glass tube while molten. The open end of the tube was then connected to a vacuum line and the liquid metal was gassed out until gas bubbles on the LBE/gas interface have disappeared.
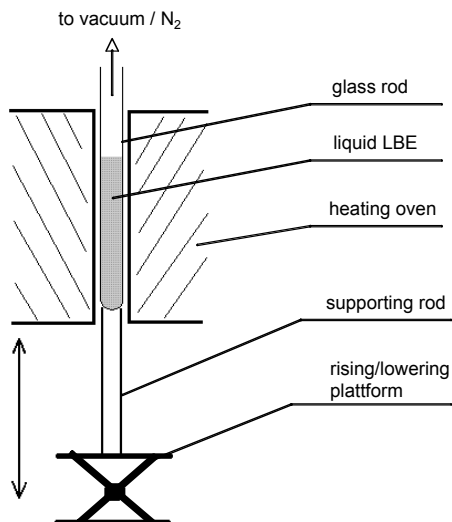
Fig. 1: Experimental setup for the preparation of cylindrical LBE samples.

The tube was then slowly lowered out of the furnace with a velocity of 5 mm/min (see figure 1). This ensures a homogeneous crystallization of the metal from bottom to top and prevents the formation of voids.

After cooling down the glass was broken and the LBE tube was cut to 10 mm long cylinders using a saw. Both front sides of each cylinder were then cut by a microtome to give a flat surface.

To study the variation of the polonium surface activity with time, four samples with shielded lateral surfaces were directly transferred to α-measuring chambers. Each chamber was evacuated to 10^{-1} mbar and spectra with 1 hour measuring time each were recorded for a period of 140 hours at room temperature.

RESULTS AND DISCUSSION

As can be seen in figure 2, the initial surface activity of all four samples equals to approx. 400 counts/h. With increasing time, however, the segregation behaviour of polonium in the four samples differs considerably. These differences may be attributed to different impurity concentrations or varying grain structure that can influence the mobility of polonium [2]. Enrichment of impurities can occur at the crystallization front moving through the LBE rod during solidification. Thus, impurities may be inhomogeneously distributed along the LBE rod. Unfortunately, it is not known from which position within the rod each of the analyzed samples initially came from. More detailed experiments will be performed in future.
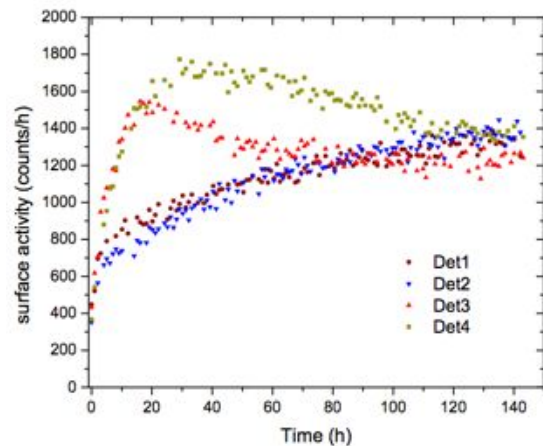
Fig. 2: The increase of surface activity with time for 4 different LBE samples.

REFERENCES

[1] F. v. Rohr et al., Ann. Rep. Lab. of Radio- & Environ. Chemistry, Uni Bern & PSI, p. 43 (2006).

[2] L. Patrizii et al., JINST 3, P07002 (2008).

PYROCHEMICAL EXTRACTION OF POLONIUM AT STATIC CONDITIONS

S. Heinitz, A. Türler (Univ. Bern & PSI), S. Luethi, J. Neuhausen, D. Schumann (PSI)

In difference to earlier experiments, the extraction performance of polonium from irradiated lead-bismuth eutectic was studied under static conditions, i.e. without a thorough mixing of both liquids using a stirrer bar. The experiments were performed under variation of the extraction time and temperature. It was found that the extraction kinetics follows a two-step process, where a fast polonium transfer to the alkaline phase is followed by a slow back-diffusion into the metal.

INTRODUCTION

The extraction of ^{210}Po using alkaline metal hydroxides represents a powerful method to decrease the radiotoxicity of irradiated lead-bismuth eutectic (LBE) used as coolant and target material in nuclear facilities. In order to improve scientific understanding on the occurring processes, a series of investigations was performed in the past [1,2]. During these experiments a continuous agitation of LBE and the hydroxide phase was maintained using a stirrer bar.

To investigate the transfer kinetics of polonium as a function of contact time, a series of experiments was performed without agitation of both liquids.

EXPERIMENTAL

For extraction experiments the same device was used as described earlier [1]. Additionally, a hole was drilled into the wall of the glassy carbon reaction vessel to fit the temperature sensor. This avoids any contact to the reactants thus increasing the lifetime of the sensor.

For each experimental run, approx. 1.0 g of eutectic NaOH/KOH mixture and 0.5 g of neutron irradiated LBE were used. Nitrogen served as gas blanket. The experimental procedure can be reviewed in [1]. The operating temperatures were chosen to be 200, 350 and 500 °C at extraction times ranging from 5 min to 8h. After each experimental run, the amount of extracted polonium was determined via liquid scintillation counting.

RESULTS AND DISCUSSION

In total, more than 60 single extractions were performed under the variation of extraction time and temperature. The results are shown in figure 1.

It was found that for short extraction times (t < 30 min) an efficient transfer of polonium is observed for every analysed temperature. Even at 200 °C polonium could be almost quantitatively extracted into the alkaline phase. This observation was not expected taking into account findings published in [1].

With increasing contact time (t > 30 min), however, the extraction efficiency steadily decreases at 200 °C. For higher extraction temperatures this effect is less pronounced or even disappears. At 350 and 500 °C the extraction efficiency remains nearly constant and does not decrease for longer contact times.
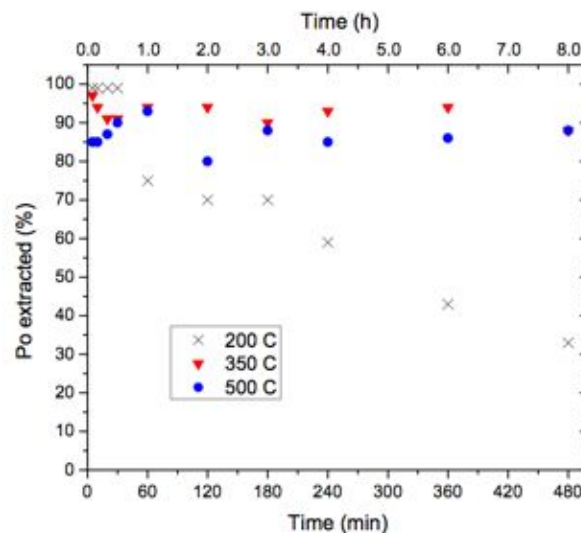
Fig. 1: Extracted polonium from LBE at different temperatures as function of time under stagnant conditions.

To explain these observations, a two-step kinetic process is proposed. In the first step a fast quantitative transfer of polonium out of the metal occurs. The time needed is probably less than a minute as screening experiments using very short reaction times have shown. In a second, slower step, polonium is forced back into the metal, thus decreasing its extraction efficiency. The reason for this may be the presence of oxygen containing species: It is known [3] that oxidative substances are inhibiting the extraction process. Consequently, impurity oxygen present in the alkaline melt or the gas blanket might influence the polonium transfer process.

At 200 °C, this second process occurs slowly, as may be seen by lower extraction efficiencies for longer contact times. At higher temperatures diffusion of oxygen containing species within the alkaline melt increases thus accelerating both occurring processes and leading to steady-state conditions appreciably faster.

REFERENCES

[1]   S. Heinitz et al., J. Nuc. Mat., **414**, pp. 221-225, (2011).

[2]   S. Heinitz et al., Ann. Rep. Lab. of Radio- & Environ. Chemistry, Univ. Bern & PSI (2008), pp. 39-41.

[3]   E.I. Yefimov et al., Mat. Res. Soc. Symp. Proc., **506**, pp. 679 – 686 (1998).

THE PRODUCTION OF POLONIUM-206 AT OCL

M. Rizzi, A. Türler (Univ. Bern & PSI), J.P. Omtvedt (Univ. Oslo), R. Eichler (Univ. Bern & PSI),
J. Neuhausen (Univ. Bern & PSI)

^{206}*Po was produced by proton irradiation of bismuth at the Oslo Cyclotron Laboratory of the University of Oslo and transported to PSI for the investigation of the chemical properties of polonium.*

INTRODUCTION

Liquid lead and liquid lead-based alloys are currently under discussion for application as spallation target in neutron sources and Accelerator Driven Systems (ADS). The main disadvantage of lead-based alloys is the formation of ^{210}Po [1]. For the investigation of chemical properties of polonium and especially its evaporation behaviour, the use of the gamma-emitting ^{206}Po radionuclide is preferable compared to the alpha-emitting ^{210}Po. One possible way to produce ^{206}Po is the proton irradiation of bismuth using the p,4n –reaction. The limited allowance for production and handling of alpha activities at the PSI Injector II cyclotron and the shut-down of the PSI Philips cyclotron in December 2010 requires us to produce such radioactive tracers abroad.

EXPERIMENTAL

Broken ingot pieces of bismuth from Goodfellow (purity > 99,9999 %, metal basis) were melted into an Aluminium target holder (shown in figure 1). Good thermal contact of the bismuth with the aluminium had to be guaranteed for an efficient heat transfer from the target itself to the aluminium-backing, which was itself water-cooled. This was achieved by first distributing a fine drop of bismuth with a spatula into the cavity of the Al-backing. Subsequently, the rest of the bismuth was molten into the backing.

The irradiation was done at the MC35 Scanditronix cyclotron at the Oslo Cyclotron Laboratory (OCL) of the University of Oslo. The aluminium target-holders with the bismuth were mounted onto a water-cooled copper backing within a vacuum chamber connected to the beam line at the SISAK position. During the irradiation, the chamber was evacuated to a total pressure between 10^{-4} and 10^{-5} mbar. The maximum cross-section of approximately 1 barn for the p,4n - reaction of bismuth is expected at 40 MeV proton energy [2]. Lower energies lead to a significantly higher cross-section for the p,3n - reaction whereas the cross-section of the desired p,4n – reaction diminishes.

With 32 MeV the highest stable proton energy available at the MC35 was used for these irradiations. At this energy the cross-section for the p,4n - reaction is around 0.4 barn.

RESULTS AND DISCUSSION

The first sample with the lowest mass of 1.297 g bismuth was irradiated for a shorter time period and a lower intensity than the other two samples to roughly estimate the yield of ^{206}Po and the ratio of ^{207}Po to ^{206}Po. The results are listed in table 1.

The results were a little disappointing, since the initial goal was to produce the maximum allowed ^{206}Po activity determined by the C-class laboratory regulations at PSI, i.e. about 10 MBq. This desired amount of ^{206}Po remains at the given beam energy out of reach. Even more, since the much higher production rate of ^{207}Po at the given irradiation conditions led to dose rates higher than 50 mSv/h in 1 m distance after one hour of cooling time after the irradiation. Since the target change had to be done manually a further increase of beam intensity or irradiation time would have been unsuitable with respect to radiation safety. However, the irradiated samples have been successfully transported from Oslo to PSI for their use in the scheduled tracer experiments.

ACKNOWLEDGEMENT

Tab. 1: Results of bismuth irradiation

N°	mass [g] Bi target	irradiation with protons Time [min]	Intensity [nA]	Energy [MeV]	activity produced [kBq] Po-206	Po-207
1	1.297	10	10	32	8.2	1899
2	1.637	60	50	32	282.8	65090

Fig. 1: Aluminium target-holder for irradiation

REFERENCES

1. J. Harrison, R. Leggett, D. Lloyd, A. Phipps, B. Scott, Journal of Radiological Protection **27**, 17-40 (2007).
2. K. Miyano, M. Sekikawa, T. Kaneko, M. Nomoto, Nuclear Physics A **230**, 1, 98-108 (1974).

RADIOCHEMICAL ANALYSIS OF THE RADIONUCLIDE INVENTORY OF SINQ-TARGET SAMPLES

T. Lorenz, A. Türler (Univ. Bern & PSI), D. Schumann, M. Ayranov, Y. Dai (PSI/GFA)

At Paul Scherrer Institute a 590 MeV proton accelerator with a beam current of 2.4 mA is driving a 1 MW class research spallation neutron source named SINQ. In this facility the proton beam is fully stopped in a lead target. One of the targets (target 4 – irradiated with a total proton dose of 10.03 Ah for 16 months from 2000 – 2001) was sawn into several disks in order to study the radionuclide distribution. First α-spectrometric results are presented.

INTRODUCTION

The spectrum of the residue nuclides within a spallation target is very complex and differs completely from the nuclide spectrum known from nuclear reactors. The precise knowledge of the radionuclide inventory, especially of safety-relevant α-emitting isotopes and long-lived radionuclides, is one of the basic topics in evaluation of risks and harms concerning the operation, decommissioning and disposal of high power targets.

Due to the complexity of the involved nuclear reactions, theoretical predictions of the radionuclide inventory are difficult and require benchmarking to improve the models and calculation codes. Within the EC-funded projects HINDAS [1] and EUROTRANS (WP NUDATRA) [2] essential progresses could be achieved concerning the development of codes and models, especially TALYS and INCL4/ABLA, to get reliable nuclear data, in particular for the target materials lead and bismuth. Experimental data for verification are urgently needed.

EXPERIMENTAL

Details on the SINQ target design from STIP-II are available in [3]. To determine the radial distribution of the radionuclide inventory, a centred rod near the beam entry has been sawn into discs (Fig. 1) in the Hot Cell Laboratory.
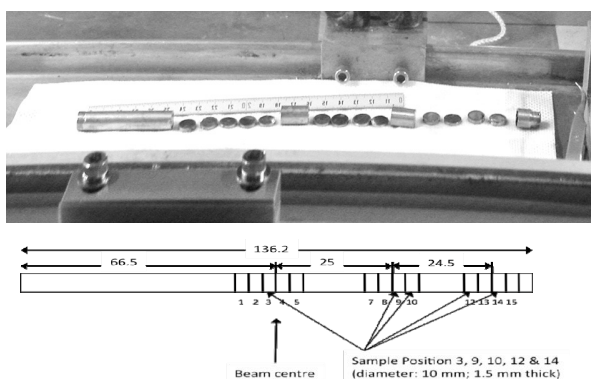
Fig. 1: Photograph and scheme: sawing the lead rod discs (dimensions in mm).

Due to the high dose rate per disc, they were fragmented into pieces of about 10 to 50 mg and a detailed γ-analysis of multiple pieces of different distances (in mm) to the beam centre was carried out. In Tab. 1 the evaluated, averaged and normalized activities, per gram of lead, of selected nuclides are given in Tab. 1.

Tab. 1: Content of selected radionuclides at different positions (measuring dates: 03/2011, 12/2011)

	D03 (1.5 mm)		D09 (25 mm)		D10 (27 mm)	
	A[Bq/g]	σ[%]	A[Bq/g]	σ[%]	A[Bq/g]	σ[%]
^{108m}Ag	$3.70 \cdot 10^5$	47.4	$3.55 \cdot 10^5$	23.1	$3.82 \cdot 10^5$	26.4
^{194}Au/^{194}Hg	$2.45 \cdot 10^7$	16.9	$1.19 \cdot 10^7$	14.5	$1.20 \cdot 10^7$	37.5
^{133}Ba	$2.32 \cdot 10^6$	41.8	$1.48 \cdot 10^6$	5.8	$1.59 \cdot 10^6$	5.1
^{207}Bi	$5.54 \cdot 10^7$	2.3	$2.82 \cdot 10^7$	9.4	$2.93 \cdot 10^7$	3.1
^{60}Co	$3.07 \cdot 10^6$	23.6	$2.01 \cdot 10^6$	5.9	$2.25 \cdot 10^6$	5.6
^{194m}Ir/^{194}Os	$1.14 \cdot 10^7$	53.6	$1.45 \cdot 10^7$	21.1	$9.59 \cdot 10^6$	49.2
^{172}Lu/^{172}Hf	$7.97 \cdot 10^6$	16.2	$4.69 \cdot 10^6$	5.6	$5.24 \cdot 10^6$	5.5
^{173}Lu	$4.26 \cdot 10^6$	29.8	$1.99 \cdot 10^6$	4.7	$2.43 \cdot 10^6$	4.6
^{102}Rh	$4.63 \cdot 10^6$	8.2	$2.12 \cdot 10^6$	5.0	$2.13 \cdot 10^6$	2.4
^{125}Sb	$6.96 \cdot 10^5$	6.8	$4.54 \cdot 10^5$	5.2	$4.91 \cdot 10^5$	10.2
^{44}Sc/^{44}Ti	$2.26 \cdot 10^5$	58.8	$2.10 \cdot 10^5$	7.5	$2.46 \cdot 10^5$	19.0

	D12 (47 mm)		D14 (49.5 mm)	
	A[Bq/g]	σ[%]	A[Bq/g]	σ[%]
^{108m}Ag	$1.91 \cdot 10^5$	6.4	$1.50 \cdot 10^5$	3.7
^{194}Au/^{194}Hg	$6.59 \cdot 10^6$	3.5	$5.08 \cdot 10^6$	21.2
^{133}Ba	$7.44 \cdot 10^5$	5.9	$6.93 \cdot 10^5$	6.6
^{207}Bi	$1.52 \cdot 10^7$	3.1	$1.18 \cdot 10^7$	3.4
^{60}Co	$1.09 \cdot 10^6$	3.4	$8.73 \cdot 10^5$	6.3
^{194m}Ir/^{194}Os	$5.29 \cdot 10^6$	48.8	$5.39 \cdot 10^6$	13.8
^{172}Lu/^{172}Hf	$2.51 \cdot 10^6$	3.6	$2.12 \cdot 10^6$	5.1
^{173}Lu	$9.73 \cdot 10^5$	6.0	$1.15 \cdot 10^6$	2.1
^{102}Rh	$9.15 \cdot 10^5$	4.0	$7.23 \cdot 10^5$	5.1
^{125}Sb	$3.83 \cdot 10^5$	10.3	$4.13 \cdot 10^5$	0.2
^{44}Sc/^{44}Ti	$1.14 \cdot 10^5$	15.8	$5.11 \cdot 10^4$	75.0

A strong dependence on the distance of the beam centre is clearly visible, according to the decreasing proton and neutron flux.

The development of chemical separation procedures for α– and β–emitting radionuclides is ongoing. The work is funded by the Swiss National Science Foundation.

REFERENCES

[1] Hindas Final Report, FIS5-00150.
[2] Report of the Numerical results from the Evaluation of the nuclear data sensitivities, FP-7 IP-EUROTRANS.
[3] Y. Dai et al., J. Nucl. Mater., 343 (2005) 33-44.

^{68}Ge - AN ISOBARIC-FREE NUCLIDE WITH HIGHEST SENSITIVITY IN AMS

A. Wallner (Univ. Vienna), D. Schumann, T. Stowasser (PSI)

^{68}Ge, one of the isobaric-free isotopes in AMS was studied for the first time. Reference material was produced at the neutron irradiation facility at PSI. First cross section measurements of the reaction ^{70}Ge(n,3n)^{68}Ge are in progress.

INTRODUCTION

Isobaric interference represents one of the major limitations in mass spectrometry. For a few cases in AMS isobaric interference is completely excluded. One example is ^{68}Ge ($t_{1/2}$ = 270.9 d), never used in AMS so far. Its respective stable isobar, ^{68}Zn does not form stable negative ions. The exceptional sensitivity of AMS for such nuclides offers important insights into different fields like nuclear astrophysics, fundamental nuclear physics and technological applications. VERA, a dedicated AMS facility is well suited for developing procedures for new and non-standard isotopes.

NATURAL SAMPLES (BLANK MATERIAL)

We investigated different Ge materials: commercially available powder, grains (Alfa Aesar, Goodfellow); and also a larger piece from a Ge crystal. They were pressed into both Al and Cu sample holders. No additional powder was added to the Ge sputter samples.

AMS results obtained at VERA for such blank samples are plotted in Fig. 1. Most of the runs were essentially without any detector events. Very rarely an event was registered, which could be either a real ^{68}Ge ion or also an ion which mimics a true event. Such events seemed to be more frequent for runs performed directly after sputtering reference samples for a longer time. Also, Cu and Al blank samples (both empty sample holders and Cu and Al_2O_3 powder pressed into sample holders) gave the same (low) number of "^{68}Ge" events as the ^{nat}Ge (blank) samples. Thus, most likely, these rare events are originating from contamination in the ion source indicating a cross talk or memory effect of the order of 10^{-4} or less.

REFERENCE MATERIAL

Reference material was produced by bombarding ^{nat}Ge material with highly energetic neutrons at PSI. The first stable isotope in mass to ^{68}Ge is ^{70}Ge, followed by ^{72,73,74,76}Ge. The neutron threshold energy for ^{70}Ge(n,3n) is 20.01 MeV. For the other isotopes much higher neutron energies for ^{68}Ge production are required, between 38.42 and 71.74 MeV. For the production of reference materials, samples with masses of ≈100 mg Ge with natural isotopic composition were exposed to these spallation neutrons with irradiation times between 1 min and 1 hour. The samples with the highest isotope ratios (> 10^{-12}) were accessible to decay counting. Their number of produced ^{68}Ge was measured through the γ-rays emitted in the decay of the daughter nuclide ^{68}Ga. ^{68}Ge/^{70}Ge isotope ratios between 10^{-14} and 10^{-12} were obtained in these neutron irradiations; with the lower isotope ratios cross-calibrated via AMS relative to the "10^{-12}" samples.

FIRST MEASUREMENT OF THE ^{70}Ge(n,3n)^{68}Ge CROSS SECTION NEAR THRESHOLD

For studying the most likely production channel in nature, the ^{70}Ge(n,3n)^{68}Ge reaction, ^{nat}Ge samples were irradiated with 18.5 to 21.5 MeV neutrons at IRMM, Belgium with the 7 MV Van de Graaff accelerator.

First results from AMS measurements showed no ^{68}Ge detector events for samples irradiated with neutrons below the (n,3n) threshold. One sample irradiated with 21.5 MeV, however, indicates isotope ratios ^{68}Ge/^{70}Ge of a few×10^{-15}, clearly above background. These measurements are in progress now.
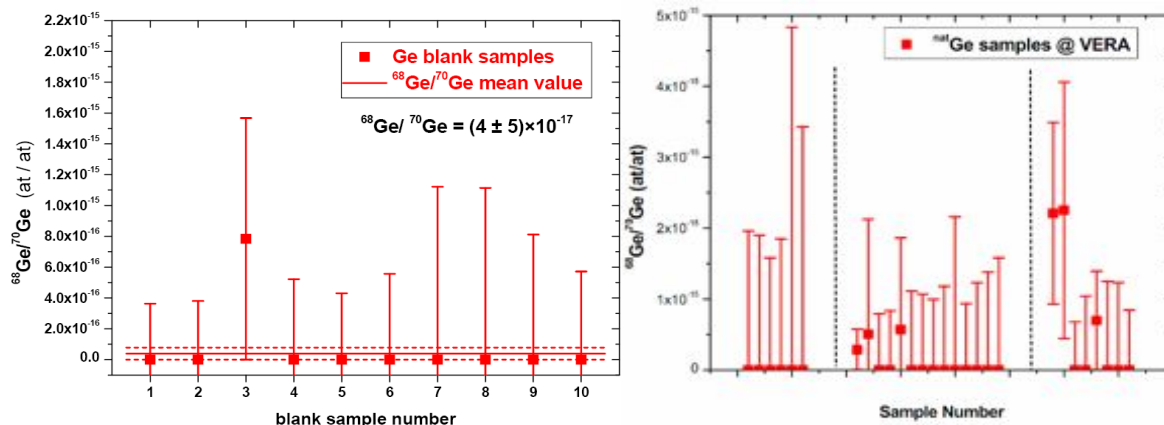
Fig. 1: Isotope ratios for blank samples. Left: first three measurement series; Right: fourth measurement.

DETERMINATION OF THE ^{36}Cl CONTENT IN INSULATED CABLES

T. Stowasser, S. Lüthi (PSI), U. Ehrlicher, P. Zimmermann, M. Egloff (PSI/LOG), D. Schumann (PSI),
C. Vockenhuber (ETHZ)

An analytical method for the determination of ^{36}Cl in electric cables exposed to particle irradiation in an accelerator environment had been developed using X-Ray Fluorescence (XRF) and Accelerator Mass Spectrometry (AMS).

INTRODUCTION

Decommissioning and disposal of accelerator waste includes also the peripheral elements like power supply, cooling systems, pumps, thermo-elements and many others. Electric cables are components, which have to be analysed as well as all other waste concerning their radionuclide content. Since plastic material used as insulation contains normally considerable amounts of Chlorine, a high production of long-lived ^{36}Cl – depending on the neutron flux – has to be expected via the nuclear reaction ^{35}Cl(n,γ)^{36}Cl.

Five different types of electric wires were analysed. As can be seen in Fig.1, showing one example, the objects of study are complex. The components were separated mechanically. All plastic materials were processed together; the metallic component was measured individually.

Fig. 1: Photo of the cable number 2 (middle) and its individual components (around).

DETERMINATION OF THE TOTAL CHLORINE CONTENT USING XRF

Since the type of plastic, and thus also the elemental composition of the cables, were not known, a determination of the total Chlorine content in the plastic parts was necessary. For this, a mobile X-Ray Fluorescence (XRF) Analyzer unit, Niton XL3t 990S (Thermo Scientific) was used, mounted on a shielded test stand. It is calibrated for different measuring modes, one especially for plastics. Measurement times for the individual cable components were set to 100s, each repeated three times. Several runs were done for correction of sample thickness and background effects. An overall uncertainty of about 30% was estimated. For Chlorine mass fractions between 20 and 30% were found.

DETERMINATION OF ^{36}Cl USING AMS

Accelerator Mass Spectrometry (AMS) is a well-known tool for determining long-lived radionuclides in relatively small amounts. The method measures the isotopic ratio (radionuclide/stable isotop) in comparison to a standard. The measurements were performed at the ETHZ.

From each type of wire two chlorine samples were prepared; one from the metal parts and one from the plastic parts.
Metal parts: The metals (mainly copper) were isolated from the plastic and between 2 to 7 mg dissolved in 7M HNO$_3$. After addition of 10mg chlorine carrier, the solution was heated until dryness. A nitrogen stream transported the generated HCl into an absorption vessel containing silver nitrate. The produced AgCl was re-precipitated two times and dried.
Plastic parts: Around 1g of cable was heated in an oven up to 450°C. During heating a nitrogen stream transported the generated gases through an absorption vessel containing AgNO$_3$. After re-precipitating the AgCl residue two times, it was dried.

RESULTS

The analysis results are shown in Table 1. It can be seen that the content of ^{36}Cl is completely determined by the production in the plastic material, values of that being 3-4 orders of magnitude higher than those for the corresponding metal parts. However, the exemption limit for ^{36}Cl (1 kBq/g) is by far not exceeded, so that disposal can be processed without any problems.

Tab. 1: Overall ^{36}Cl content in the metal and plastics parts.

No	metal content [%]	^{36}Cl [Bq/g] in metal	Cl content in plastic in [%]	^{36}Cl [Bq/g] in plastic
1	34.9	3.72E-04	26.9	1.75E-01
2	51.0	7.61E-04	26.1	2.79E-01
3	63.8	1.47E-04	21.1	1.54E-01
4	39.3	4.65E-05	33.7	1.69E-03
5	29.1	1.67E-03	30.6	4.69E-01

CYCLOTRON PRODUCTION OF SCANDIUM-44

M. Bunka (Univ. Bern & PSI), K. Zhernosekov (PSI), Y. Eichholzer (PSI/ZRW), R. Schibli (ETH & PSI),
A. Türler (Univ. Bern & PSI)

The production of ^{44}Sc via the ^{44}Ca(p, n)^{44}Sc nuclear reaction has been developed at the PSI Injector II cyclotron. Extraction chromatography was evaluated for chemical isolation of scandium-44 from irradiated calcium targets. ^{44}Sc was successfully separated from the Ca-target and used for radiolabelling of biomolecules.

INTRODUCTION

With a half-life of 3.97 h the positron emitter ^{44}Sc is attractive for positron emission tomography (PET) and might be a better alternative to currently used short-lived ^{68}Ga ($t_{1/2}$ = 1.1 h). Trivalent ^{44}Sc can be effectively used for radiolabelling with already established chemical strategies via bifunctional chelators. It can be produced from a ^{44}Ti/^{44}Sc radionuclide generator as daughter nuclide of ^{44}Ti. Alternatively, the ^{44}Ca(p, n)^{44}Sc nuclear reaction at a cyclotron can be used [1], which was developed in this work. For the chemical isolation of Sc extraction chromatography with DGA resin (N,N,N′, N′-tetra-n-octyl-diglycolamide (DGA) as extractant) was evaluated. The DGA resin demonstrates high affinity for rare earth elements in concentrated hydrochloric acid solutions and low affinity for Ca(II) [2]. There is, however, no data for Sc(III), those were determined in this work.

EXPERIMENTAL

Irradiation at the PSI cyclotron. Targets up to 200 mg mass of ^{nat}CaCO$_3$ or 5 mg of ^{44}CaCO$_3$ mixed with ≈160 g graphite were prepared for model experiments to estimate irradiation yields, radionuclide purity and to assess target stability. Pellets of 0.5 mm thickness were pressed (Fig. 1 a) and b)) and encapsulated in aluminium (Fig. 1 c)). Irradiation with protons in an energy range of about 14→12 MeV and beam currents of 50 µAh were performed at the PSI Injector II cyclotron.

Fig. 1: Preparation of Ca-targets: a) and b) pressing of ~200 mg CaCO$_3$, c) encapsulating of the targets

Chemical separation with DGA. For the determination of the distribution coefficients of Sc(III) on DGA at different hydrochloric acid concentrations, batch experiments of ^{46}Sc(III) uptake were performed and the observed values are shown in Fig. 2 (left). At low acid concentrations up to 1 M HCl Sc^{3+} has only minimal adsorption. It increases rapidly with increasing HCl concentration and approaches its maximum at 6 M HCl. For the separation of Sc a column of 5×55 mm packed with 50 mg of DGA resin was used.
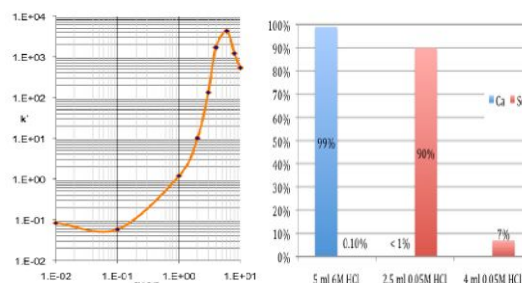
Fig. 2: Estimated k'-values for Sc(III) on DGA resin (left) and the separation of ^{44}Sc from Ca-targets (right)

The irradiated Ca-target was dissolved in 2 ml of 6 M HCl and directly loaded onto the column. Then the column was washed with additional 3 ml of 6 M HCl. Sc remained on the column while Ca was not adsorbed under these conditions. ^{44}Sc is eluted within 2.5 ml of 0.05 M HCl and the column is rinsed with 4 ml of 0.05 M HCl (Fig. 2 (right)). The Ca-solution can be used for recycling of ^{44}CaCO$_3$ for further irradiations.

RESULTS AND DISCUSSION

Enriched ^{44}CaCO$_3$, irradiated with protons, provides high radionuclide purity containing only ^{44}Sc and ^{44m}Sc (see γ-spectrum of the target Fig. 3).
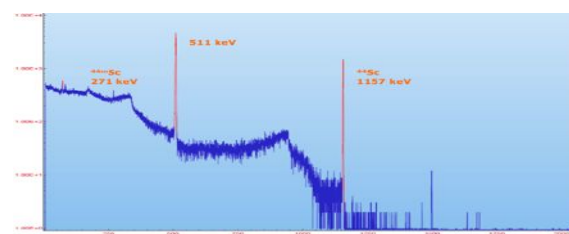
Fig. 3: The γ-spectrum of the irradiated ^{44}CaCO$_3$

The irradiation yields are up to 200 MBq/µAh per 200 mg ^{44}CaCO$_3$ target (extrapolated) and the ratio of ^{44m}Sc/^{44}Sc is less than 1 %. For the chemical separation of ^{44}Sc from Ca DGA resin shows excellent results. Sc(III) is quantitatively adsorbed on the resin from 6 M HCl and 90 % of it eluted in a small volume of 0.05 M HCl, which was successfully used for radiolabelling experiments.

REFERENCES

[1] A. Bilewicz et al., 3rd-INCC, Italy (2011).
[2] E. P. Horwitz et al., Solvent Extraction Ion Exch., **23**, (2005).

TEST-PRODUCTION OF THE THERAPEUTIC ALPHA-EMITTER ^{149}Tb VIA PROTON INDUCED SPALLATION OF TANTALUM

H. Dorrer (Univ. Bern & PSI), K. Zhernosekov, C. Müller (PSI/ZRW),
U. Köster, K. Johnston (CERN), R. Schibli (ETHZ & PSI), A. Türler (Univ. Bern & PSI)

The alpha-emitting, therapeutic radionuclide ^{149}Tb was produced by proton induced spallation of tantalum and on-line mass separation at ISOLDE, CERN. It was successfully isolated from isobaric and pseudo-isobaric impurities and used for radiolabeling experiments at PSI. The radionuclide allows optimization of alpha radionuclide therapy.

INTRODUCTION

^{149}Tb is a promising candidate for targeted radionuclide therapy with α-particles. It can be produced via proton induced spallation reactions on tantalum followed by online mass separation at ISOLDE [1].
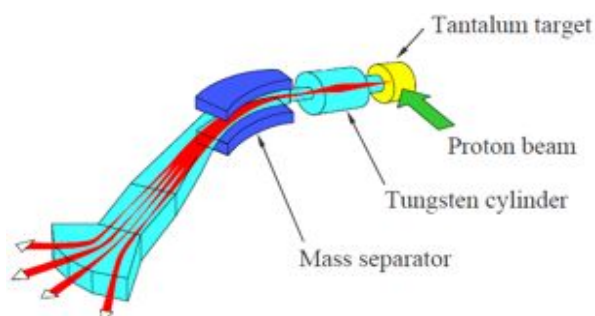
Fig. 1: Schematic principal of ISOLDE.

The principle schema of ISOLDE is presented in Fig. 1. High energy protons (1 GeV) induce the spallation reaction on a heated tantalum target (up to 2400 °C). Spallation products emitted by diffusion out of the target are ionized and separated online in the mass separator. Beams of isobar and pseudo-isobar ions are produced. For transportation of the terbium radioisotope to PSI, deposition of the ion beam onto a metal foil is required.

In the proof of concept study we develop a one-step separation procedure for the chemical isolation of ^{149}Tb from isobaric and pseudo-isobaric impurities based on a miniaturized chromatographic column. The radionuclide should be finally obtained with high chemical and radionuclidic purity in a form directly applicable for radiolabeling of biomolecules.

EXPERIMENTAL

The radionuclide ^{149}Tb was produced by spallation of tantalum and following mass separation at ISOLDE. The ion beam was deposited onto self-made one-sided zinc-covered gold foils containing a mass of up to 5 mg of zinc.

The zinc layer containing the deposited ions was dissolved in 1 ml 0.1 M HCl. 100 µl of 1 M NH$_4$Cl solution were added. The chemical isolation of ^{149}Tb from isobaric and pseudo-isobaric by-products as well as stable zinc was done by cation exchange chromatography with the complexing agent α-HIB (α–hydroxyisobutyrate).

To optimize the separation time and elution volume a miniaturized chromatographic column of 50 x 5 mm dimensions, filled with a strong cation exchange resin in NH$_4^+$-form, was applied. The mixture of radionuclides was loaded onto the column. The isolation of ^{149}Tb from impurities was performed by gradient elution of the chromatographic column in order to minimize the volume of the terbium-fraction. The obtained ^{149}Tb in form of its α-HIB-complex was directly used for radiolabeling reactions.

The produced ^{149}Tb was used for radiolabeling of the tumor specific tracer DOTA-folate. For this propose 12 nmol of DOTA-folate were radiolabeled with 5 MBq ^{149}Tb in 1000 µl total volume of reaction mixture at pH = 4.75. The mixture was incubated at 95°C for 10 minutes. The radiolabeling yield was monitored by means of HPLC.

RESULTS AND DISCUSSION

In the proof of concept study up to about 23 MBq of ^{149}Tb were produced at ISOLDE. It could be successfully isolated from impurities of ^{149}Gd, ^{133m}Ce as well as from stable zinc. The radionuclide was obtained in a small volume (< 1 ml) and in a chemical form, which is usable for radiolabeling reactions. Finally up to 6 MBq of ^{149}Tb were available at PSI for radiopharmaceutical purposes. The vitamin derivate DOTA-folate was successfully radiolabeled with a reaction yield > 96 %, confirming the high chemical purity of the radionuclide preparation.

CONCLUSION AND OUTLOOK

We developed an efficient production strategy for ^{149}Tb available from ISOLDE. In a proof of concept study the radionuclide was successfully used for the preparation of novel therapeutic radiolabeled compounds. The availability of this radionuclide allows optimization of alpha radionuclide therapy. The next step is the scale up of the radionuclide production and introduction of ^{149}Tb in systematic preclinical trials.

ACKNOWLEDGEMENT

REFERENCE

[1] G.-J. Beyer et al., Eur. J. Nucl. Med., **31** (2004), p. 547-554.

PRODUCTION OF [161]Tb IN THERAPEUTIC AMOUNTS AT THE PSI SPALLATION INDUCED NEUTRON SOURCE SINQ

H. Dorrer (Univ. Bern & PSI), K. Zhernosekov, A. Vögele (PSI),
R. Schibli (ETHZ & PSI), A. Türler (Univ. Bern & PSI)

The therapeutic radionuclide [161]Tb was produced at the PSI spallation neutron source SINQ in quantities adequate for medical applications. It can be isolated very effectively from irradiated [160]Gd-targets. We demonstrated that SINQ is a reliable source for [161]Tb production in order to provide the nuclide for advanced radiopharmaceutical science at CRS.

INTRODUCTION

[161]Tb is a very appropriate candidate for targeted radionuclide therapy in nuclear oncology [1, 2]. Recently, we reported the production of [161]Tb at PSI based on up to 15 mg [160]Gd-targets irradiated at the ILL high flux reactor (thermal neutron flux: $\sim 1 \cdot 10^{15}$ cm^{-2}s^{-1}) [3]. For the chemical separation of [161]Tb from the irradiated [160]Gd we implemented one-step cation exchange chromatography. In this study we present the production of therapeutic amounts of [161]Tb at the spallation induced neutron source SINQ (thermal neutron flux: $\sim 4 \cdot 10^{13}$ cm^{-2}s^{-1}). To produce comparable quantities of [161]Tb at the lower thermal neutron flux an increase of the mass of the [160]Gd-target by a factor of more than 10 is required. The increased lanthanide mass leads, however, to a degradation of the separation performance. Therefore, the chemical procedure applied must be optimized.

EXPERIMENTAL

Targets with up to 160 mg of highly enriched [160]Gd in its nitrate form were irradiated at SINQ with a thermal neutron flux of up to $4 \cdot 10^{13}$ cm^{-2}s^{-1} for about 20 days.

The separation of [161]Tb from the massive [160]Gd-target was performed by cation exchange chromatography with the complexing agent α-HIB (α–hydroxyl-isobutyrate) on a 300 x 9 mm dimensions sized column, filled with a strong cation exchange resin in NH_4^+-form. The irradiated target material was dissolved in 0.05 M NH_4Cl solution and loaded onto the separation column. To improve the elution profile of [161]Tb, gradient elution of the separation column was applied. The fraction of [161]Tb, separated from gadolinium, was acidified with 3 ml 1 M HCl and loaded on a 12 x 5 mm secondary cation exchange column. The column was eluted with 5 M HCl. The resulting solution was evaporated to dryness under nitrogen and the residue redissolved in 300 μl of 0.05 M HCl.

For assessment of the radionuclide quality, 0.6 nmol to 2.8 nmol of DOTA-Tyr3-octreotate (DOTATATE) were radiolabeled with 200 MBq [161]Tb, resulting in molar metal to ligand ratios from 1:2 to 1:10. The radiolabeling reaction was performed in 65 μl volume of reaction mixture, pH = 4.5, for 30 min at 95 °C. The radiolabeling yield was determined by means of HPLC.

RESULTS AND DISCUSSION

Up to about 18 GBq of [161]Tb (EOB) were produced at SINQ. Optimization of the chemical separation could be successfully achieved by gradient elution of the chromatographic column without changes to the established separation facility. More than 95 % of [161]Tb was obtained in ~15 ml fraction whereby the Gd-amount was reduced by factor of more than 10^5 (Fig. 1).
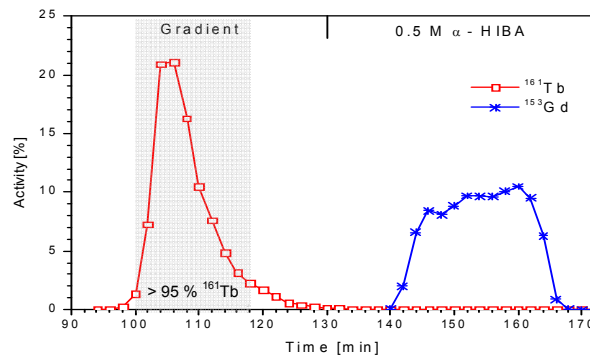
Fig. 1: Test separation of a 300 mg Gd-target.

Quantities of [161]Tb adequate for medical applications of up to 14.5 GBq could be obtained after processing the targets irradiated at SINQ. The DOTA-peptide DOTATATE could be radiolabeled at molar [161]Tb to peptide ratios of 1:6 with labelling yields > 99 %, evidencing high specific activity and chemical purity of [161]Tb.

CONCLUSION

We developed and established the production of [161]Tb in therapeutic amounts at SINQ providing an independent and reliable source of the novel therapeutic radionuclide. Currently the radionuclide is successfully introduced into preclinical trials at CRS.

ACKNOWLEDGEMENT

REFERENCES

[1] H. Uusijärvi et al., J. Nucl. Med., **47** (2006)., p 807-814.

[2] S. Lehenberger et al., Nucl. Med. and Biol., **38** (2011), p 917-924.

[3] H. Dorrer et al., Ann. Rep. Lab. of Radio- & Environ. Chemistry, Uni. Bern & PSI (2010), p. 58.

THE NEW GMP (GOOD MANUFACTURING PRACTICE) COMPLIANT RADIO-PHARMACEUTICAL LABORATORY AT THE INSEL HOSPITAL IN BERN

A. Türler (Univ. Bern & PSI), K. Zhernosekov (PSI), K. von Bremen, Ch. Schweinsberg, C. Dumas (SWAN),
T. Krause, M. Walter (INSELSPITAL), S. Braccini (Univ. Bern)

The Laboratory for Radiochemistry and Environmental Chemistry (Univ. Bern & PSI) in collaboration with SWAN Isotopen AG has completed the installation of a modern research and development laboratory for the small-scale production of radiopharmaceuticals on the premises of the Insel University hospital. Five hotcells and a sterile isolator were delivered and set-up by TEMA Sinergie Srl and the site acceptance tests were completed by the end of 2011.

INTRODUCTION

The advances of modern nuclear medicine in the diagnosis and treatment of malignant diseases, cardiology and neurology has prompted the formation of SWAN Isotopen AG, an innovative private company dedicated to the production and marketing of radiopharmaceuticals for positron emission tomography (PET). SWAN Isotopen AG decided to build and operate a dedicated facility on the premises of the Insel University hospital in Bern.

INFRASTRUCTURE

The five story building contains in the basement a multifunctional cyclotron Cyclone® 18/9 by IBA, equipped with an external beam line, which ends in a separate irradiation cave. The basement also contains the control room for the accelerator and additional laboratories operated by the laboratory for high energy physics (LHEP) for detector tests and radiology. The cyclotron was delivered on June 16, 2011 and lowered into the cyclotron bunker. First beam is expected in February 2012.

On the first floor, space for four radiopharmaceutical laboratories was planned. Three laboratories were equipped with hotcells. Two of the labs are reserved for SWAN Isotopen AG and contain the production facilities for ^{18}FDG (^{18}F-desoxyglucose), a radiopharmaceutical for PET. One lab is leased to Bern University as radiopharmaceutical research and development laboratory. The LCH was charged with planning and equipping the laboratory with hotcells. As supplier TEMA Sinergie Srl was chosen to assure compatibility of the equipment with SWAN. The laboratory was equipped with three multi-purpose research and development hotcells, which will house automated synthesis modules, that are either own developments or commercial products. The hotcells can be connected through shielded capillaries to the cyclotron. Two of the hotcells are shielded with 7.5 cm (one front access door only) and one with 5 cm of Pb. The hotcells comply with air quality class C, as does the laboratory environment. One hotcell with air quality A is dedicated to sterile filtration and dispensing of radiopharmaceuticals to vials or syringes and connected to the 3 research hotcells by capillaries. A larger, general purpose hotcell with telemanipulators (air class C) and integrated autoclave allows the small scale production and testing of novel radiopharmaceuticals. The hotcells are complemented by a sterile isolator box (air class A) to handle inactive or biohazardous materials under sterile conditions. All hotcells are equipped with a continuous radiation monitor on the exhaust air and a relevant switch to the emergency compression system. A view of the laboratory is shown in Fig. 1.

Fig. 1: Photograph of the GMP compliant R&D laboratory equipped with hotcells (see text).

Adjacent to the room containing the hotcells, a quality control laboratory can be reached by means of an airlock pass through box (Fig. 2).
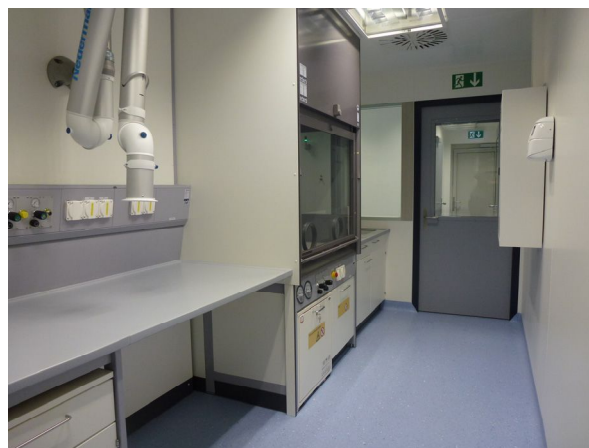
Fig. 2: Photograph of the quality control laboratory. A GC- and HPLC system will be installed later.

The upper floors of the SWAN house contain offices and two modern patient wards. One dedicated to palliative care and one for patients of nuclear medicine.

The building will be officially inaugurated on January 12, 2012 and presented to the public.

THE NEW ^{14}C AMS LABORATORY AT THE UNIVERSITY OF BERN: PROGRESS REPORT

S. Szidat, E. Vogel, M. Battaglia (Univ. Bern), A. Türler (Univ. Bern & PSI), L. Wacker, H.A. Synal (ETHZ)

We will establish a new ^{14}C accelerator mass spectrometry (AMS) laboratory at the University of Bern, which shall become operational in 2012. This report elucidates the progress of this project during 2011.

INTRODUCTION

Precise determinations of the radionuclide ^{14}C have widespread applications in many branches of natural sciences, ranging from geochemistry, archaeology, and climate science to biomedical and pharmacological applications. In order to strengthen ^{14}C-based research in our laboratory and at the University of Bern in general, the decision was made in 2010 to install an accelerator mass spectrometry (AMS) system on site [1], which shall be operational in 2012. In the following, the preparations made so far are presented.

AMS SYSTEM

The setup of the AMS system MICADAS [2] was planned in detail in 2011. Recent improvements and adaptations of the original prototype have been implemented carefully. Many individual parts were already manufactured by the workshop of ETH Zurich or commissioned from industrial providers.

An updated version of the gas inlet system for the supply of the gas-capable ion source with carbon dioxide [3] was produced at the workshop of the University of Bern. This gas inlet system will allow feeding of the AMS with CO_2 from small samples sealed in glass ampoules for automated ^{14}C measurement. Furthermore, this device establishes a basis for the coupling of an elemental analyser (EA) with the AMS for routine combustion and online ^{14}C analysis of small solid samples [4].

SAMPLE PREPARATION LABORATORY

For routine ^{14}C measurement of archaeological and environmental samples, chemical pre-treatment procedures are required to remove contaminations and to isolate the fractions of interest [5]. For this, a new sample preparation laboratory was installed and equipped with instruments dedicated for ^{14}C analysis (Fig. 1).

Fig. 1: The new ^{14}C sample preparation laboratory.

AUTOMATED GRAPHITISATION EQUIPMENT

After pre-treatment, most samples will be combusted to carbon dioxide, which in turn will be converted into graphite-like carbon, the solid target material for AMS measurement. For routine operation of this process, an automated graphitisation equipment (AGE) [6] was built up (Fig. 2). This device combines an EA with seven reduction reactors fully controlled by a Lab-VIEW programme.

Fig. 2: The automated graphitisation equipment (AGE) for routine production of solid AMS targets.

ACKNOWLEDGEMENTS

REFERENCES

[1] S. Szidat et al., Ann. Rep. Lab. of Radio & Environ. Chem., Uni Bern & PSI (2010), p. 63.

[2] H.A. Synal et al., Nucl. Instrum. Meth. Phys. Res. B, **259**, 7 (2007).

[3] M. Ruff et al., Nucl. Instrum. Meth. Phys. Res. B, **268**, 790 (2010).

[4] M. Ruff et al., Radiocarbon, **52**, 1645 (2010).

[5] I. Hajdas et al., Nucl. Instrum. Meth. Phys. Res. B, **223-224**, 267 (2004).

[6] L. Wacker et al., Nucl. Instrum. Meth. Phys. Res. B, **268**, 931 (2010).

FOSSIL VERSUS NON-FOSSIL SOURCES OF FINE ELEMENTAL AND ORGANIC CARBONACEOUS PARTICULATE MATTER IN NORTHEAST SPAIN

M.C. Minguillón, X. Querol (CSIC), S. Szidat, S.M. Fahrni (Univ. Bern), L. Wacker (ETHZ),
N. Perron, U. Baltensperger, A.S.H. Prévôt (PSI/LAC)

Submicron fine particulate matter samples were collected during summer and winter at an urban background site in Barcelona (BCN) and at a forested regional background site in Montseny (MSY) in Northeast Spain. We present radiocarbon (^{14}C) analysis for elemental and organic carbon (EC and OC) for these campaigns aiming at the apportionment of fossil and non-fossil sources.

INTRODUCTION

Submicron particulate matter (PM_1, particles with an aerodynamic diameter <1 µm) contains substantial fractions of carbonaceous aerosol [1]. Carbonaceous aerosol comprises a wide variety of organic compounds, collectively referred to as organic carbon (OC), elemental carbon (EC). An accurate knowledge of the sources of EC and OC is necessary to design strategies aimed at mitigating the effects of aerosols. Radiocarbon (^{14}C) analysis is a powerful tool used to help apportion the sources of carbonaceous aerosols [2], due to its ability to differentiate between contemporary and fossil sources. Since EC and OC may have different origins, source apportionment of EC and OC separately (as opposed to only total carbon, TC) provides additional valuable information.

METHODOLOGY

During the DAURE campaign (Determination of the sources of atmospheric Aerosols in Urban and Rural Environments in the Western Mediterranean) [3], two sampling sites were selected in Northeast Spain: Barcelona (BCN), an urban background site (80 m a.s.l.), and Montseny (MSY), a forested regional background site 50 km away from Barcelona (720 m a.s.l.). PM_1 samples were collected on quartz fibre filters. Sampling periods were 48 h in winter (February-March 2009) and 24 h in summer (July 2009). OC and EC were isolated and combusted to carbon dioxide as described in [3], a method similar to [4]. ^{14}C measurements were performed at the accelerator mass spectrometer MICADAS at ETH Zurich [5].

RESULTS

During the winter period, fossil sources (mainly from road traffic) accounted for 87±1% of EC at BCN, whereas at MSY this percentage was 66±3 % (Fig .1). In summertime, these values were 91±1% and 79±4% at BCN and MSY, respectively. In both seasons, the fossil contribution to EC at the urban site is higher than at the rural site, as expected. In absolute values, the difference is larger. Fossil EC at BCN was 6.3 times higher than at MSY in winter and 4.5 times higher in summer. The higher contributions of non-fossil EC in winter with respect to summer are likely due to higher emissions from residential heating using wood and open burning of agricultural biomass [3].

During the winter period, fossil OC was 40±4% of OC at BCN and 31±4% at MSY. These values are similar to those obtained during winter at Zurich, Switzerland (32%) [2], and at Gothenburg, Sweden (35–45% at an urban site and 35–40% at a rural site) [6]. In summer fossil OC was 48±4% of OC at BCN and 25±5% at MSY; this again being comparable to contributions at Gothenburg in summer (31–47 %) [6]. Non-fossil OC mainly stemmed from biomass burning and biogenic secondary organic aerosols during winter and summer, respectively.
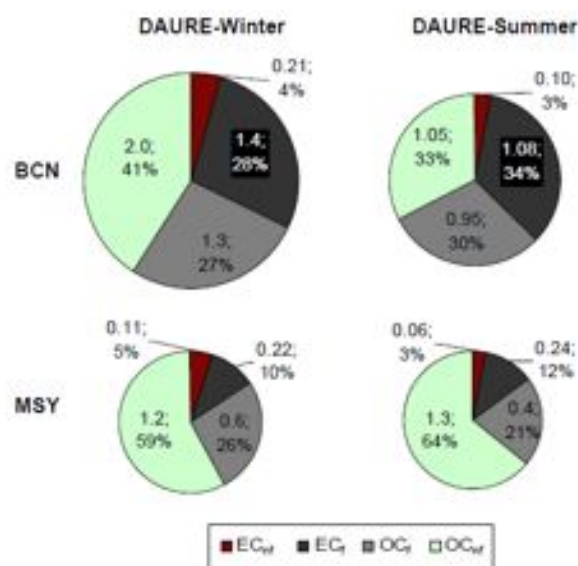
Fig. 1: Fossil (f) and non-fossil (nf) fractions of total carbon; concentrations in µgm^{-3} and % of total carbon [3].

REFERENCES

[1] J.L. Jimenez et al., Science, **326**, 1525 (2009).
[2] S. Szidat et al., J. Geophys. Res., **111**, D07206 (2006).
[3] M.C. Minguillón et al., Atmos. Chem. Phys., **11**, 12067 (2011).
[4] Y.L. Zhang et al., this report, p. 65.
[5] M. Ruff et al., Radiocarbon, **49**, 307 (2007).
[6] S. Szidat et al., Atmos. Chem. Phys., **9**, 1521 (2009).

ON THE ISOLATION OF OC AND EC OF CARBONACEOUS AEROSOLS FOR ^{14}C MEASUREMENT: A MODIFIED THERMAL-OPTICAL METHOD

Y.L. Zhang (Univ. Bern & PSI), S. Szidat (Univ. Bern), N. Perron, P. Zotter, M.C. Minguillón,
A.S.H. Prévôt, U. Baltensperger (PSI/LAC), L. Wacker (ETHZ)

[14]C/^{12}C values of carbonaceous aerosol particles give a unique and absolute measure of the contemporary-to-fossil carbon source ratio, which can be used for apportionment of biogenic and anthropogenic emissions. Here, we present a new thermal-optical method for the collection of organic carbon (OC) and elemental carbon (EC) for ^{14}C measurement, which reduces the uncertainty of the source apportionment results of the individual carbon fractions.

INTRODUCTION

Carbonaceous aerosols, which comprise the large fractions of elemental carbon (EC) and organic carbon (OC), badly affect climate and human health. However, there is a considerable uncertainty about detailed apportionment and quantification of its sources due to the large number of origins and chemical compounds associated with the aerosols. Radiocarbon (^{14}C) measurements of EC and OC allow an improvement in carbonaceous aerosol source apportionment, leading to a full and unambiguous distinction and quantification of the contributions from non-fossil and fossil sources [1, 2].

Thermal-optical analysis (TOA) has been widely used for the determination of EC and OC [3]. However, such TOA methods have not yet been applied successfully to isolate EC and OC for ^{14}C analyses. The biggest challenge is to define a split point to isolate EC and OC for ^{14}C analyses. This split point between OC and EC applied in previous TOA methods cannot be directly used to isolate the individual carbon fraction for ^{14}C measurement, since it does not provide a physical split or boundary of OC and EC. As the non-fossil fractions of EC and OC may differ significantly [1], incomplete OC removal will substantially bias the ^{14}C result of the EC fraction. This study presents a new TOA method for OC/EC collection for ^{14}C measurement.

NEW TOA PROTOCOL: OC/EC ISOLATION FOR ^{14}C ANALYSIS

If OC removal is performed in oxygen after water extraction of the filters [4], charring can be reduced to less than 10% for all studied filters including winter/summer and rural/city samples. This demonstrates that the optimal method to isolate EC from TC for ^{14}C measurement should be based on the oxidation of OC in pure oxygen for water-extracted sample filters.

The TOA protocol in this study employs pure O_2 as the carrier gas and sets the duration of each temperature step long enough to yield well-resolved carbon peaks for ^{14}C measurement of individual carbon fractions. The temperature setup must be optimized to assure the complete decomposition of OC, and both charring and premature EC evolution should be minimized.

The new protocol (Fig. 1) consists of four steps aiming at complete removal of OC prior to EC collection with the best possible EC recovery: (1) T1 is set at 375°C during 150 s to allow OC removal with negligible premature EC loss. (2) T2 is then increased to an intermediate value between 425°C and 600°C to remove refractory OC with minimal EC loss and prevent OC from charring in the following step (T3 and T4). The duration is set to 120 s to allow different chosen temperatures (from 425 and 600°C) to remain close to the set value for about 20 s. (3) T3 not only removes any remaining OC, but also evaluates whether there is still residual unevolved and uncharred OC evolving in the last fraction (T4). For this, helium is used as carrier gas. The thermal parameter in T3 is similar to the last two helium steps in conventional protocols like EUSAAR2 and IMPROVE [3]. For a limited number of samples, the different temperatures in step T3 were also investigated by OC/EC analyser and ^{14}C measurement. (4) T4 is set to 760°C for 150s. The carbon released in this step can be regarded as pure EC and thus collected for AMS measurement.

The new method allows collecting 70–80% EC without positive bias from charring and negative bias from premature EC oxidation.
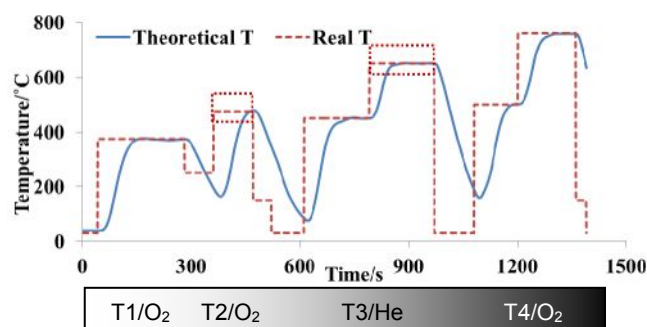
Fig. 1: Four steps thermal-optical OC/EC separation method for ^{14}C analysis.

REFERENCES

[1] S. Szidat et al., Atmos. Chem. Phys., **9**, 1521 (2009).
[2] S. Szidat, Chimia, **63**, 157 (2009).
[3] F. Cavalli et al., Atmos. Meas. Tech., **3**, 79 (2010).
[4] N. Perron et al., Ann. Rep. Lab. of Radio & Environ. Chem., Uni Bern & PSI (2008), p. 49.

DIURNAL CYCLE OF FOSSIL AND NON-FOSSIL TOTAL CARBON USING ^{14}C ANALYSES DURING CALNEX

P. Zotter, A.S.H. Prévôt, U. Baltensperger (PSI/LAC), Y.L. Zhang (Univ. Bern & PSI), S. Szidat (Univ. Bern),
L. Wacker (ETHZ), X. Zhang, R. Weber (GA Tech), Y.H. Lin, J.D. Surratt (Univ. NC), P. Hayes,
J.L. Jimenez (Univ. CO)

For the first time, radiocarbon measurements were performed on aerosol filters with a sampling time of only 3 and 4 h. As a result, a diurnal pattern with the fossil and non-fossil composition of carbonaceous aerosols can be resolved for a suburban site near Los Angeles.

INTRODUCTION

Aerosols are important for the Earth's climate and have a negative impact on human health [1]. Carbonaceous particles (total carbon, TC) are a major fraction of the fine aerosol and are classified into the subfractions elemental carbon (EC) and organic carbon (OC) [2]. EC originates from fossil-fuel combustion and biomass burning. OC can be emitted directly as primary organic aerosol from biogenic sources, wood burning and fossil fuel combustion or can be formed in the atmosphere as secondary organic aerosol [3].

Analysis of the radioactive isotope ^{14}C is a unique tool for distinguishing fossil and non-fossil sources of carbonaceous aerosol, because ^{14}C in fossil fuels is completely depleted, whereas other sources have a contemporary ^{14}C level [3]. The ^{14}C/^{12}C content in the EC and OC fractions provides a quantitative and unambiguous measurement of the fossil/non-fossil carbon, thereby directly addressing a major uncertainty in the present understanding of organic aerosol sources.

This study presents the first ^{14}C measurements performed on high time resolution (3-4 h) filter samples. As a result, a diurnal pattern with the fossil and non-fossil composition of carbonaceous aerosols can be resolved.

METHODS

Filter sampling was conducted during the CalNex-2010 field campaign from May 15 to the June 16, 2010 at the California Institute of Technology (CAL-TECH), located about 20 km northeast of downtown Los Angeles using a high-volume sampler with PM1 inlet.

Isolation of TC is carried out using the THEODORE system [4] and a Sunset ECOC Analyzer [5]. The evolving CO_2 is cryo-trapped and sealed in glass ampoules for ^{14}C measurements which are then performed with the mini radiocarbon dating system MI-CADAS [6] at ETH Zürich.

RESULTS

First results for TC for June 4 and 14 (see Fig. 1) show a distinct diurnal variation with a peak for fossil TC (TC_f) in the early afternoon after the plume of the L.A. basin is transported to Pasadena with the sea breeze (wind direction SW). The low concentration of EC (max. 0.8 and 1.0 µg/m^3 for June 4 and June 14,

respectively) and aerosol and gas-phase measurements from other groups (e.g. [7]) indicate that the increase of TC_f in the early afternoon is mainly due to SOA formed from anthropogenic precursor gases in the L.A. plume.

The non-fossil TC (TC_{nf}) is on average 41% and 45% for June 4 and June 14, respectively, and stays roughly constant between 2 and 3 µg/m^3 throughout both days, even though the Los Angeles area is strongly influenced by traffic-related emissions. This indicates that biogenic, cooking or other contemporary carbon sources also significantly affect the total carbon budget in urban areas.
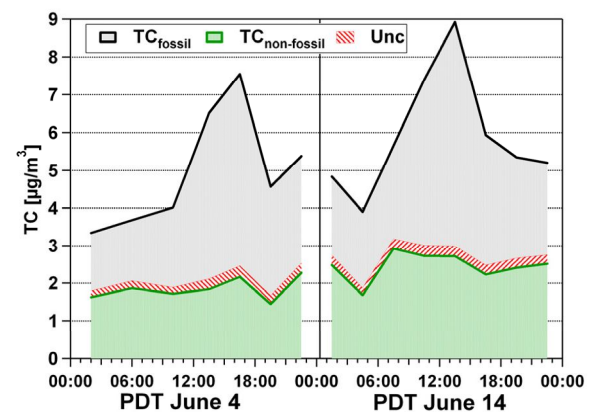
Fig. 1: Daily cycle of TC_f and TC_{nf} for June 4 and 14, 2010. The red shaded area is the uncertainty for the discrimination between TC_f and TC_{nf}

ACKNOWLEDGEMENT

REFERENCES

[1] C.A. Pope III and D.W. Dockery, J. Air Waste Manage. Assoc., **56**, 709(2006).
[2] M.C. Jacobson et al., Rev. Geophys., **38**, 267 (2000).
[3] S. Szidat et al., J. Geophys. Res., **111**, D07206 (2006).
[4] S. Szidat et al., Radiocarbon, **46**, 475(2004).
[5] Y.L. Zhang et al., this report, p. 65.
[6] M. Ruff et al., Radiocarbon, **49**, 307 (2007).
[7] X. Zhang et al., Geophys. Res. Lett., **38**, L21810 (2011).

QUANTIFICATION OF THE CARBONACEOUS MATTER ORIGIN IN SUBMICRON MARINE AEROSOL BY ^{13}C AND ^{14}C ISOTOPE ANALYSIS

D. Ceburnis, C.D. O'Dowd (NUI Galway), A. Garbaras (CPST Vilnius), S.M. Fahrni, S. Szidat (Univ. Bern), N. Perron, A.S.H. Prévôt (PSI/LAC), L. Wacker (ETHZ), M. Rinaldi, M.C. Facchini (NRC Bologna)

Dual carbon isotope analysis of marine aerosol samples has been performed for the first time demonstrating a potential in organic matter apportionment between three principal sources: marine, terrestrial (non-fossil) and fossil fuel due to unique isotopic signatures. The results presented here provide conclusive evidence of a dominant biogenic organic fraction to organic aerosol over biologically active oceans.

INTRODUCTION

Recent studies revealed significant enrichments of carbonaceous aerosol in marine air during periods of high plankton activity, suggesting a biogenic source from both organically-enriched sea-spray and condensable ocean-derived organic vapours [1]. This enrichment of organic matter in sea-spray has important implications for marine aerosol haze and cloud layers, ultimately contributing to climate change.

For source identification of carbonaceous marine aerosol, a dual isotopic approach has been applied [2]: on the one hand, the ^{14}C/^{12}C ratio was used to elucidate the contributions of contemporary carbon biomass emissions and fossil fuel emissions; on the other hand, the ratio of ^{13}C/^{12}C was employed to determine carbon emissions associated with different plants, both terrestrial and oceanic, due to preferential photosynthesis uptake routes of heavier or lighter inorganic carbon isotopes. This allowed the quantification of the biogenic marine carbon (i.e. carbon derived from marine plants), continental non-fossil carbon (i.e. carbon derived from terrestrial plant emissions and/or biomass burning emissions), and fossil fuel carbon emissions.

METHODS

Marine aerosol samples were collected over the N.E. Atlantic at Mace Head (western Ireland) from April to October 2006 [2]. Fine particulate matter samples (<1.5 μm) were collected on a weekly basis using automated sector control system to separate clean marine and polluted air masses.

For three samples of each of these source regimes, ^{13}C and ^{14}C isotope analyses were performed using isotope mixing equations, which yielded reference source ratios by an error minimisation approach [2]. For marine, continental and fossil sources, the respective δ^{13}C ratios of −20 ‰, −26 ‰, −29 ‰, and Δ^{14}C ratios of −50 ‰, +100 ‰, −1000 ‰ were obtained from this approach.

RESULTS

On average, as shown in Fig. 1, carbon in marine samples comprised 79% marine biogenic carbon, 14% fossil fuel carbon and 7% continental non-fossil carbon while in non-marine air masses 37% are attributed to fossil fuel, 31% continental (non-fossil carbon) and 32% marine biogenic carbon. The presence of a marine source in polluted air masses (and of similar magnitude to the continental non-fossil source) has significant implications in interpreting other experimental results where dual isotope analysis is not performed and all organic matter is typically attributed to terrestrial (continental non-fossil and fossil fuel) sources.

REFERENCES

[1] C.D. O'Dowd et al., Nature, **431**, 676 (2004).
[2] D. Ceburnis et al., Atmos. Chem. Phys., **11**, 8593 (2011).
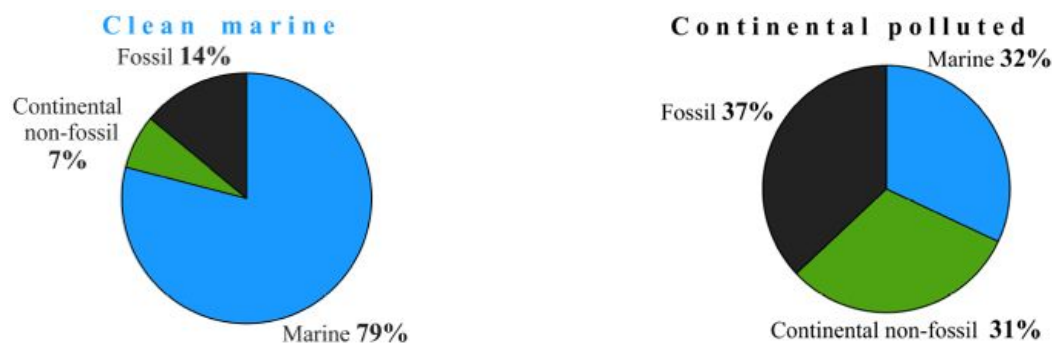
Fig. 1: Average source contribution to organic matter in terms of fossil fuel carbon (black), non-fossil fuel continental carbon (dark green), and marine biogenic carbon (blue) sources for clean marine and continental polluted air masses at Mace Head [2].

LIST OF PUBLICATIONS

Heavy Elements

J. Even, J. Ballof, W. Brüchle, R.A. Buda, Ch.E. Düllmann, K. Eberhardt, A. Gorshkov, E. Gromm, D. Hild, E. Jäger, J. Khuyagbaatar, J.V. Kratz, J. Krier, D. Liebe, M. Mendel, D. Nayak, K. Opel, J.P. Omtvedt, P. Reichert, J. Runke, A. Sabelnikov, F. Samadani, M. Schädel, B. Schausten, N. Scheid, E. Schimpf, A. Semchenkov, P. Thörle-Pospiech, A. Toyoshima, A. Türler, V. Vilas, N. Wiehl, T. Wunderlich, A. Yakushev
The recoil transfer chamber-An interface to connect the physical preseparator TASCA with chemistry and counting setups
Nucl. Instrum. Methods Phys. Res. Sect. A 638, 157–164 (2011).

H.W. Gäggeler
Gas chemical properties of heaviest elements
Radiochim. Acta **99** (7-8): 503-513 (2011).

J.M. Gates, Ch.E. Düllmann, M. Schädel, A. Yakushev, A. Türler, K. Eberhardt, J.V. Kratz, D. Ackermann, L.L. Andersson, M. Block, W. Brüchle, J. Dvorak, H.G. Essel, P.A. Ellison, J. Even, U. Forsberg, J. Gellanki, A. Gorshkov, R. Graeger, K.E. Gregorich, W. Hartmann, R.D. Herzberg, F.P. Heßberger, D. Hild, A. Hübner, E. Jäger, J. Khuyagbaatar, B. Kindler, J. Krier, N. Kurz, S. Lahiri, D. Liebe, B. Lommel, M. Maiti, H. Nitsche, J.P. Omtvedt, E. Parr, D. Rudolph, J. Runke, H. Schaffner, B. Schausten, E. Schimpf, A. Semchenkov, J. Steiner, P. Thörle-Pospiech, J. Uusitalo, M. Wegrzecki, N. Wiehl
First superheavy element experiments at the GSI recoil separator TASCA: The production and decay of element 114 in the $^{244}Pu(^{48}Ca,3$-$4n)$ reaction
Phys. Rev. C 83, 054618 (2011).

W. Maneschg, L. Baudis, R. Dressler, K. Eberhardt, R. Eichler, H. Keller, R. Lackner, B. Praast, R. Santorelli, J. Schreiner, M. Tarka, B. Wiegel, A. Zimbal
Production and characterization of a custom-made Th-228 source with reduced neutron source strength for the borexino experiment
arXiv.org (2011).

A. Serov, N.V. Aksenov, G.A. Bozhikov, R. Eichler, R. Dressler, V.Y. Lebedev, O. Petrushkin, D. Piguet, S. Shishkin, E. Tereshatov, A. Türler, A. Vögele, D. Wittwer, H.W. Gäggeler
Adsorption interaction of astatine species with quartz and gold surfaces
Radiochim. Acta **99** (9): 593-600 (2011).

A. Serov, R. Eichler, R. Dressler, D. Piguet, A. Türler, A. Vögele, D. Wittwer, H.W. Gäggeler
Gas chromatography of indium in macroscopic and carrier-free amounts using quartz and gold as stationary phases
Radiochim. Acta **99** (2): 95-101 (2011).

D. Wittwer, R. Dressler, R. Eichler, H.W. Gäggeler, D. Piguet, A. Serov, A. Türler, A. Vögele
The thermal release of scandium from titanium metal – a simple way to produce pure SC-44 for pet application
Radiochim. Acta **99** (3): 193-196 (2011).

L. Canella, P. Kudejova, R. Schulze, A. Türler, J. Jolie
Characterisation and optimisation of the new Prompt Gamma-ray Activation Analysis (PGAA) facility at FRM II
Nucl. Instrum. Methods Phys. Res. Sect. A 638, 108–113 (2011).

Surface Chemistry

T. Bartels-Rausch, G. Krysztofiak, A. Bernhard, M. Schläppi, M. Schwikowski, M. Ammann
Photoinduced reduction of divalent mercury in ice by organic matter
Chemosphere **82** (2): 199-203 (2011).

T. Bartels-Rausch, T. Ulrich, T. Huthwelker, M. Ammann
A novel synthesis of the N-13 labelled atmospheric trace gas peroxynitric acid
Radiochim. Acta **99** (5): 285-292 (2011).

F. Enzmann, M.M. Miedaner, M. Kersten, N. von Blohn, K. Diehl, S. Borrmann, M. Stampanoni, M. Ammann, T. Huthwelker
3-D imaging and quantification of graupel porosity by synchrotron-based micro-tomography
Atmos. Meas. Tech. **4** (10): 2225-2234 (2011).

M. Shiraiwa, M. Ammann, T. Koop, U. Pöschl
Gas uptake and chemical aging of semisolid organic aerosol particles
Proc. Nat. Acad. Sci. **108** (27): 11003-11008 (2011).

M. Shiraiwa, Y. Sosedova, A. Rouvière, H. Yang, Y. Zhang, J.P.D. Abbatt, M. Ammann, U. Pöschl
The role of long-lived reactive oxygen intermediates in the reaction of ozone with aerosol particles
Nat. Chem. **3** (4): 291-295 (2011).

Y. Sosedova, A. Rouviere, T. Bartels-Rausch, M. Ammann
UVA/VIS-induced nitrous acid formation on polyphenolic films exposed to gaseous NO_2
Photochem. Photobiol. **10** (10): 1680-1690 (2011).

D.E. Starr, D. Pan, J.T. Newberg, M. Ammann, E.G. Wang, A. Michaelides, H. Bluhm
Acetone adsorption on ice investigated by X-ray spectroscopy and density functional theory
Phys. Chem. Chem. Phys. **13** (44): 19988-19996 (2011).

V. Zelenay, M. Ammann, A. Krepelová, M. Birrer, G. Tzvetkov, M.G.C. Vernooij, J. Raabe, T. Huthwelker
Direct observation of water uptake and release in individual submicrometer sized ammonium sulfate and ammonium sulfate/adipic acid particles using X-ray microspectroscopy
J. Aerosol Sci **42** (1): 38-51 (2011).

V. Zelenay, T. Huthwelker, A. Křepelová, Y. Rudich, M. Ammann
Humidity driven nanoscale chemical separation in complex organic matter
Environ. Chem. **8** (4): 450-460 (2011).

V. Zelenay, M.E. Monge, B. D'Anna, C. George, S.A. Styler, T. Huthwelker, M. Ammann
Increased steady state uptake of ozone on soot due to UV/VIS radiation
J. Geophys. Res. **116** (D11): D11301 (2011).

ANALYTICAL CHEMISTRY

N. Bukowiecki, P. Zieger, E. Weingartner, Z. Jurányi, M. Gysel, B. Neininger, B. Schneider, C. Hueglin, A. Ulrich, A. Wichser, S. Henne, D. Brunner, R. Kaegi, M. Schwikowski, L. Tobler, F.G. Wienhold, I. Engel, B. Buchmann, T. Peter, U. Baltensperger
Ground-based and airborne in-situ measurements of the Eyjafjallajökull volcanic aerosol plume in Switzerland in spring 2010
Atmos. Chem. Phys. **11** (19): 10011-10030 (2011).

A. Eichler, W. Tinner, S. Brütsch, S. Olivier, T. Papina, M. Schwikowski
An ice-core based history of siberian forest fires since AD 1250
Quat. Sci. Rev. **30** (9-10): 1027-1034 (2011).

J. Gabrieli, G. Cozzi, P. Vallelonga, M. Schwikowski, M. Sigl, J. Eickenberg, L. Wacker, C. Boutron, H.W. Gäggeler, P. Cescon, C. Barbante
Contamination of alpine snow and ice at Colle Gnifetti, Swiss/Italian alps, from nuclear weapons tests
Atmos. Environ. **45** (3): 587-593 (2011).

S.D. Kaspari, M. Schwikowski, M. Gysel, M.G. Flanner, S. Kang, S. Hou, P.A. Mayewski
Recent increase in black carbon concentrations from a Mt. Everest ice core spanning 1860-2000 AD
Geophys. Res. Lett. **38** (4): L04703 (2011).

S. Maus, S. Müller, J. Büttner, S. Brütsch, T. Huthwelker, M. Schwikowski, F. Enzmann, A. Vähätolo
Ion fractionation in young sea ice from Kongsfjorden, Svalbard
Ann. Glaciology **52** (57): 301-310 (2011).

O. Sidorova, M. Saurer, V. Myglan, A. Eichler, M. Schwikowski, A. Kirdyanov, M. Bryukhanova, O. Gerasimova, I. Kalugin, A. Daryin, R. Siegwolf
A multi-proxy approach for revealing recent climatic changes in the Russian Altai
Clim. Dyn. **38** (1-2): 175-188 (2011).

RADWASTE ANALYTICS

S. Heinitz, J. Neuhausen, D. Schumann
Alkaline extraction of polonium from liquid lead bismuth eutectic
J. Nucl. Mater. **414** (2): 221-225 (2011).

M. Medarde, R. Moormann, R. Frison, R. J. Puźniak, E. Pomjakushina, K. Conder, E. Platacis, Y. Dai, D. Kiselev, L. Zanini, S. Török, P. Zagyvai, S. Heinitz, J. Neuhausen, D. Schumann, K. Thomsen
Lead–gold eutectic: An alternative liquid target material candidate for high power spallation neutron sources
J. Nucl. Mater. **411** (1-3): 72-82 (2011).

J. Neuhausen, D. Schumann
Vapour phase concentrations of volatile nuclear reaction products in the Megapie cover gas
J. Nucl. Mater. **415** (3): 361-366 (2011).

J. Neuhausen, D. Schumann, R. Dressler, B. Eichler, S. Lüthi, S. Horn, T. Stora, M. Eller
Radiochemical aspects of liquid mercury spallation targets
J. Nucl. Mat. 2011, doi:10.1016/j.jnucmat.2011.11.019.

E. Noah, V. Boutellier, R. Brütsch, R. Catherall, D. Gavillet, J. Krbanjevic, H.P. Linder, M. Martin, J. Neuhausen, D. Schumann, T. Stora, L. Zanini
Post-irradiation analysis of the tantalum container of an ISOLDE LBE target
J. Nucl. Mat. 2011, doi: 10.1016/j.jnucmat.2011.11.034.

D. Schumann, J. Neuhausen, R. Michel, V. Alfimov, H.A. Synal, J.C. David, A. Wallner
Excitation functions for the production of long-lived residue nuclides in the reaction nat Bi(p;xn,yp)Z
J. Phys. G: Nucl. Part. Phys. **38** (6): 065103 (2011).

RADIONUCLIDE DEVELOPMENT - CHEMISTRY

S. Lehenberger, C. Barkhausen, S. Cohrs, E. Fischer, J. Grünberg, A. Hohn, U. Köster, R. Schibli, A. Türler, K. Zhernosekov
The low-energy β− and electron emitter Tb-161 as an alternative to Lu-177 for targeted radionuclide therapy
Nuclear medicine and biology **38** (6): 917-924 (2011).

N.S. Loktionova, A.N. Belozub, D.V. Filosofov, K. Zhernosekov, T. Wagner, A. Türler, F. Rösch
Improved column-based radiochemical processing of the generator produced Ga-68
Appl. Radiat. Isot. **69** (7): 942-946 (2011).

ENVIRONMENTAL RADIONUCLIDES UNIVERSITÄT BERN

D. Ceburnis, A. Garbaras, S. Szidat, M. Rinaldi, S. Fahrni, N. Perron, L. Wacker, S. Leinert, V. Remeikis, M.C. Facchini, A.S.H. Prevot, S.G. Jennings, M. Ramonet, C.D. O'Dowd
Quantification of the carbonaceous matter origin in submicron marine aerosol by C-13 and C-14 isotope analysis
Atmos. Chem. Phys. **11** (16): 8593-8606 (2011).

S. Farooq, S.A. Eqani, R.N. Malik, A. Katsoyiannis, G. Zhang, Y.L. Zhang, J. Li, X. Liu, K.C. Jones, Z.K. Shinwari
Occurrence, finger printing and ecological risk assessment of polycyclic aromatic hydrocarbons (PAHs) in the Chenab River, Pakistan
J. Environ. Monit., 13, 3207-3215 (2011).

J. Li, Q.L. Li, R. Gioia, Y.L. Zhang, G. Zhang, X.D. Li, B. Spiro, R.S. Bhatia, K.C. Jones
PBDEs in the atmosphere over the Asian marginal seas, and the Indian and Atlantic oceans.
Atmos Environ, 2011, 45(37): 6622-6628. DOI: 10.1016/j.atmosenv.2011.09.010.

S.F.L. Mertens, M. Gara, A.S. Sologubenko, J. Mayer, S. Szidat, K.W. Krämer, T. Jacob, D.J. Schiffrin, T. Wandlowski
Au@Hg nanoalloy formation through direct amalgamation: Structural, spectroscopic, and computational evidence for slow nanoscale diffusion
Adv. Funct. Mater. **21** (17): 3259-3267 (2011).

M.C. Minguillón, N. Perron, X. Querol, S. Szidat, S.M. Fahrni, A. Alastuey, J.L. Jimenez, C. Mohr, A.M. Ortega, D.A. Day, V.A. Lanz, L. Wacker, C. Reche, M. Cusack, F. Amato, G. Kiss, A. Hoffer, S. Decesari, F. Moretti, R. Hillamo, K. Teinilä, R. Seco, J. Peñuelas, A. Metzger, S. Schallhart, M. Müller, A. Hansel, J.F. Burkhart, U. Baltensperger, A.S.H. Prévôt
Fossil versus contemporary sources of fine elemental and organic carbonaceous particulate matter during the Daure campaign
in northeast spain
Atmos. Chem. Phys. **11** (23): 12067-12084 (2011).

Y.L. Zhang, X.Q. Lee, F. Cao
Chemical characteristics and sources of organic acids in precipitation at a semi-urban site in Southwest China
Atmos. Environ. **45**, 413-419, doi:10.1016/j.atmosenv.2010.09.067 (2011).

Y.L. Zhang, X.Q. Lee, F. Cao, D.K. Huang
Seasonal variation and sources of low molecular weight organic acids in precipitation in the rural area of Anshun
Chinese Science Bulletin **56**, 1005-1010, doi:10.1007/s11434-011-4411-5 (2011).

REPORTS AND TECHNICAL NOTES

Y. Dai, J. Neuhausen, D. Schumann, C. Zumbach, H. Leu, H. Schweikert, A. Spahr
Specimen extraction plan for MEGAPIE PIE
MPR-11-DY34-001-3, 13.01.2011, Villigen, Switzerland.

J. Neuhausen, M. Wohlmuther
Betrachtungen zur Verdampfung von Po-Isotopen und Hg-194 bei Fräsvorgängen
TM-24-11-01/0, MPR-11-NJ24-001/0, 21.03.2011, Villigen, Switzerland.

P. Suter, Ch. Zumbach, M. Wohlmuther, J. Neuhausen, D. Schumann, V. Boutellier
Anforderungen an die Werkzeuge zur Probenerzeugung aus dem MEGAPIE Target im Hotlabor des PSI
MPR-1-WM85-019/2, 03.05.2011, Villigen, Switzerland.

M. Wohlmuther, J. Neuhausen, D. Schumann
Betrachtungen zu den Aktivitätsmengen bei Reinigung der MEGAPIE PIE-Proben in Öl sowie HNO_3
MPR-1-WM85-046/1, 09.05.2011, Villigen, Switzerland.

L. Zanini, N. Baluc, A. De Simone, R. Eichler, S. Joray, E. Manfrin, M. Pouchon, S. Rabaioli, D. Schumann, J. Welte, K. Zhernosekov
Conceptual Design, Neutronic and Radioprotection Study of a Fast Neutron Irradiation Station at SINQ
PSI-Report Nr. 11-04, December 2011, ISSN 1019-0643, Villigen, Switzerland.

CONTRIBUTIONS TO CONFERENCES, WORKSHOPS AND SEMINARS

HEAVY ELEMENTS

M. Ayranov, M. Bunka, R. Dressler, I. Günther-Leopold, S. Heinitz, N. Kivel, S. Lüthi, D. Schumann, T. Stowasser, A. Vögele, D. Wittwer, M. Wohlmuther
Repetition of the re-measurement of the ^{60}Fe half-life
ERAWAST II workshop, PSI, Switzerland, August – September, 2011.

R. Dressler
Chemical investigation of element 114 - Indication for a massive relativistic effect in chemistry
International Conference on Advances in Radioactive Isotope Science (ARIS), Leuven, Belgium, June, 2011.

R. Dressler, P. Rassmussen
pureCOLD fast electronics for β-α pile-up suppression first on-line measurements
4th International Conference on the Chemistry and Physics of the Transactinide Elements (TAN'11), Sochi, Russia, September, 2011.

R. Dressler
Plan to measure the half-life and neutron capture cross section of ^{53}Mn
ERAWAST II workshop, PSI, Villigen, Switzerland, August – September, 2011.

R. Eichler
Chemistry with the newly discovered Superheavy Elements
General Physics Seminar, University Aarhus, Denmark, 3 March, 2011.

R. Eichler
First foot prints of chemistry on the shore of The Island of SHE
4th International Conference on the Chemistry and Physics of the Transactinide Elements (TAN'11), Sochi, Russia, 7 September, 2011.

H.W. Gäggeler, J. Dvorak
Deep inelastic transfer studies at GSI: Historical reminiscences & New developments.
Department of Nuclear Physics, Australian National University (ANU), Canberra, Australia, 25 March, 2011.

H.W. Gäggeler
Heavy ion production of heaviest elements and recent achievements in their chemical studies,
Institute of Modern Physics of the Chinese Academy of Sciences, Lanchou, China, 22 August, 2011.

H.W. Gäggeler, J.V. Kratz, M. Schädel
Revival of deep inelastic transfer reactions for production of neutron-rich isotopes of heavy elements
4th International Conference on the Chemistry and Physics of the Transactinide Elements (TAN'11), Sochi, Russia, 5-9 September, 2011.

H.W. Gäggeler
Recent achievements in chemical studies of heaviest elements at FLNR in Dubna
XXXII Mazurian Lakes Conference of Nuclear Physics, Piaski, Poland, 11-18 September, 2011.

J. Neuhausen, D. Schumann, R. Dressler, B. Eichler, S. Heinitz, B. Hammer, F. von Rohr, L. Zanini, V. Boutellier, M. Rüthi, J. Eikenberg, E. Noah
Radiochemical aspects of liquid metal spallation targets
DAE-BRNS Symposium on Nuclear and Radiochemistry, Visakhapatnam, India, February, 2011.

S. Söllradl
Prompt Gamma Activation Analysis - Principles of the methodology, example measurements, and plans for the future upgrade of the former PSI instrument at FRM-II in Munich
Seminar of the Laboratory of Radiochemistry and Environmental Chemistry, Paul Scherrer Institute and University of Berne, Switzerland, 25 March, 2011.

P. Steinegger
Diamond Detectors for α-Spectroscopy at High Temperatures
4th International Conference on the Chemistry and Physics of the Transactinide Elements (TAN'11), Sochi, Russia, September 2011.

P. Steinegger
Diamond Detectors for Transactinide Chemistry
3rd CARAT Workshop, GSI Darmstadt, Germany, 11-13 December, 2011.

A. Türler, R. Eichler, H.W. Gäggeler, A. Yakushev, C.E. Düllmann, M. Schädel, S.N. Dimitriev, J.V. Kratz, K.J. Moody, H. Nitsche, N. Trautmann
Chemical Properties of Element 114
241st ACS National Meeting & Exposition, 2011, Anaheim, California, USA, 27-31 March, 2011.

A. Türler for a TUM, GSI, JINR, Mainz, JAEA, LBNL, UCB, Oslo, Lund, IET, IMP, PSI collaboration
Nuclear and Chemical Studies with Hassium Isotopes
4th International Conference on the Chemistry and Physics of the Transactinide Elements (TAN'11), Sochi, Russia, September, 2011.

I. Usoltsev
Attempts to produce intermetallic targets for heavy ion irradiations
4th International Conference on the Chemistry and Physics of the Transactinide Elements (TAN'11), Sochi, Russia, September 2011.

I. Usoltsev
Attempts to produce intermetallic targets for heavy ion irradiations
Seminar of the Laboratory of Radiochemistry and Environmental Chemistry, Paul Scherrer Institute and University of Berne, Switzerland, 11 November, 2011.

D. Wittwer
Thermal release investigation of radioacvtive tracers from metal matrices
Seminar of the Laboratory of Radiochemistry and Environmental Chemistry, Paul Scherrer Institute and University of Berne, Switzerland, 4 March, 2011.

D. Wittwer
Thermal release of p-elements from metal matrice
4th International Conference on the Chemistry and Physics of the Transactinide Elements (TAN'11), Sochi, Russia, 9 September, 2011.

SURFACE CHEMISTRY

M. Ammann
The ice - air interface in snow - the molecular to micron scale perspective
Third workshop on Air-Ice Chemical Interactions (AICI), New York, USA, 6-8 June, 2011.

M. Ammann
Reactivity at the sea salt - air interface: Spectroscopy and kinetics
American Chemical Society 242nd National Meeting & Exposition, Denver, USA, 28 August - 1 September, 2011.

M. Ammann
Ambient pressure photoelectron spectroscopy for basic surface science studies related to urea-scr technology
NADiP Workshop, PSI, Villigen, Switzerland, 21 October, 2011.

T. Bartels-Rausch, F. Riche, S. Wren, S. Schreiber, J. Donaldson, M. Schneebeli, M. Ammann
The microstructure of ice and effective diffusion of VOCs in snow: A laboratory study
European Geoscience Union General Assembly, Vienna, Austria, 3-8 April, 2011.

T. Bartels-Rausch
Parameterizing trace gas - ice interactions: A look into laboratories
Snow Chemistry Modelling Workshop, New York, USA, 8 June, 2011.

T. Bartels-Rausch, S. Schreiber, T. Ulrich, F. Riche, G. Krysztofiak, M. Brigante, Y.F. Elshorbany, S. Wren, A. Bernhard, B. D'Anna, M. Ndour, K. Stemmler, M. Schläppi, C. George, J. Kleffmann, M. Schneebeli, M. Schwikowski, M. Ammann
How chemistry in snow alters the atmospheric composition
EuCheMS International Conference on Chemistry and the Environment, Zürich, Switzerland, 11-15 September, 2011.

M. Brown, M. Ammann, J. v. Bokhoven
Fast moving liquid interfaces for Swissfel studies: Spectroscopy, scattering and diffraction experiments
Workshop on hard X-ray instrumentation at the SwissFEL X-ray Free Electron Laser facility, Zürich, Switzerland, 12 September, 2011.

G. Grzinic
Production and detection of N-13 labeled N2O5
Seminar of the Laboratory of Radiochemistry and Environmental Chemistry, Paul Scherrer Institute and University of Berne, Switzerland, 25 March, 2011.

M. Lampimäki
X-ray microscopy and photoelectron spectroscopy studies on iron oxide particles
Seminar of the Laboratory of Radiochemistry and Environmental Chemistry, Paul Scherrer Institute and University of Berne, Switzerland, 25 March, 2011.

M. Lampimäki, V. Zelenay, A. Křepelová, S. Steimer, M. Ammann
Nanostructure and hygroscopicity of tannic acid particles: Influence of O3 and UV-radiation
ECASIA'11: 14th European Conference on Applications of Surface and Interface Analysis, Cardiff, UK, 4-9 September, 2011.

M. Lampimäki, V. Zelenay, A. Křepelová, S. Steimer, M. Ammann
Mineral dust and iron oxide particles studied under oxidizing and acidic conditions
JUM@P'11: Joint Users' meeting at PSI, Villigen, Switzerland, 15-16 September, 2011.

S. Schreiber
The interaction of nitrogen oxides with ice - a lab study at atmospherical partial pressures
Seminar of the Laboratory of Radiochemistry and Environmental Chemistry, Paul Scherrer Institute and University of Berne, Switzerland, 21 October, 2011.

S. Steimer, M. Lampimäki, V. Zelenay, A. Křepelová, M. Ammann
Morphology and composition of individual tannic and shikimic acid particles studied at oxidizing environmental conditions
JUM@P'11: Joint Users' meeting at PSI, Villigen, Switzerland, 15-16 September, 2011.

T. Ulrich, M. Ammann, S. Leutwyler, T. Bartels-Rausch
The adsorption of HNO$_4$ on ice and its temperature dependence
Seminar of the Laboratory of Radiochemistry and Environmental Chemistry, Paul Scherrer Institute and University of Berne, Switzerland, 25 March, 2011.

T. Ulrich, M. Ammann, S. Leutwyler, T. Bartels-Rausch
The adsorption of HNO$_4$ on ice
European Geoscience Union General Assembly, Vienna, Austria, 3-8 April, 2011.

V. Zelenay, T. Tritscher, A. Krepelova, M.F. Heringa, R. Chirico, A.S.H. Prévôt, E. Weingartner, U. Baltensperger, J. Dommen, B. Watts, J. Raabe, T. Huthwelker, M. Ammann
The climate effect of soot particles caught in act
15th ETH Conference on Combustion Generated Nanoparticles, Zurich, Switzerland, 26-29 June, 2011.

ANALYTICAL CHEMISTRY

E. Bühlmann
Particulate matter and its influence on the albedo of Plaine Morte glacier
Seminar of the Laboratory of Radiochemistry and Environmental Chemistry, Paul Scherrer Institut, Switzerland,
21 October, 2011.

E. Bühlmann
Influence of particulate matter on observed albedo reductions on Plaine Morte glacier, Swiss Alps
Swiss Geoscience Master Congress, ETH Zurich, Switzerland, 10 November, 2011.

F. Cao, S. Szidat, M. Schwikowski
Radiocarbon analysis of organic carbon and elemental carbon in ice/firn samples
The first TTORCH Summer School, Hyytiälä Forestry Field Station, Finland, 27 September - 4 October, 2011.

A. Eichler, S. Kaspari, M. Gysel, M. Schwikowski, M.G. Flanner, S. Kang, S. Hou, P.A. Mayewski
Ice core derived changes in Black Carbon concentrations
15th ETH-Conference on Combustion Generated Nanoparticles, Zurich, Switzerland, 26-29 June, 2011.

A. Eichler, M. Schwikowski
Climate reconstructions from high-alpine ice cores.
Conference on „Climate Change in High Mountain Regions - from Understanding of the past to Modelling of the Future
Salzburg, Austria, 29 August - 1 September, 2011.

H.W. Gäggeler
Ice core dating
Lecture, Graduate students, Nanjing University, China, 26 September, 2011.

H.W. Gäggeler
Pollution records and climate information deduced from alpine ice cores
Nanjing University, China, 28 September, 2011.

H.W. Gäggeler, M. Schwikowski, A. Eichler, L. Tobler, S. Olivier, T. Papina
Isotope and chemical studies of a firn/ice core from Belukha, Russian Altai
Int. Symp. on Changing Cryosphere, Water Availability and Sustainable Development in Central Asia, Urumqi, China,
8-10 October, 2011.

H.W. Gäggeler
Pollution records and climate information deduced from ice cores from the Andes, Alps, and Altai
Cold and Arid Environmental Research Institute, Lanzhou, China, 13 October, 2011.

H.W. Gäggeler
Pollution records and climate information deduced from ice cores from the Andes, Alps, and Altai
Institute of Tibetan Plateau (ITP) of CAS, Beijing, China, 29 October, 2011.

H.W. Gäggeler
Drei Jahrzehnte Umweltforschung auf alpinen Gletschern, Fachvortrag
Prix de Quervin Verleihung, Naturhistorisches Museum Bern, Switzerland, 3 November, 2011.

P.A. Herren
Paleo climate reconstruction from the continental Mongolian Altai
Seminar of the Laboratory of Radiochemistry and Environmental Chemistry, Paul Scherrer Institut, Switzerland,
6 May, 2011.

P.A. Herren, S. Brütsch, A. Eichler, S. Olivier, T. Papina, W. Tinner, M. Schwikowski
An ice-core based history of Siberian forest fires since AD 1250
XVIII INQUA Congress Bern, Switzerland, 21-27 July, 2011.

P.A. Herren, A. Eichler, J. Eikenberg, H. Machguth, T. Papina, L. Tobler, E. Vogel, A. Zapf, M. Schwikowski
Ice core based climate reconstruction of the Mongolian Altai
9th Swiss Geoscience Meeting, ETH Zurich, Switzerland, 11-13 November, 2011.

S. Kaspari, M. Schwikowski, M. Gysel, T.H. Painter
Spatial and seasonal variations in black carbon concentrations in snow and ice in the Solu-Khumbu
Nepal, AGU Fall Meeting, San Francisco, USA, 5-9 December, 2011.

T. Kirchgeorg, J. Gabrieli, A. Dreyer, Z. Xie1, M. Sigl, M. Schwikowski, C. Barbante, C. Boutron, R. Ebinghaus
Perfluorinated compounds in ice core samples from the Alps
SETAC meeting "Ecosystem Protection in a Sustainable World: a Challenge for Science and Regulation", Milan, Italy, 15-19 May, 2011.

I. Mariani, T. Jenk, M. Sigl, M. Schwikowski
Ice core proxies as indicators of moisture source areas for the Alps
European Research Course on Atmospheres (ERCA), Grenoble, France, 10 January – 11 February, 2011.

I. Mariani
Precipitation and temperature signals from two ice cores in the Alps
Seminar of the Laboratory of Radiochemistry and Environmental Chemistry, Paul Scherrer Institut, Switzerland, 6 May, 2011.

I. Mariani, M. Sigl, A. Eichler, J. Gabrieli, D. Bolius, C. Barbante, C. Boutron, H.W. Gäggeler, M. Schwikowski
A 1000-year record of Saharan dust from an Alpine ice core
9th Swiss Geoscience Meeting, ETH Zurich, Switzerland, 11-13 November, 2011.

P. Pavlova, P. Schmid, M. Schwikowski
Accelerated release of persistent organic pollutants from Alpine glaciers
EAWAG Summer school 2011: "Sediments as archives of environmental change", Kastanienbaum, Switzerland, 4-15 July, 2011.

P. Pavlova
Accelerated release of POPs from Alpine glaciers: PCB/DDT record from lake sediments
Seminar of the Laboratory of Radiochemistry and Environmental Chemistry, Paul Scherrer Institut, Switzerland, 21 October, 2011.

P. Pavlova, P. Schmid, M. Schwikowski
Accelerated release of persistent organic pollutants from Alpine glaciers: PCB/DDT record from lake sediments
Internal seminar of the Analytical chemistry department, Empa, Dübendorf, Switzerland, 8 November, 2011.

M. Schwikowski
Palaeo climate reconstructions derived from high-alpine ice cores
Seminar Geography Universität Bern, Switzerland, 2 March, 2011.

M. Schwikowski, E. Bühlmann, P.A. Herren
Effects of soot, algae, and mineral dust on the albedo of the Plaine Morte Glacier, Switzerland
IASC Workshop on the use of automated measuring systems on glaciers, Pontresina, Switzerland, 23-26 March, 2011.

M. Schwikowski
Klimawandel - auf Spurensuche in hochalpinen Gletschern
Vortragsreihe "Forschung live erleben", Paul Scherrer Institut, Villigen, Switzerland, 6 April, 2011.

M. Schwikowski
Effects of impurities on the albedo of snow and ice
PhD disputation Kimberly Ann Casey, University of Oslo, Oslo, 15 September, 2011.

M. Schwikowski, P.A. Pavlova
Accelerated release of persistent organic pollutants (POPs) from Alpine glaciers
OCCR WP3 fall meeting, Zollikofen, Switzerland, 20 October, 2011.

I. Wendl, E. Isaksson, M. Schwikowski
Study of a new Svalbard ice core
9th Swiss Geoscience Meeting, ETH Zurich, Switzerland, 11-13 November, 2011.

I. Wendl
Black carbon analysis in ice cores
Seminar of the Laboratory of Radiochemistry and Environmental Chemistry, Paul Scherrer Institut, Villigen, Switzerland, 9 December, 2011.

A. Zapf
Radiocarbon dating of ice cores
Seminar of the Laboratory of Radiochemistry and Environmental Chemistry, Paul Scherrer Institut, Villigen, Switzerland, 6 May, 2011.

A. Zapf, S. Szidat, M. Schwikowski
Radiocarbon Dating of Ice Cores, "Pushing the size limits of Radiocarbon Analysis", An International Exploratory Workshop
ETH Zurich, Switzerland, 13-16 September, 2011.

A. Zapf, S. Szidat, M. Schwikowski
Radiocarbon dating of glacier ice, 9th Swiss Geoscience Meeting
ETH Zurich, Switzerland, 11-13 November, 2011.

A. Zapf
Radiocarbon dating of high alpine glaciers, Seminar of the Laboratory of Ion Beam Physics
ETH Zurich, Switzerland, 21 December, 2011.

RADWASTE ANALYTICS

M. Ayranov, D. Schumann, R. Dressler
Preparation of ^{60}Fe, ^{44}Ti, ^{53}Mn, ^{26}Al and $^{7/10}$Be samples for astrophysical experiments
Nuclear Physic in Astrophysic 5, Eilat, Israel, 5-9 April, 2011.

M. Ayranov, D. Schumann, R. Dressler, N. Kivel
Exotic radionuclides extraction from proton irradiated copper beam dump and SINQ cooling water
ERAWAST II workshop, PSI, Switzerland, 29 August - 2 September, 2011.

D. Bemmerer, T. Al-Abdullah, R. Dressler, D. Schumann
Is it possible to study the ^{44}Ti(α,p)^{47}V reaction with a radioactive target?
ERAWAST II workshop, Paul Scherrer Institut, Villigen, Switzerland, August - September, 2011.

R. Dressler, D. Schumann
Plans to measure neutron capture cross-sections and half-lives of cosmogenic radio-nuclides
Annual n_TOF meeting Lisbon, Portugal, December, 2011.

B. Hammer
Production and distribution of long-lived radionuclides in a lead-bismuth target from ISOLDE
Seminar of the Laboratory of Radiochemistry and Environmental Chemistry, Paul Scherrer Institut, Villigen, Switzerland, 11 November, 2011.

S. Heinitz
On the diffusion of polonium through metals
Seminar of the Laboratory of Radiochemistry and Environmental Chemistry, Paul Scherrer Institut, Villigen, Switzerland, 4 March, 2011.

D. Kiselev, P. Baumann, M. Gandel, Y.J. Lee, D. Schumann, A. Strinning, A. Konobeyev
Examination of a copper collimator irradiated in the 590 MeV proton beam line at PSI
4th High Power Targetry Workshop, Malmö, Schweden, 2-6 May, 2011.

W. Kutschera, K. Buzcak, O. Forstner, R. Golser, A. Priller, P. Steier, A. Wallner, D. Schumann, R. Dressler, G. Wallner, M. Bichler, G. Steinhauser, P. Collon, M. Bowers, K. Chamberlin, M. Couder, W. Lu, D. Robertson, M. Troy, A. Stoltz, S. Austin, I. Ahmad, J. Green, D. Graczyk, M. Paul
The half-life of ^{60}Fe revisited
ERAWAST II workshop, Paul Scherrer Institut, Villigen, Switzerland, August - September, 2011.

T. Lorenz, B. Hammer
www.Nucleonica.net - web driven nuclear science
ASI Seminar, Villigen, Switzerland, 11 October, 2011.

J. Neuhausen, H. Glasbrenner, S. Heinitz, M. Jolkkonen, Y. Kurata, T. Obara, N. Thiolliere, L. Zanini
Chapter 5: Properties of irradiated LBE and Pb
Meeting of the WPFC Expert Group on Heavy Liquid Metal Technologies
OECD, NEA offices, Issy-les-Moulineaux, France, 17-18 January, 2011.

J. Neuhausen
Release of volatiles from liquid Pb-alloy: PSI-radiochemistry contribution to Myrrha
Preparation Meeting for the FP7-Project SEARCH, Brussels, Belgium, 3 February, 2011.

J. Neuhausen, D. Schumann, R. Dressler, B. Eichler, S. Heinitz, B. Hammer, F. von Rohr, L. Zanini, V. Boutellier, M. Rüthi, J. Eikenberg, E. Noah
Radiochemical aspects of liquid metal spallation targets
Proceedings of DAE-BRNS Symposium on Nuclear and Radiochemistry, Visakhapatnam, India, 22-26 February, 2011.

J. Neuhausen, M. Wohlmuther
Betrachtungen zur Verdampfung von Po-Isotopen und Hg-194 bei Schmelz- und Trennvorgängen
Fachgespräch zu Sicherheit und Entsorgung im Rahmen der MEGAPIE-Nachuntersuchungen, ENSI, Brugg, Switzerland, 28 April, 2011.

J. Neuhausen, D. Schumann, V. Boutellier, Ch. Zumbach, M. Dubs
Sampling and radiochemical investigations of the MEGAPIE-Target
MEGAPIE PSC/PCG-Meeting, Villigen, Switzerland, 30 June, 2011.

J. Neuhausen, M. Wohlmuther, D. Gavillet
Evaluation of Po and Hg-194 evaporation during melting and cutting of MEGAPIE samples
MEGAPIE PSC/PCG-Meeting, Villigen, Switzerland, 30 June, 2011.

J. Neuhausen
Spallation product release and distribution in a liquid target: Possible PSI-Radiochemistry contributions to ESS
ESS WP6-Meeting, Riga, Latvia, 26 October, 2011.

J. Neuhausen
SEARCH WP6: Release and capture of volatiles from liquid LBE
Overview: Objectives, Structure, Budget
SEARCH Kick-off Meeting, Brussels, Belgium, 23 November, 2011.

J. Neuhausen
SEARCH WP6: Release and capture of volatiles from liquid LBE
PSI-contribution – Task 6.1
SEARCH Kick-off Meeting, Brussels, Belgium, 23 November, 2011.

J. Neuhausen
Radiochemical aspects of liquid metal spallation targets
Meeting of the Myrrha-LBE Conditioning and Chemistry group, Mol, Belgium, 25 November, 2011.

M. Rizzi, J. Neuhausen
Polonium evaporation studies from liquid metal spallation targets
4th High Power Targetry Workshop 2011, hosted by European Spallation Source (ESS)
Malmö, Schweden, 2-6 May, 2011.

D. Schumann
ERAWAST – Nuclear Chemistry for Nuclear Science
2nd ERAWAST workshop, Villigen, Switzerland, 29 August - 2 September, 2011.

D. Schumann, M. Ayranov, R. Dressler
Possibilities for the preparation of exotic targets at PSI
Annual n_TOF meeting, Lisbon, Portugal, 13-15 December, 2011.

S. Söllradl, L. Canella, P. Kudejova, Zs. Reva, R. Dressler, D. Schumann, M. Ayranov, A. Türler
Plan to measure the neutron capture cross-section of ^{60}Fe with cold neutrons at the PGAA facility in munich
ERAWAST II workshop, PSI, Switzerland, August - September, 2011.

A. Wallner, K. Buczak, A. Plompen, D. Schumann, V. Semkova
New exotic and non-standard radionuclides in AMS
12th Accelerator Mass Spectrometry Conference, Wellington, New Zealand 20-25 March, 2011.

RADIONUCLIDE DEVELOPMENT

M. Bunka, K. Zhernosekov, A. Hohn, R. Schibli, A. Türler
Entwicklung von ^{44}Ti-Produktion für $^{44}Ti/^{44}Sc$ Radionuklidgenerator
GDCh-Wissenschaftsforum 2011, Bremen, Germany, 4-7 September, 2011.

H. Dorrer
Production of terbium radioisotopes for diagnostic and therapeutic applications in nuclear medicine
Seminar of the Laboratory of Radiochemistry and Environmental Chemistry, Paul Scherrer Institute and University of Berne, Switzerland, 25 March, 2011.

H. Dorrer, K. Zhernosekov, U. Köster, K. Johnston, R. Schibli, A. Türler
Herstellung von Terbium-Radioisotopen für diagnostische und therapeutische Anwendungen in der Nuklearmedizin
GDCh-Wissenschaftsforum, Bremen, Germany, 4-7 September, 2011.

H. Dorrer, U. Köster, C. Müller, K. Johnston, R. Schibli, A. Türler, K. Zhernosekov
Herstellung von Terbium-Radioisotopen für diagnostische und therapeutische Anwendungen in der Nuklearmedizin
19. Jahrestagung der Arbeitsgemeinschaft Radiochemie/Radiopharmazie, Ochsenfurt bei Würzburg, Germany, 15-17 September, 2011.

H. Dorrer
Production of Terbium radioisotopes for diagnostic and therapeutic applications in nuclear medicine
Seminar of the Laboratory of Radiochemistry and Environmental Chemistry, Paul Scherrer Institute and University of Berne, Switzerland, 9 December, 2011.

K. Zhernosekov, S. Geistlich, A. Blanc, H. Dorrer, S. Landolt, A. Türler, R. Schibli
^{177}Lu quality and limitations analysis for an efficient preparation of ^{177}Lu -labeled compounds
Gemeinsame Jahrestagung der Deutschen, Österreichischen und Schweizerischen Gesellschaft für Nuklearmedizin Bregenz, Austria, 13-16 April, 2011.

K. Zhernosekov
$^{68}Ge/^{68}Ga$ radionuclides generators & synthesis modules
Pre Symposium, 1st World Congress on Gallium-68 and Peptide Receptor Radionuclide therapy (PRRNT).
Bad Berka, Germany 27-29 June, 2011.

ENVIRONMENTAL RADIONUCLIDES UNIVERSITÄT BERN

D. Ceburnis, A. Garbaras, S. Szidat, K.E. Yttri, V. Remeikis, C.D. O'Dowd
Source apportionment of ambient particulate carbonaceous matter at Mace Head during the joint EMEP/EUCAARI intensive measurement periods in fall 2008 and spring 2009
European Aerosol Conference 2011, Manchester, U.K., 4-9 September, 2011.

U. Dusek, M. Monaco, M. Prokopiou, F. Gongriep, R. Holzinger, S. Szidat, R. Hitzenberger, T. Röckmann
Thermal separation and purification of organic and elemental carbon from small aerosol samples for ^{14}C analysis
International Workshop on Small Scale Radiocarbon Analysis, Zurich, Switzerland, 13-16 September, 2011.

S.M. Fahrni, S. Szidat, H.A. Synal, L. Wacker
Improving a gas ion source for ^{14}C AMS
International Workshop on Small Scale Radiocarbon Analysis, Zurich, Switzerland, 13-16 September, 2011.

M. Furger, M. Crippa, F. Freutel, L. Poulain, S. Visser, S. Szidat, P. Zotter, A.S.H. Prevot, U. Baltensperger
Regional vs. local aerosol sources during the MEGAPOLI Paris campaigns
25th General Assembly of the International Union of Geodesy and Geophysics (IUGG), Melbourne, Australia, 28 June - 7 July, 2011.

S. Szidat
New infrastructure at the Oeschger Centre: ^{14}C Accelerator Mass Spectrometry
Plenary Meeting Oeschger Centre 2011, Bern, Switzerland, 16 February, 2011.

S. Szidat, S.M. Fahrni, N. Perron, A.S.H. Prévôt, M. Rzaca, H. Bauer, H. Puxbaum, L. Wacker
Compound-specific ^{14}C analysis of acidic aerosol components
12th Accelerator Mass Spectrometry Conference, Wellington, New Zealand, 20-25 March, 2011.

S. Szidat, S.M. Fahrni, L. Wacker, H.A. Synal
Improving and understanding a gas ion source for ^{14}C AMS
12th Accelerator Mass Spectrometry Conference, Wellington, New Zealand, 20-25 March, 2011.

S. Szidat, Y.L. Zhang, N. Perron , A.S.H. Prévôt, L. Wacker
Radiocarbon measurements of carbonaceous aerosols: the new sample preparation line at University of Bern
12th Accelerator Mass Spectrometry Conference, Wellington, New Zealand, 20-25 March, 2011.

S. Szidat, S.M. Fahrni, N. Perron, A.S.H. Prévôt, L. Wacker, M. Rzaca, H. Bauer, H. Puxbaum
^{14}C source apportionment of dicarboxylic acids and humic-like substances in atmospheric aerosols
10th International Conference on Carbonaceous Particles in the Atmosphere, Vienna, Austria, 26-29 June, 2011.

S. Szidat
Radiocarbon analysis of black and brown carbon: what can we learn?
23rd International Symposium on Polycyclic Aromatic Compounds, Münster, Germany, 4-8 September, 2011.

S. Szidat
^{14}C accelerator mass spectrometry: status of the new installations at University of Bern
Oeschger Centre WP3 Meeting 2011, Zollikofen, Switzerland, 20 October, 2011.

L. Wacker, S. Bernasconi, A. Birkholz, S. Fahrni, M. Gigera, I. Hajdas, N. Perron, M. Ruff, T. Schulze-Koenig, R. Smittenberg, H.A. Synal, S. Szidat, Y.L. Zhang
A versatile gas interface for routine radiocarbon analyses with a gas ion source
12th Accelerator Mass Spectrometry Conference, Wellington, New Zealand, 20-25 March, 2011.

Y.L. Zhang, N. Perron, A.S.H. Prévôt, L. Wacker, S. Szidat
Radiocarbon measurements of carbonaceous aerosols: the new sample preparation line at University of Bern
12th Swiss Global Change Day, Bern, Switzerland, 19 April, 2011.

Y.L. Zhang
On the quantification of OC and EC and their isolation for ^{14}C measurement: a modified thermal-optical method
Seminar Laboratory of Atmospheric Chemistry, PSI, Switzerland, 2 May, 2011.

Y.L. Zhang, N. Perron, A.S.H. Prévôt, L. Wacker, S. Szidat
On the quantification of OC and EC and their isolation for ^{14}C measurement: a modified thermal-optical method
10th International Conference on Carbonaceous Particles in the Atmosphere, Vienna, Austria, 26-29 June, 2011.

Y.L. Zhang, A. Zapf, M. Schwikowski, A.S.H. Prévôt, S. Fahrni, L. Wacker, S. Szidat
Microgram level radiocarbon determination on carbonaceous aerosol particles in the environment
International Workshop on Small Scale Radiocarbon Analysis, Zurich, Switzerland, 13-16 September, 2011.

Y.L. Zhang
Source appointment of carbonaceous aerosol by C-14 analysis: method development and applications
Seminar of the Laboratory of Radiochemistry and Environmental Chemistry, Paul Scherrer Institut, Villigen, Switzerland, 11 November, 2011.

P. Zotter, A.S.H. Prévôt, Y.L. Zhang, S. Szidat, X. Zhang, Y.H. Lin, P. Hayes, J. Schnelle-Kreis, G. Seibert, R. Zimmermann, J.D. Surratt, J.L. Jimenez, R. Weber, U. Baltensperger
Diurnal cycle of fossil and non-fossil total carbon using ^{14}C analyses during CalNex
CalNex Data Analysis Workshop, Sacramento, USA, 16-19 May, 2011.

P. Zotter, A.S.H. Prévôt, Y. Zhang, S. Szidat, X. Zhang, Y.H. Lin, P. Hayes, J. D. Surratt, J.L. Jimenez, R. Weber, J. Slowik, U. Baltensperger
Diurnal cycle of fossil and non-fossil total carbon using ^{14}C analyses during CalNex
European Aerosol Conference 2011, Manchester, U.K., 4-9 September, 2011.

P. Zotter, A.S.H. Prévôt, Y.L. Zhang, S. Szidat, X. Zhang, Y.H. Lin, P. Hayes, J.D. Surratt, J.L. Jimenez, R. Weber, U. Baltensperger
Diurnal cycle of fossil and non-fossil total carbon using ^{14}C analyses during CalNex
International Workshop on Small Scale Radiocarbon Analysis, Zurich, Switzerland, 13-16 September, 2011.

P. Zotter, A.S.H. Prévôt, S. Szidat, J. Surratt, J.L. Jimenez, R. Weber, Y.L. Zhang, S. Szidat, X. Zhang, Y.H. Lin, P. Hayes, U. Baltensperger
Diurnal cycle of fossil and non-fossil total carbon using ^{14}C analyses in Pasadena
American Association for Aerosol Research (AAAR) 30th Annual Conference, Orlando, USA, 3-7 October, 2011.

PUBLIC RELATIONS AND OUTREACH ACTIVITIES

Analytical Chemistry

Wissenschaft aktuell (http://www.wissenschaft-aktuell.de)
Ruß auf dem Everest
25 January 2011

Welt der Physik (http://www.weltderphysik.de)
Ruß auf dem Everest
25 January 2011

Zentralschweiz am Sonntag
Russ und Dreck auf dem Dach der Welt
30 January 2011

PSI Media release
Russ lässt Himalaya-Gletscher schneller schmelzen
21 February 2011

Schweizerische Depeschenagentur AG
Klimaforschung Russ lässt Himalaya-Gletscher schneller schmelzen
21 February 2011

NZZ Online
Russ lässt Himalaya-Gletscher schneller schmelzen
22 February 2011

Die Botschaft
Nicht nur eine Folge der Klimaerwärmung, Russ lässt Himalaya-Gletscher schneller schmelzen
23 February 2011

Tages-Anzeiger
Russ lässt das Eis im Himalaja schmelzen
23 February 2011

Süddeutsche Zeitung
Dreck auf Eis
23 February 2011

Chemie Plus/Labor Flash
Russ mitschuldig an Gletscherschmelze
7 March 2011

Demonstration
Tag der offenen Tür am PSI
Chemie im Gletschereis - Gletscher archivieren die Luftverschmutzung
16 October 2011

http://www.oeschger.unibe.ch/people/profiles/alexander_zapf_en.html
Analysing African ice before it disappears forever
12 December 2011

Heavy Elements

Forum für Universität und Gesellschaft, Universität Bern
A. Türler, „Radioaktivität: Grundlagen und Strahlungsmessung"
1 April 2011

DRS1 (Radiosendung Doppelpunkt)
A. Türler,"Marie Curie und ihre Entdeckungen"
17 June 2011

Demonstration
Tag der offenen Tür am PSI
Die Kleinsten sind die Wichtigsten – auch in der Chemie
16 October 2011

Demonstration
Tag der offenen Tür am PSI
Superschwere Elemente mit ungewöhnlicher Chemie?
16 October 2011

Surface Chemistry

Demonstration
Tag der offenen Tür am PSI
Klimaeffekt von Feinstaub im Fokus
16 October 2011

Environmental Radionuclides Universität Bern

Homepage Department of Chemistry and Biochemistry, Uni Bern
Molecule of the month: Terbium-161 - A New Radionuclide for Tumor Therapy
http://www.dcb-server.unibe.ch/dcbneu/mom/mom_2011-08.html
August 2011

LECTURES AND COURSES

Prof. Dr. A. Türler
Universität Bern, FS2011:
Bachelor
- Instrumentalanalytik II (with Dr. K. Krämer and Prof. M. Schwikowski) (3 ECTS)
- Allgemeine Chemie (Einführung Radioaktivität) (with Prof. R. Hähner and Prof. J. Hulliger) (4 ECTS)

Universität Bern, HS2011:
Bachelor
- Physikalische Chemie IV (with Prof. T. Wandlowski) (3,75 ECTS)
- Praktikum Phys. Chemie II (with others) (4 ECTS)
- Biochemische Methoden I (with others) (3 ECTS)

Master
- Nuclear and Radiochemistry (with R. Eichler) (3 ECTS)
- Lab course: Nuclear and Radiochemistry at Bern, Basel, ETHZ and PSI (with others) (4 ECTS)
- Seminar Radio- und Umweltchemie in collaboration with Paul Scherrer Institut
  (organized by D. Schumann FS2011 and S. Szidat HS2011)

Prof. Dr. M. Schwikowski
Universität Bern, FS2011:
Bachelor
- Instrumentalanalytik II (with Prof. A. Türler and Dr. K. Krämer) (3 ECTS)

Master
- Summer Course am Paul Scherrer Institut. 2months International Summer Student Programme
  (with Prof. A. Türler) (4 ECTS)

Universität Bern, HS2011
Master
- Atmospheric and Aerosol Chemistry (3 ECTS)

Dr. M. Ammann
ETH Zürich, FS2011:
- Systempraktikum Atmosphäre und Klima, (7 ECTS)

Dr. T. Bartels-Rausch
Universität Bern, HS2011
Master
- Lab course: Nuclear and Radiochemistry at the PSI (with Prof. A. Türler and S. Szidat) (4 ECTS)

Dr. R. Dressler
Course for PhD students at PSI
- Nuclear Radiation Measurement Part 1
- Nuclear Radiation Measurement Part 2

Dr. R. Eichler

Universität Bern, HS2011:
- Praktikum Phys. Chemie II (with Prof. A. Türler) (4 ECTS)
- Master Lab course Radiochemistry
- Lab course: Nuclear and Radiochemistry (with Prof. A. Türler and S. Szidat) (4 ECTS)

Prof. Dr. H.W. Gäggeler

University Lanzhou, China, HS 2011:
- Introduction into Radiochemistry and some applications

Dr. J. Neuhausen

Universität Bern, HS2011:
- Praktikum Physikalische Chemie II (with Prof. A. Türler) (4 ECTS)

Dr. D. Schumann

FS2011:
- Seminar Radio- und Umweltchemie in collaboration with Paul Scherrer Institut

PD Dr. S. Szidat

Universität Bern, FS2011:
- Ergänzungen zur analytischen Chemie für Pharmazeuten (2 ECTS)

Universität Bern, HS2011:
- Chemie für Studierende der Veterinärmedizin (with C. Leumann) (4.5 ECTS)
- Environmental Radionuclides and Nuclear Dating (1.5 ECTS)
- Praktikum Physikalische Chemie II (with others) (4 ECTS)
- Lab Course Nuclear and Radiochemistry (with A. Türler and R. Eichler) (4 ECTS)
- Seminar Radio- und Umweltchemie in collaboration with Paul Scherrer Institut

MEMBERS OF SCIENTIFIC COMMITTEES
EXTERNAL ACTIVITIES

Dr. Markus Ammann:
- Atmospheric Chemistry and Physics: member of editorial board
- Member of the IUPAC Subcommittee on gas kinetic data evaluation
- PSI internal research commission (FoKo), member

Dr. Thorsten Bartels-Rausch:
- Air-Ice Chemical Interactions (AICI), Member of Steering Committee

Dr. Robert Eichler:
- PSI internal research commission (FoKo), member
- Associate Editor of the International Journal of Modern Physics E (IJMPE)
  World Scientific Publishing

Dr. Dorothea Schumann:
- Member of the Nuklearforum Schweiz
- Member of the Schweizerische Gesellschaft der Kernfachleute
- Member of the PSI internal Neutron Source Development Group

Prof. Dr. Margit Schwikowski:
- Member of the Coordinating Committee of the Pages/IGBP initiative LOTRED SA
  (Long-Term climate Reconstruction and Diagnosis of (southern) South America)
- Schweizerische Gesellschaft für Schnee, Eis und Permafrost (SEP), board member
- Member of the Oeschger Centre for Climate Change Research (OCCR)
- Council of the International Glaciological Society, elective member
- PhD thesis committee Kimberley Ann Casey, Supraglacial dust and debris characterization via in situ and
  optical remote sensing methods, University of Oslo, 15 September 2011
- PhD thesis committee Irene Wientjes, A study of the dark region in the western ablation zone of the
  Greenland ice sheet, Utrecht University, 7 October 2011

PD Dr. Sönke Szidat:
- Member of the Oeschger Centre for Climate Change Research (OCCR)
- Treasurer of the Bernese Chemical Society (Berner Chemische Gesellschaft, BCG)

Prof. Dr. Andreas Türler:
- Eidgenössische Kommission für Strahlenschutz und Überwachung der Radioaktivität (KSR), member
- GSI Helmholtzzentrum für Schwerionenforschung GmbH, member of the General Program Advisory
  Committee (G-PAC) and GSI Users Group, member of the Executive Committee (UEC)
- Gesellschaft Deutscher Chemiker (GDCh), Fachgruppe Nuklearchemie, Vorstands-Beirat
- Radiochimica Acta, member of the advisory board
- Oeschger Centre for Climate Change Research (OCCR), Mitglied des Wissenschaftlichen Ausschusses
- Nuklearforum Schweiz, Mitglied des Vorstandes

DOCTORAL THESIS

Veronika Zelenay

Water uptake and chemical composition in single submicron particles analyzed by X-ray microspectroscopy

Prof. Dr. T. Peter / ETHZ
Dr. M. Ammann / PSI
January 2011

Simon Fahrni

New methods for radiocarbon measurements of atmospheric di- and polycarboxylic acids with accelerator mass spectrometry

Prof. Dr. H. W. Gäggeler / PSI & Uni Bern
PD Dr. S. Szidat / Uni Bern
February 2011

Yulia Sosedova

Heterogenous chemistry of nitrogen dioxide and its impact on atmospheric nitrous acid

Prof. Dr. H. W. Gäggeler / PSI & Uni Bern
Dr. M. Ammann / PSI
May 2011

C. Barkhausen

Production of non carrier added (n.c.a.) ^{177}Lu for radiopharmaceutical Applications

PhD thesis at TU Munich
Prof. Dr. A. Türler / PSI & Uni Bern
Dr. K. Zhernosekov / PSI
September 2011

MASTER THESIS

Eva Bühlmann

Influence of particulate matter on observed albedo reductions on Plaine Morte glacier, Swiss Alps

Prof. Dr. M. Schwikowski / PSI & Uni Bern
Prof. Dr. M. Hoelzle / University of Fribourg
October 2011

Emanuel Hammer

Calculation and interpretation of cloud peak supersaturations at the Jungfraujoch

Prof. Dr. Urs Baltensperger / PSI
Dr. E. Weingartner / PSI
Prof. Dr. M. Schwikowski / PSI & Uni Bern
March 2011

Christine Ketterer

Investigation of the planetary boundary layer using remote sensing and in-situ measurements at the Kleine Scheidegg and at the Jungfraujoch

Dr. E. Weingartner / PSI
Prof. Dr. M. Schwikowski / PSI & Uni Bern
December 2011

BACHELOR THESIS

Yvonne Hari

System set-up for the isolation of humic-like substances from aerosols

PD Dr. S. Szidat / Uni Bern
June 2011

AWARD

P.A. Herren, A. Eichler, J. Eikenberg, H. Machguth, T. Papina, L. Tobler, E. Vogel, A. Zapf, M. Schwikowski

First Prize for Young Researchers of the Swiss Snow, Ice and Permafrost Society (SEP)
Ice core based climate reconstruction of the Mongolian Altai

9th Swiss Geoscience Meeting, ETH Zurich, 11-13 November 2011

SUMMER STUDENTS

Francois Chenuet
A new dye to probe the water-air and ice-air interface
University of Orleans, France
April - August 2011

Sebastian Crespo
Chemical analysis of major ion concentrations and stable isotope ratios ($\delta^{18}O$) in samples of river water, ground water, rain, snow, and glacier ice using ion chromatography and stable isotope mass spectrometry
Instituto Argentino de Nivología, Glaciología y Ciencias Ambientales, Mendoza, Argentina
July - September 2011

Valentine Grimaudo
Analysis of Lomonosovfonna ice cores in Svalbard
University Bern
September - December 2011

Adam Hasenfratz
Chemical analyses of major ion concentrations and stable isotope ratios in glacier ice
University Bern
July - September 2011

Gregorz Mazur
Alkaline extraction of polonium from LBE
University of Warshaw
July - August 2011

Patrick Steinegger
Diamond detectors for vacuum chromatography
University Bern
March - May 2011

Michelle Frei
Purification of the ^{53}Mn fraction from stable chromium – Stip I stainless steel samples
Kantonsschule Baden
July - September 2011

Fabian Haumann
3-wöchiges Berufspraktikum zur chemischen Analyse von Gletschereis
Kantonsschule Wettingen
February - March 2011

Fabio Masero und Lukas Kupferschmied
Maturarbeit: Können wir die Konzentrationen von POPs in Schneeproben bestimmen?
Gymnasium Thun Seefeld
April - October 2011

VISITING GUESTS AT PSI 2011

19 January
Yinon Rudich, Weizmann Institut, Israel
Discussion new options for imaging liquid - liquid separation in environmental nanoparticles

23-25 February
Andrej Semchenkov, Oslo Cyclotron Laboratory
Discussion on moving the ECR source form the PSI Injector I to the OCL

23-25 February
Jon Petter Omtvedt, Oslo Cyclotron Laboratory
Discussion on moving the ECR source form the PSI Injector I to the OCL

4 March
Jan John, University of Prague
Spent nuclear fuel recycling studies at the CTU in Prague

7 March - 3 April
Sumi Wren, University of Toronto
Collaborative experiments on transport processes in snow

21 March
D. James Donaldson, University of Toronto
Revisiting the strategy for new photochemistry in the atmosphere

17-22 April
Manabu Shiraiwa, Max Planck Institut, Mainz, Germany
Collaborative kinetic experiments

27-29 April
Hou Shugui, Nanjing University, China
Ice core research in the Tibetan Plateau

3 May
Jürg Beer, EAWAG
Solar variability and climate change

6 May
Mauro Bonardi, University of Milano, Italy
Production and use of high specific activity radiotracers for metallobiochemical, toxicological and environmental studies

19 May
Jakob Liebl, University of Vienna, Vienna, Austria
^{14}C bomb peak dating of human DNA samples at the microgram level

5-17 June
Alexander Aerts, SCK·CEN, Mol, Belgium
Experiments studying the evaporation of volatiles from LBE

22 June
Mattia Monaco, Utrecht University, Utrecht, The Netherlands
^{14}C analysis of carbonaceous particles from the Netherlands

16 August
Tatyana Papina, IWEP SRRAS, Institute for Water and Environmental Problems, Barnaul, Russia
Discussion on the Mongolia Altai ice core project

19 August - 2 September
Gunther Korschinek, TU Munich, Germany
Accelerator waste, accelerator mass spectrometry and more

28 August - 2 September
Alessia Di Pietro, INFN Catania, Italy
Reactions induces by radioactive Be beams

13 September
Guaciara dos Santos and Xiaomei Xu, University of California, Irvine, USA
Isolation of organic carbon and elemental carbon from aerosols for ^{14}C analysis

21 October
Michael Kerbrat, Laboratoire de Glaciologie et Géophysique de l'Environnement, University of Grenoble, Grenoble, France
Nitrous acid measurements in Antarctica

11 November
Alexander Aerts, Belgian Nuclear Research Centre, Mol, Belgium
Chemistry research and development for MYRRHA (Multi-purpose hybrid research reactor for high-tech applications)

17 November
Jonathan P. Reid, University of Bristol, UK
Seminar and exchange of knowledge in the context of microstrucute and microphysics of atmospheric particles

9 December
Reto Knutti, Institute for Atmospheric and Climate Science, ETH Zürich, Switzerland
Should we believe model predictions of future climate change?

OBITUARY

Mit tiefem Bedauern mussten wir am 11. Februar 2012 von Beat Rufibach Abschied nehmen. Er ist bei einem Bergunfall in seinem geliebten Grimselgebiet ums Leben gekommen. Beat hat uns über viele Jahre als Bergführer und Eisbohrer zu Gletschern in aller Welt begleitet.

Wir werden sein Lächeln, seine warmherzige Art und seinen immensen Tatendrang sehr vermissen. Mit ihm verlieren wir nicht nur einen kompetenten Mitarbeiter sondern auch einen wahren Freund. Beat hat jede Expedition sowohl wissenschaftlich wie auch menschlich bereichert.

Unsere Gedanken sind in dieser schweren Zeit bei seiner Familie.

We are deeply saddened by the loss of Beat Rufibach. Over many years he was our mountain guide and colleague on various field expeditions to glaciers all over the world. We lose a competent fellow and true friend.

Our thoughts are with his family.

PAUL SCHERRER INSTITUT
PSI

LABOR FÜR RADIO- UND UMWELTCHEMIE
DES PAUL SCHERRER INSTITUTS UND DER UNIVERSITÄT BERN
31.12.2011

u^b

UNIVERSITÄT
BERN

PSI **Prof. Dr. Andreas Türler** **Uni Bern**

Angela Blattmann (Secretary / 80 %) Catrina Veraguth (Secretary / 40 %)

Prof. Dr. Margit Schwikowski (Deputy)

SURFACE CHEMISTRY
Dr. Markus Ammann
Dr. Thorsten Bartels-Rausch
Dr. Markus Lampimäki
Mario Birrer
Thomas Ulrich [1]
Sepp Schreiber [1]
Goran Grzinic [1]
Sarah Steimer [1]

ANALYTICAL CHEMISTRY
Prof. Dr. Margit Schwikowski
Leonhard Tobler
Dr. Anja Eichler (50%)
Dr. Gabriela Gramlich (50%)
Roman Bentz
Sabina Brütsch
Silvia Köchli
Pierre-Alain Herren [1]
Isabella Mariani [1]   *Isabel Wendl* [1]
Alexander Zapf [1]   *Fang Cao* [1]
Pavlina Pavlova [1]

ENVIRONMENTAL RADIONUCLIDES
PD Dr. Sönke Szidat
Edith Vogel
Michael Battaglia
Yanlin Zhang [1]

HEAVY ELEMENTS
Dr. Robert Eichler
Dr. Rugard Dressler
Dave Piguet
Alexander Vögele
David Wittwer [1]
Stefan Söllradl [1]
Patrick Steinegger [1]
Ilya Usoltsev [1]

RADWASTE ANALYTICS
Dr. Dorothea Schumann
Dr. Jörg Neuhausen
Dr. Marin Ayranov
Sabrina Lüthi
Tanja Stowasser (50%)
Stephan Heinitz [1]
Matthias Rizzi [1]
Bernadette Hammer [1]
Tobias Lorenz [1]

RADIONUCLIDE DEVELOPMENT
Dr. Konstantin Zhernosekov
Dr. Alexander Hohn (ZRW)
Holger Dorrer [1]
Maruta Bunka [1]

[1] Graduate student

AUTHOR INDEX

AFFILIATION INDEX

ASI	Abteilung für Strahlenschutz und Sicherheit, Paul Scherrer Institut, CH-5232 Villigen PSI, Switzerland
CERN	European Organization for Nuclear Research, CERN CH-1211, Genève 23, Switzerland
CIC	Niels Bohr Institute, Centre for Ice and Climate, Juliane Maries Vej 30, DK-2100 København, Denmark
CIEMAT	Avda. Complutense, 40, 28040 Madrid, Spain
CPST Vilnius	Center for Physical Sciences and Technology, Institute of Physics, Vilnius, Lithuania
CSIC	Institute of Environmental Assessment and Water Research, CSIC, Barcelona, Spain
EMPA	Forschungsinstitution im ETH-Bereich, Überlandstrasse 129, CH-8600 Dübendorf, Switzerland
ETHZ	Eidgen. Technische Hochschule Zürich, CH-8092 Zürich, Switzerland
FLNR Dubna	Flerov Laboratory of Nuclear Reactions, Joliot Curie 6, 141980 Dubna, Russia
GA Tech	School of Earth and Atmospheric Sciences, Georgia Institute of Technology, Atlanta, GA, USA
GFA	Large Research Facilities (GFA), Paul Scherrer Institut, CH-5232 Villigen PSI, Switzerland
GIG CAS	Guangzhou Institute of Geochemistry, Chinese Academy of Sciences, 511 Kehua Street, Wushan, Tianhe District, Guangzhou, GD 510640, China
GSI	GSI Helmholtzzentrum für Schwerionenforschung GmbH, Postfach 11 05 52, 64220 Darmstadt, Germany
HIM	Helmholtz-Institut Mainz, Johannes Gutenberg-Universität, D-55099 Mainz, Germany
Hotlab	The Hot Laboratory Division (AHL) of the Nuclear Energy and Safety Department (NES) of the Paul Scherrer Institut (PSI), Switzerland
Hovd University	Hovd University,213500 Hovd, Mongolia
IANIGLA-Conicet	Instituto Argentino de Nivología, Glaciología y Ciencias Ambientales, C.C. 330, 5500 Mendoza, Argentina
IMP	Institute of Modern Physics, Chinese Academy of Sciences, Add: 509 Nanchang Rd., Lanzhou**,** 730000, China
INFN Bologna	National Institute of Nuclear Physics, Viale B. Pichat, 6/2, I-40127 Bologna, Italy
Inselspital	Inselspital, Nuclearmedizin, 3010 Bern, Switzerland
ITE	Instytut Technologii Elektronowej, Al. Lotników 32/46 02-668 Warszawa, Poland
IWEP	Institute for Water and Environmental Problems, Siberian Branch of the Russian Academy of Sciences, 105 Papanintsev Str., RU-Barnaul 656099, Russia
JAEA	Japan Atomic Energy Agency, Tokai Research and Development Center, (Nuclear Science Research Institute), 2-4 Shirane Shirakata, Tokai-mura, Naka-gun, Ibaraki 319-1195, Japan
KIT	Karlsruher Institut für Technologie, Hermann-von-Helmholtz-Platz 1, 76344 Eggenstein-Leopoldshafen, Germany
FRM II	Forschungs-Neutronenquelle Heinz Maier-Leibnitz (FRM II), Lichtenbergstr. 1, 85748 Garching, Germany
KUP	Climate and Environmental Physics, Physics Institute, University of Bern, Sidlerstrasse 5, CH-3012 Bern, Switzerland
LAC	Laboratory of Atmospheric Chemistry, Paul Scherrer Institut, CH-5232 Villigen PSI, Switzerland

LBNL	Lawrence Berkeley National Laboratory, Berkeley, CA 94720, USA
LLNL	Lawrence Livermore National Laboratory, 7000 East Ave., Livermore, CA 94550-9234, USA
LOG	Fachbereich Logistik, Paul Scherrer Institut, CH-5232 Villigen PSI, Switzerland
MAS	Social Economy Research Center of Mongolian Academy of Sciences, Mongolia
MPI-CH	Max-Planck-Institut für Chemie (Otto-Hahn-Institut), Joh.-Joachim-Becher-Weg 27, 55128 Mainz, Germany
NES	Nuclear Energy and Safety Research Department, Paul Scherrer Institut, CH-5232 Villigen PSI, Switzerland
NPI	Norwegian Polar Institute, N-9296 Tromsø, Norway
NRC	Bologna Institute of Atmospheric Sciences and Climate, National Research Council, Bologna, Italy
NUI Galway	School of Physics and Centre for Climate & Air Pollution Studies, Ryan Institute, National University of Ireland, Galway, University Road, Galway, Ireland
PSI	Paul Scherrer Institut, CH-232 Villigen PSI, Switzerland
SLF	Institut für Schnee- und Lawinenforschung, Flüelastr. 11, CH-7260 Davos, Switzerland
SLS	Swiss Light Source, Paul Scherrer Institut, CH-232 Villigen PSI, Switzerland
State Key Lab. of Cryospheric Sciences	Chinese Academy of Sciences, Lanzhou, 730000, China.
SWAN	SWAN Isotopen AG, Freiburgstrasse 18, 3010 Bern, Switzerland
TUM	Technische Universität München, Arcisstraße 21, 80333 München, Germany
Univ. Bergen	Department of Earth Science, University of Bergen, Allégt. 41, N-5007 Bergen, Norway
Univ. Bern	Departement für Chemie und Biochemie, Universität Bern, Freiestr. 3, CH-3012 Bern, Switzerland
Univ. Bielefeld	Universität Bielefeld, Postfach 10 01 31, D-33501 Bielefeld, Germany
Univ. CO	Department of Chemistry and CIRES, University of Colorado, Boulder, CO, USA
Univ. Fribourg	Université de Fribourg, Av. Europe 20 - 1700 Fribourg, Switzerland
Univ. Mainz	Universität Johann Gutenberg, Institut für Kernchemie, D-55128 Mainz, Germany
Univ. NC	Department of Environmental Sciences & Engineering, University of North Carolina, NC, USA
Univ. Oslo	University of Oslo P.O. Box 1072 Blindern 0316 Oslo, Norway
Univ. Stuttgart	Universität Stuttgart, Postfach 10 60 37, 70049 Stuttgart, Germany
Univ. Tallinn	Institute of Geology, Tallinn University of Technology, 10143 Tallinn, Estonia
Univ. Vienna	University of Vienna, Dr.-Karl-Lueger-Ring 1, 1010 Wien, Austria
Univ. Zürich	University of Zurich, Winterthurerstr. 190, CH-8057 Zürich, Switzerland
UMass	Climate System Research Center and Department of Geosciences, University of Massachusetts, Morrill Science Center, Amherst, MA, USA
Victoria Univ. Wellington	Victoria University of Wellington, PO Box 600, Wellington 6140, New Zealand
Weizmann Institute	Weizmann Institute of Science, 234 Herzl Street, Rehovot 76100, Israel
ZRW	Center for Radiopharmaceutical Sciences, Paul Scherrer Institut, CH-5232 Villigen PSI, Switzerland